Tennessee Valley Authority, 1101 Market Street, Chattanooga, TN 37402

CNL-16-170

October 28, 2016

10 CFR 2.101
10 CFR 52.15

ATTN: Document Control Desk
U.S. Nuclear Regulatory Commission
Washington, DC 20555-0001

Clinch River Nuclear Site
NRC Project No. 785

Subject: Submittal of Supplemental Information Related to Vibratory Ground Motion in Support of Early Site Permit Application for Clinch River Nuclear Site

References:
1. Letter from TVA to NRC, CNL-16-081, "Application for Early Site Permit for Clinch River Nuclear Site," dated May 12, 2016
2. Letter from TVA to NRC, CNL-16-134, "Schedule for Submittal of Supplemental Information in Support of Early Site Permit Application for Clinch River Nuclear Site," dated August 11, 2016
3. Letter from TVA to NRC, CNL-16-162, “Submittal of Supplemental Information Related to Geologic Characterization Information, Surface Deformation, and Stability of Subsurface Materials and Foundation in Support of Early Site Permit Application for Clinch River Nuclear Site,” dated October 21, 2016

By letter dated May 12, 2016 (Reference 1), Tennessee Valley Authority (TVA) submitted an application for an early site permit (ESP) for the Clinch River Nuclear (CRN) Site in Oak Ridge, TN. Subsequent to the submittal of the application, and consistent with interactions with NRC staff, TVA identified certain aspects of the application that it intends to supplement. By letter dated August 11, 2016 (Reference 2), TVA provided a plan for submitting the identified supplemental information. By letter dated October 21, 2016 (Reference 3), TVA submitted supplemental information related to Geologic Characterization Information, Surface Deformation, and Stability of Subsurface Materials and Foundation in support of Early Site Permit Application (ESPA) for the CRN Site.

Enclosure 1 to this letter provides supplemental information, including markups of the affected Site Safety Analysis Report (SSAR) sections, related to Vibratory Ground Motion as described in the Enclosure submitted in Reference 2. Enclosure 2 provides additional supplemental information related to SSAR Subsection 2.5.3 and revised ESPA SSAR Figures in Subsection 2.5.1, 2.5.2, 2.5.3 and 2.5.4 provided in Reference 1. These changes will be incorporated into a future revision of the ESPA.

There are no new regulatory commitments associated with this submittal. If any additional information is needed, please contact Dan Stout at (423) 751-7642.

I declare under penalty of perjury that the foregoing is true and correct. Executed on this 28th day of October 2016.

Respectfully,

J. W. Shea
Vice President, Nuclear Licensing

Enclosures:

1. Supplemental Information Related to Vibratory Ground Motion of the Early Site Permit Application for Clinch River Nuclear Site
2. Supplemental Information Related to SSAR Subsection 2.5.3 and Revised SSARFigures of the Early Site Permit Application for Clinch River Nuclear Site

cc (Enclosures):

Project Manager, Division of New Reactor Licensing

cc (without Enclosures):

V. McCree, Executive Director of Operations, USNRC
C. Haney, Regional Administrator, Region II, USNRC
M. Johnson, Deputy Executive Director for Reactor and Preparedness Programs, USNRC
J. Uhle, Director, Office of New Reactors, USNRC
F. Akstulewicz, Director, Division of New Reactor Licensing, USNRC
A. Fetter, Acting Branch Chief, Division of New Reactor Licensing, USNRC
P. Vokoun, Project Manager, Division of New Reactor Licensing, USNRC
T. Dozier, Project Manager, Division of New Reactor Licensing, USNRC
S. Johnson, Deputy Assistant Secretary, Nuclear Technology Demonstration & Deployment, DOE
T. O'Connor, Director, Office of Advanced Reactor Deployment, DOE
T. Beville, SMR Licensing Technical Support Program, DOE
M. Shields, SMR Licensing Technical Support Program, DOE
M. M. McIntosh, Regulatory Specialist, Eastern Regulatory Field Office, Nashville District, USACE

ENCLOSURE 1

SUPPLEMENTAL INFORMATION RELATED TO VIBRATORY GROUND MOTION OF THE EARLY SITE PERMIT APPLICATION FOR CLINCH RIVER NUCLEAR SITE

By letter dated May 12, 2016 (Reference 1), Tennessee Valley Authority (TVA) submitted an application for an early site permit for the Clinch River Nuclear (CRN) Site in Oak Ridge, TN. Subsequent to the submittal of the application, and consistent with interactions with NRC staff, TVA identified certain aspects of the application that it intends to supplement. By letter dated August 11, 2016 (Reference 2), TVA provided a plan for submitting the identified supplemental information.

This enclosure provides supplemental information related to Vibratory Ground Motion to support the NRC staff's review. This enclosure also includes proposed changes to the affected Site Safety Analysis Report (SSAR) sections. These changes will be incorporated into a future revision of the ESPA.

Supplement Item A (from Reference 2)

A. TVA will provide a markup of the applicable ESPA sections to provide the technical bases for key physical parameters used in the site response calculations. Supplemental information will include:

- *Descriptions of the 1D versus 2D site response comparisons and information to justify the use of the 1D site response in the site-specific seismic hazard analysis.*
- *Assumptions and technical justifications used in determining key site-response parameters, such as the shear wave velocity profiles, degradation curves, and their uncertainties.*
- *Information supporting the use of the generalized regional geologic cross-section information for a site-specific seismic hazards analysis, including the deeper velocity structure.*
- *Information supporting the estimated site kappa value used for the site-specific seismic hazards analysis, including an evaluation of uncertainties.*

Supplemental Information

TVA has provided a markup of the applicable ESPA sections to provide the technical bases for key physical parameters used in the site response calculations. Specifically, the SSAR Subsections within 2.5.2.5, "Seismic Wave Transmission Characteristics of the Site," and 2.5.2.6, "2D Sensitivity Analysis," have been replaced in their entirety, and a roadmap of changes is included in this response.

To address the four areas of Supplement Item A, Subsections 2.5.2.5 and 2.5.2.6 have been revised as described below:

- Descriptions of the 1D versus 2D site response comparisons and information to justify the use of the 1D site response in the site-specific seismic hazard analysis.

TVA performed a 2D sensitivity analysis in response to the letter from Nuclear Regulatory Commission (NRC) to TVA, “Pre-Application Readiness Assessment Observations on the Draft Early Site Permit Application for the Clinch River Nuclear Site,“ dated November 19, 2015 (Reference 3). This letter stated: “The application should provide additional justification supporting adequacy of a 1-D approach for the proposed site, including a 2-D sensitivity analysis.” This 2D sensitivity analysis was performed to determine if the dipping strata had any influence on the site response. Consequently, a 1D response analysis, utilizing best estimate profiles, was performed for locations A and B. In addition, a 2D SASSI analysis was performed using best estimate profiles across the top the hardrock foundation where the ground motion is imputed as an outcrop motion. Surfaces responses were then computed at the corners and center for locations A and B at the Clinch River SMR Site, where the mean of the results were compared to a 1D model.

SSAR Subsection 2.5.2.6 has been updated with additional detail from the 2D sensitivity analysis and, in summary, the resulting 2D response for the best-estimate profile properties indicates no significant exceedance of the 1D response. This is due to the site shear wave velocity (V_S) being high for this site and the differences in velocities between rock layers not being significant, reducing the magnitude of the 2D effects at lower frequencies of interest. Therefore, no adjustment of the Ground Motion Response Spectra (GMRS) for 2D effects is required based on the implementation of multiple basecase V_s profiles in the site response analysis and the results of the 2D sensitivity analysis.

- Assumptions and technical justifications used in determining key site-response parameters, such as the shear wave velocity profiles, degradation curves, and their uncertainties.

  SSAR Subsection 2.5.2.5 has been updated to include additional justifications of key site response parameters assumptions from the previously performed analyses.

- Information supporting the use of the generalized regional geologic cross-section information for a site-specific seismic hazards analysis, including the deeper velocity structure.

  SSAR Subsection 2.5.2.5 has been updated to provide additional detail regarding the generalized regional geologic cross section. The generalized regional geologic cross section information was developed by a member of the University of Tennessee faculty with substantial experience researching, developing and authoring papers and reports regarding geologic formations in the Tennessee Valley. The profiles were developed in a structured approach based upon topographic profiles and exploratory activities at TVA dams and nearby nuclear facilities, that resulted in an accurate representation of geologic structures and formations for the CRN Site. In addition, it should be further noted that development of the full geologic cross section was significantly enhanced by insights received from a high quality seismic reflection line, produced for the oil and gas industry, that provided insight into the geometry being projected from the surface as well as the depth to the basement surface and its geometry. The professor has high confidence in the quality and validity of the developed cross sections. However, appropriate epistemic uncertainties were included in the response analysis to account for any minor uncertainties in the geologic profile.

- Information supporting the estimated site kappa value used for the site-specific seismic hazards analysis, including an evaluation of uncertainties.

  The description of the determination of the site kappa has been significantly increased in Subsection 2.5.2.5.2, "Estimation of Kappa." Additional text, tables and figures have been added to Subsection 2.5.2.5.2. based on the work previously performed for the submittal. The determination of site kappa was developed based upon industry information with additional information obtained from nearby strong motion data collected at Tellico Dam.

To incorporate the changes described above, existing Subsections 2.5.2.5 and 2.5.2.6 have been revised. This enclosure includes the proposed changes to the affected SSAR sections. An ESPA Change Request has been initiated to incorporate these changes into a future revision of the ESPA.

Specific revisions to Subsection 2.5.2.5 and 2.5.2.6 include:

- The following existing SSAR Subsections have been revised:

	Subsection	Subsection Title
a.	2.5.2.5	Seismic Wave Transmission Characteristics of the Site
b.	2.5.2.5.1	Basecase Site-Specific Geologic Profiles and Uncertainties (Revised in its entirety and title also changed from Basecase Site Specific Soil Columns and Uncertainties)

- The following existing Subsections have been revised and renumbered:

	Existing Subsection	New Subsection	Subsection Title
a.	2.5.2.5.2	2.5.2.5.4	Capturing Site-Specific Geologic Column Properties, Uncertainties, and Correlations
b.	2.5.2.5.3	2.5.2.5.5	Site Response Analysis
c.	2.5.2.5.3.1	2.5.2.5.5.1	Implementation of Approach 3
d.	2.5.2.5.3.2	2.5.2.5.5.2	RVT-Based Equivalent-Linear Site Response Approach
e.	2.5.2.5.3.3	2.5.2.5.5.3	Horizontal Amplification Factors
f.	2.5.2.5.4	2.5.2.5.6	Development of V/H Ratios
g.	2.5.2.5.5	2.5.2.5.7	Site-Specific Horizontal and Vertical UHRS
h.	2.5.2.6	2.5.2.5.8	Site-Specific GMRS
i.	2.5.2.6.1	2.5.2.6	2D Sensitivity Analysis

- The following Subsections have been added to 2.5.2.5:

	Subsection	Subsection Title
a.	2.5.2.5.1.1	Epistemic Uncertainties in V_S
b.	2.5.2.5.1.2	Unit Weights
c.	2.5.2.5.2	Estimation of Kappa
d.	2.5.2.5.2.1	Tellico Dam Site: Kappa Analog for the CRN Site
e.	2.5.2.5.2.1.1	Tellico Dam Instrumentation
f.	2.5.2.5.2.1.2	Linear Elastic Transfer Function
g.	2.5.2.5.2.1.3	Earthquake Data Recorded at Tellico Dam

h. 2.5.2.5.2.2 Methods Used for the Estimation of Kappa
i. 2.5.2.5.2.2.1 Response Spectral Shape
j. 2.5.2.5.2.2.2 Direct Measurement from the Slope of the FAS
k. 2.5.2.5.2.3 Estimates of Kappa
l. 2.5.2.5.2.3.1 Response Spectral Shape
m. 2.5.2.5.2.3.2 Direct Measurement from the Slope of the FAS
n. 2.5.2.5.2.3.3 Kappa Based on V_S30
o. 2.5.2.5.2.3.4 Summary
p. 2.5.2.5.3 Dynamic Material Nonlinearity
q. 2.5.2.5.3.1 Linear Analyses
r. 2.5.2.5.3.2 Total Effective Kappa

References

1. Letter from TVA to NRC, CNL-16-081, "Application for Early Site Permit for Clinch River Nuclear Site," dated May 12, 2016

2. Letter from TVA to NRC, CNL-16-134, "Schedule for Submittal of Supplemental Information in Support of Early Site Permit Application for Clinch River Nuclear Site," dated August 11, 2016

3. Letter from NRC to TVA, “Pre-Application Readiness Assessment Observations on the Draft Early Site Permit Application for the Clinch River Nuclear Site,“ dated November 19, 2015

SSAR Subsection 2.5.2.5 is revised as indicated: (Note - deletions are shown as "~~strike-through~~" text and additions are shown as "<u>underlined</u>" text.)

2.5.2.5 Seismic Wave Transmission Characteristics of the Site

This subsection describes the development of the site amplification factors that results from the transmission of the seismic waves through the site-specific geologic profile above the hard rock, which consists of various dipping rock formations as described in Subsections 2.5.4.2 and 2.5.4.7. The site amplification factors are used in determination of the UHRS and the GMRS for the site. ~~It is noted that the potential effects of increased confining pressure due to overburden on the GMRS have not been captured in the depth-dependent cyclic strain dependencies characterizing the unweathered firm to hard rock site profile. With the lowest and shallowest shear-wave velocities ranging from about 2000 to 3000 ft/s combined with depth dependent nonlinear properties, increased confining pressure, slightly changing the depth dependencies of the nonlinear dynamic properties, was expected to have a minimal effect on the GRMS. The overburden effects were addressed through sensitivity analyses (Subsection 2.5.2.6) based on an estimate of an expected overburden depth of 42 ft. As indicated in Subsection 2.5.2.6, the effects of increased confining pressure due to overburden material on the firm to hard rock nonlinear properties are insignificant.~~

Due to the dipping stratigraphy beneath the CRN Site (about 33 degrees) potential two-dimensional (2D) effects on ground motions were evaluated using an expanded version of the computer code SASSI (System for Analysis of Soil Structure Interaction). The 2D effects were addressed through a sensitivity analysis (Subsection 2.5.2.6~~.1~~).

A geologic cross-section at the site that illustrates the depth to Precambrian rock, drawn perpendicular to the strike direction, is shown on Figure 2.5.1-63. Planned surface grade at the site is at Elevation 821 ft. The planned bottom of the foundation for Reactor Service Buildings (RSB) is taken at Elevation 683 ft. The top of competent rock varies across the areas of Locations A and B as shown on Figure 2.5.4-2. Based on the data to the top of unweathered rock from the suspension data, competent rock ranges from about Elevation 749 to 770 ft at Location A and Elevation 738 to 758 ft at Location B. Given that no specific technology has been selected, the elevation of the GMRS is chosen to be Elevation 683 ft corresponding to the bottom of the RSB foundations below the top of unweathered rock. All elevations cited in this subsection are based on the North American Vertical Datum of 1988 (NAVD88).

Recognizing the assessment of epistemic uncertainty must necessarily reflect a significant degree of judgment and the range in basecase shear-wave velocities (<u>V_S</u>) at CRN Site must necessarily accommodate two separate aspects of the site conditions. For the depth ranges for which measured velocities were available, the dipping structure (Figure 2.5.4-13) results in the same unit and associated dynamic material properties occurring at different depths across each site footprint.

Providing impedance contrasts are relatively small, broad-band resonance effects due to the dipping structure, such as a basin edge, are not expected to significantly exceed (Reference 2.5.2-169) one-dimensional (1D) resonances, particularly if they are broadened through the use of multiple basecases. Extending epistemic uncertainty through the shallow portion of the profile (approximately 300 ft) where sufficient measurements exist to constrain a single basecase profile was considered essential to accommodate the potential effects of the shallow dipping structure.

For the deeper structure (Knox Group and below, Figure 2.5.4-13) uncertainty in V_S exists due principally to the limited site-specific measurements. Below the Knox group, 2D effects are expected to be less than the shallower structure, particularly at frequencies of interest (greater than 0.5 Hz), due to the smaller impedance contrasts and the shallowing of the dip and more uneven nature of the very deep structure (Figure 2.5.4-13). As a result the same relative factor expressing epistemic uncertainty was used for both the shallow structure with direct measurements as well as the deep structure lacking site-specific velocity measurements.

The hard rock UHRS described in Subsection 2.5.2.4 defines the seismic motion on the hard rock. Hard rock is characterized with a minimum ~~shear wave velocity (V_S)~~of 2800 m/s (9200 ft/s). While the profiles for 1D site response analysis could have been truncated at shallower depths and placed on top of the full midcontinent crustal model with little effect at high-frequency, to consider the minimum depth at which the ~~shear wave velocity~~V_S exceeds 9200 ft/s in all deeper strata and to accommodate amplification to at least the lowest frequency defined by the hard rock hazard (0.5 Hz), the profiles are truncated at depths of 12,644 ft and 12,601 ft for Locations A and B, respectively.

2.5.2.5.1 Basecase Site-Specific ~~Soil Columns~~ Geologic Profiles and Uncertainties

V_S basecase profiles were developed for Locations A and B at the CRN site (Figure 2.5.4-11) down to Precambrian basement rock. Although a thick layer of hard rock (Chickamauga and Knox Groups and Maynardville limestone) underlies the site to a depth of more than 1 km, there are layers of lower velocity rock (Conasauga shale and Pumpkin Valley shale) at greater depth beneath CRN Site extending nearly to basement rock (Figures 2.5.4-12 and 2.5.4-13). The data consisted of primarily V_S profiles from OYO suspension logging as described in Subsection 2.5.4.4. OYO suspension data from similar lithologies as at CRN collected at several TVA dams were also reviewed in addition to spectral-analysis-of-surface-wave (SASW) data collected at WBN2 by the University of Texas at Austin (Reference 2.5.2-172).

Geologic profiles were estimated based on the stratigraphic cross-section C-C' for the shallow units above the Knox Group as shown on Figure 2.5.4-12 and the cross-section developed by Hatcher (Reference 2.5.2-173) for the Knox Group and deeper units (Figure 2.5.4-13). With the stratigraphy dipping to the southeast, geologic profiles were developed at the northwest and southeast boundaries of both Locations A and B to assess the variability across the locations.

Based upon a review of the geologic profiles of Locations A and B, a single best-estimate (mean) basecase V_S profile was developed for each area. The epistemic uncertainty in the mean basecase profile was addressed by developing lower-range and upper-range basecase profiles. The aleatory variability across the locations was addressed through the profile randomization used in the site response analysis. A compilation of all the V_S profiles that were computed for each area provided a lognormal mean profile (Figures 2.5.4-14 and 2.5.4-15). The profiles utilized are indicated on Figures 2.5.4-14 and 2.5.4-15, those that were contained or just outside the locations (within 100 ft) as shown on Figures 2.5.4-11 and 2.5.4-12. The variation in the V_S profiles was approximately ± 20 percent about the mean (Figures 2.5.4-14 and 2.5.4-15). The V_S above unweathered rock was not included in the best-estimate profiles. The top of unweathered (competent) rock corresponds to the elevation of the GMRS. Table 2.5.4-3 provides the top of unweathered rock in each borehole. The top of unweathered rock in each profile was normalized to zero depth. The lognormal mean profiles are used to develop the shallow portion of the basecase profile. The lognormal mean profiles extend to depths of about 300 ft and 350 ft for Locations A and B, respectively. Note that the lognormal mean profiles were only used to depths where there were at least two Vs profiles.

At depths below the shallow lognormal Vs profiles where there are no measured V_S data in the two locations, the geologic profiles shown in Figures 2.5.4-16 and 2.5.4-17 were used to extend the profiles. An average velocity was assigned to each geological unit down to and including the uppermost unit of the Knox Formation (Newala unit) based on the mean V_S shown in Table 2.5.4-16. Examination of the V_S profiles for each unit showed generally constant V_S with depth, thereby a single mean V_S value for each unit was utilized. The lower and upper range basecase profiles will account for the epistemic uncertainty in the mean basecase profile. The mean V_S adopted for the Newala unit was used for the rest of the Knox unit (rounded up to 11,000 ft/sec) due to their similar lithologies. Figures 2.5.4-16 to 2.5.4-17 show the two V_S profiles down to the Newala unit.

Beneath the Knox unit, there are no data for the deeper units at the CRN site, which include the Conasauga shale, Rome Formation sandstone, and Pumpkin Valley shale. These units repeat themselves with depth because of the overthrusting (Figure 2.5.4-13). V_S data were available for all three formations from the deep SASW surveys that were performed at WBN2 (Reference 2.5.2-172). At a depth of 500 ft, the Conasauga shale and Pumpkin Valley shale have measured V_S values of 6,000 ft/sec and 6,000 to 7,000 ft/sec, respectively at WBN2. The Rome sandstone had measured values of 9,000 to 10,000 ft/sec at a depth of 1,500 ft (Reference 2.5.2-172). An unconfined free-free resonant column (URC) test also measured a Vs of almost 9,000 ft/sec for a sample of Rome Formation (Reference 2.5.2-172, Appendix B). Although these V_S values are not site-specific, they likely are representative of the V_S for these units beneath the CRN Site at depths below the OYO surveys based on regional stratigraphic relationships.

To estimate the V_S of the units below depths of 500 to 1500 ft, a review was performed of the deep V_S profiles available in the literature that went down several kilometers. Based on the review, the generic V_S profile for CEUS hard rock developed by Boore and Joyner (Reference 2.5.2-174) was selected. No region-specific V_S profile information was available. Examination of the central and eastern U.S. V_S database compiled by PE&A support the use of the Boore and Joyner (Reference 2.5.2-174) generic profile. The generic profile was anchored to the value of 6,000 ft/sec at a depth of 500 ft for the Conasauga shale and 9,000 ft/sec at a depth of 1,500 ft for the Rome Formation and the Pumpkin Valley shale (Figure 2.5.4-13). The adjusted Boore and Joyner (Reference 2.5.2-174) generic profiles were then used to estimate the V_S for the deeper units (Figures 2.5.4-18 and 2.5.4-19). Once Precambrian rock was reached, the V_S profiles were truncated at a V_S of 11,000 ft/sec.

For the site response analysis, the shallow suspension logging-measured portion of the V_S profiles were smoothed to produce the mean basecase profiles. The lognormal mean V_S profiles (Figures 2.5.4-14 and 2.5.4-15) were converted to a layered model with uniform velocities by preserving the travel time in each layer. Figures 2.5.4-18 and 2.5.4-19 show the final V_S profiles for Locations A and B (Tables 2.5.4-30 and 2.5.4-31).

2.5.2.5.1.1 Epistemic Uncertainties in V_S

To address the epistemic uncertainty in the mean basecase profile, the uncertainties in the 25 V_S profiles measured within the CRN Site and at 18 TVA damsites (measured by Geovision Geophysical Services) were examined through a statistical analysis that looked at several aspects of the data. For the TVA dam V_S profiles, the material above rock (embankment material, alluvium, etc.) was removed and not considered in the statistical analysis. All V_S profiles were smoothed prior to performing the statistical analysis. First, the V_S profiles for each of the subunits of the CRN Chickamauga Group were compiled and the sigmas and coefficient of variations (COVs) were computed (Figures 2.5.2-92 and 2.5.2-93). The right side of the figures show the number of profiles used to compute the statistics. The actual depths of the

subunits were preserved. The sigmas and COVs average are relatively small and are fairly uniform with depth at about 0.08 and reflect within unit differences. In a similar fashion, the CRN Chickamauga Group was divided up by general rock type (dolomite, limestone, and siltstone) and Figures 2.5.2-94 and 2.5.2-95 show the trends. For the subunits that were a mix of dolomite and limestone, the dominant rock types were used. The dolomite and limestone showed smaller sigma and COVs than the shale (Figures 2.5.2-94 and 2.5.2-95). Finally, the sigma and COV were computed for the CRN and TVA damsite V_S profiles (Figures 2.5.2-96 and 2.5.2-97). The sigma and COV average about 0.15 and 0.30, respectively, from 50 to 200 ft where there were a sufficient number of profiles. Not surprisingly, the sigma and COV were higher for the TVA dams because they were located on a wider range of geology covering three Appalachian states compared to the CRN profiles.

Using these results as well as the sigma across units at the CRN Site in Figure 2.5.2-96 to inform judgment in developing depth-independent epistemic uncertainty, a standard deviation of 0.15 was selected to accommodate potential 2D effects in the top 300 ft where 2D effects may be expected to be the strongest in the shallow strata but still minor, as well as lack of site-specific measurements below a depth of about 300 ft. Considering a three-point approximation to the distribution weights of 0.2, 0.6, and 0.2 for lower (P2)-, middle (P1)-, and upper (P3)-range estimates results in a velocity scale factor of approximately 1.25, a ± 25% variation about the mean (best estimate) basecase. The resulting base-case (P1) as well as lower-range (P2) and upper-range (P3) basecases are illustrated in Figure 2.5.4-20 and 2.5.4-21 for Locations A and B, respectively. The resulting range in V_S from the lower- to upper- base-cases is about 1.6 and well within the range for such materials (Reference 2.5.2-208), acknowledging a portion of the range was taken to accommodate the dipping structure.

Basecase profiles (P1) for Locations A and B, illustrated in Figures 2.5.4-20 and 2.5.4-21, reflect high V_S throughout, particularly within the Knox Group and below. The limestones as well as some of the shales exceed at depth the V_S (2.83 km/sec) of the top layer of the generic Midcontinent crustal model (Subsection 2.5.2.5.5). As a result, to accommodate a more realistic crustal profile, the roughly 12,000 ft (3.6 km) of the CRN Site profile was taken to replace the top layer of the Midcontinent crust, with the second layer at a V_S of 3.52 km/sec (11,550 ft/sec) assumed to effectively reflect basement conditions (Figure 2.5.4-13). The assumed basement condition is depicted in Figures 2.5.4-20 and 2.5.4-21as the deepest layer. The upper-range base-case profiles (P3) within the Knox Group and Rome and Pumpkin Valley Units were truncated at the assumed basement V_S of 3.52 km/sec.

2.5.2.5.1.2 Unit Weights

The unit weights for the rock units above the Newala Formation (Mascot and Kingsport the top two undifferentiated formations of the Knox Group) were taken from Table 2.5.4-21. It was assumed that the Newala and the deeper portions of the Knox Group had the same unit weight of 168 pcf (Figure 2.5.4-13). Ken Stokoe (Reference 2.5.2-172) measured unit weights for the Rome, Pumpkin Valley and Conasauga of 167.5, 167.4, and 166.8 pcf, respectively, for several core samples taken at shallow depths (< 200 ft). We considered these unit weights to be minimums given their shallow depths and relied on their V_S and the values given in Table 2.5.4-21 to estimate units weights for the Rome/Pumpkin Valley and Conasauga Formations (Table 2.5.2-30). Unit weights were converted to densities by dividing by 62.4. Densities play only a minor role in site-specific amplification (Reference 2.5.2-139).

2.5.2.5.2 Estimation of Kappa

For typical rock and deep soil sites that display an overall increase in stiffness with depth due primarily to increasing confining pressure, kappa reflects the major contribution to seismic

energy dissipation through both intrinsic energy absorption as well as wave scattering that occurs over the top several kilometers of the crust at close rupture distances (< about 50 km) (Reference 2.5.2-175); (Reference 2.5.2-176)). This observation was first recognized and subsequently characterized as a site parameter by Anderson and Hough (Reference 2.5.2-175), specifically as kappa at zero epicentral distance. At sites that reflect significant departures from an overall increase in stiffness with depth due to geology, such as layered basalt and sedimentary soil or rock sequences, significant contributions to kappa may occur at depths well beyond 1 to 2 km This damping appears to be largely frequency-independent (hysteretic), occurs at low strains, and is the principal site or path parameter controlling the limitation of high-frequency (> 5 Hz) strong ground motion at close-in sites (≤ 50 km). As a result, its value or range of values is important in characterizing strong ground motions for engineering design, particularly in regions of sparse seismicity. Additionally, small local or regional earthquakes may be used to estimate its value or range in values because it is generally independent of the level of motion at rock or very stiff sites. As such kappa measures the cumulative low-strain damping over the top several kilometers of the crust and clearly defined as the amplitude decay of seismic waves (Reference 2.5.2-155) rather than intrinsic damping which is a dynamic material property. This distinction is particularly relevant to site response as the "effective damping" (Reference 2.5.2-155) controls non-geometric frequency-independent energy loss and has contributions from both intrinsic damping as well as other mechanisms such as wave scattering. Because kappa reflects an observational parameter incorporating the above effects, it was used to constrain the total effective damping (Campbell, 2009) (Reference 2.5.2-155) throughout the CRN profile.

In this study, two methods were used to estimate kappa for use in the site response analysis of the CRN site. They are: 1) evaluation of peak frequency and shape of normalized acceleration response spectrum (5% damped PSA/PGA) (Reference 2.5.2-176); (Reference 2.5.2-142); (Reference 2.5.2-177)) and 2) direct measurement of the high-frequency decay of the S-wave Fourier amplitude spectrum (FAS) (Reference 2.5.2-175).

The Tellico Dam site area is an analog to the CRN site that has soft weathered rock overlying a thick sequence of Paleozoic rocks over crystalline basement. At this site, estimation of the damping in the Paleozoic sequence, a significant contributor to kappa, is important to assessing appropriate levels of high-frequency design motions.

2.5.2.5.2.1 Tellico Dam Site: Kappa Analog for the CRN Site

A strong motion recording site is located near Tellico Dam at 35.778^{o} N, 84.261^{o} W (Figure 2.5.2-98). The CRN Site is located only 10 miles (16.7 km) northwest of Tellico Dam. The geologic structure at the Tellico Dam site is shown in Figure 2.5.2-99. For comparison, the geologic structure at CRN is shown in Figure 2.5.4-13. Both of these sites are located in the Valley and Ridge physiographic province of the southern Appalachians. The Tellico Dam site is located on southeastward-dipping Paleozoic rocks of middle Ordovician age which correspond to sedimentary rocks of the same age and orientation at the CRN Site (Figure 2.5.2-99). Because the Tellico site is somewhat farther to the east than the CRN Site, the middle Ordovician rocks at Tellico are somewhat thicker and tend to have a higher percentage of clastic components. Both sites are believed to be underlain by Paleozoic sedimentary rock units of lower Cambrian to middle Ordovician age. Specifically, the Rome Formation and the Conasauga, Knox and Chickamauga Group rocks are believed to be present under both sites.

An OYO P-S suspension log has been completed at the Tellico Dam strong motion site down to a depth of 56.7 m (186 ft) (Figure 2.5.2-100). With the exception of a relatively thin layer of soil and weathered rock near the surface (about 6.1 m, 20 ft), the suspension logging results indicate intact rock with consistently high V_S of about 2,700 m/sec (9,000 ft/sec). Based on core

log descriptions and projection of the rock units measured along strike at Tellico and Fort Loudoun Dams, the rock measured in the suspension logging borehole at Tellico Dam is assigned to a lower member of the middle Ordovician age Ottosee Formation.

The geologic structure beneath the Tellico Dam site is similar in style to that of the CRN Site (Figures 2.5.2-99 and 2.5.4-13); however, the geologic structure at Tellico Dam is somewhat simpler because only two major thrust sheets are shown under the Tellico Dam site. In contrast, the CRN Site is believed to be underlain by four significant thrust faults (Figure 2.5.4-13). Hatcher et al. (Reference 2.5.2-178) interprets a gradual deepening of the top of basement rock from northwest to southeast through eastern Tennessee and, therefore, the depth to basement is somewhat deeper at Tellico (~4420 m [14,500 ft]) than at the CRN Site (~3690 m [12,100 ft]). The average V_S of the rocks from the surface to the interpreted top of basement at Tellico Dam (~2865 m/sec [~9,400 ft/sec]) is essentially identical to the average V_S estimated at the CRN Site. However, the sedimentary sequence underlying the CRN Site (Figure 2.5.4-13) has significantly more lower velocity shale than exists below the Tellico Dam site, whereas there is more high velocity limestone at the Tellico Dam site (Figure 2.5.2-99). The increased proportion of lower velocity shales would suggest an increased kappa value for CRN compared to Tellico Dam, providing the shales represent a significant contribution to the total effective kappa.

In summary, the geologic setting and expected dynamic response at Tellico Dam and the CRN Site are similar with differences mostly related to the depth of basement, extent of structural complexity beneath the two sites, and more shales beneath the CRN Site. Hence it was assumed in these analyses that kappa estimates at the Tellico Dam site may be used as a conservative estimate (analog) for kappa at the CRN Site due to proximity and similar geologic and V_S structure beneath the two sites.

2.5.2.5.2.1.1 Tellico Dam Instrumentation

The Tellico Dam site is instrumented with a Kinemetrics K2 (Serial Number 2229) that has recorded several small, local earthquakes. The accelerograph recordings have a sampling rate of 200 sps with a high-frequency limit of 80 Hz defined by the frequency response of the K2 instrument from DC to 80 Hz. The high frequency limit is controlled by the low-pass anti-alias filter with a steep rolloff (120 dB down at 100 Hz Nyquist frequency) . The recorder is mounted on a concrete pad that is within about 3 m (10 ft) of top of rock.

2.5.2.5.2.1.2 Linear Elastic Transfer Function

Figure 2.5.2-101 shows the smoothed and interpreted V_S at the site based on the OYO suspension logging. The top 6.1 m (20 ft) of soil and weathered rock is represented as a single layer with a V_S of 1,524 m/s (5,000 fps) overlying hard rock with a V_S of 2,830 m/s (9,285 fps).

The presence of the relatively thin layer of shallow soil and weathered rock over hard rock was expected to dominate and distort the high-frequency amplification, resulting in a biased estimate of kappa (Reference 2.5.2-179). To correct for the presence of high-frequency distortion, amplification from the shallow crustal profile was estimated from the interpreted V_S profile (Figure 2.5.2-101) from source depth to the surface. The relatively high V_s and depths in the structure beneath the shallow soil and weathered rock, which reflect low-frequency resonances (Figure 2.5.2-99), was not expected to affect estimates of kappa (Subsection 2.5.2.5.4). The smoothed linear (damping 0.01%) transfer function as implemented (Subsection 2.5.2.5.2.3.1) is shown in Figure 2.5.2-102 and is dominated by a high-frequency (near 60 Hz) resonance caused by the 6.1m (20 ft) soil and weathered rock layer over the hard rock layer. The peak amplification is around a factor of 2.5.

2.5.2.5.2.1.3 Earthquake Data Recorded at Tellico Dam

In total the dataset included 59 recordings from 2004 to 2008. A subset of these events that had been identified as earthquakes and had estimates of both magnitude and location were selected for processing. A further subset of the processed earthquake data with deep (≥ 5 km) hypocenters were selected for analysis based on a comparison of signal verses noise level (Table 2.5.2-31). The hypocentral depth criterion was implemented to both fully sample the Paleozoic sedimentary rocks and to avoid possible double paths in the Paleozoic section for downgoing paths at distant sites. Table 2.5.2-31 lists the magnitudes, hypocentral depths, and distances for the twenty selected earthquakes.

Data processing for the Tellico Dam time series generally followed the NGA-West2 process as described in Reference 2.5.2-180. The main differences are the selection of several windows for the calculation of Fourier amplitude spectra, including the S-wave window used for kappa estimation (Reference 2.5.2-181).

2.5.2.5.2.2 Methods Used for the Estimation of Kappa

The methods used to estimate kappa were: 1) evaluation of the peak frequency and shape of normalized acceleration response spectra (Reference 2.5.2-176); (Reference 2.5.2-142); (Reference 2.5.2-179)) and 2) direct measurement of the high-frequency decay of the S-wave FAS (Reference 2.5.2-175). Ktenidou et al. (Reference 2.5.2-179) provide a summary of these and additional methods to estimate kappa at a site.

Each method made use of either 5%-damped acceleration response spectrum or FAS from the recordings at Tellico Dam (Table 2.5.2-31). Magnitude, distance and bandwidth were considered when selecting data appropriate for each method from Table 2.5.2-31. For example, robust estimates of the average response spectral shape require averaging data from earthquakes with similar magnitude and distance.

2.5.2.5.2.2.1 Response Spectral Shape

The approach of using response spectral shapes (5%-damped PSA/PGA) computed from recordings made at rock sites at close distances to estimate kappa was developed in (Reference 2.5.2-176) and (Reference 2.5.2-142). Differences in response spectral content or shape at sites are significant and may be interpreted as primarily resulting from differences in the V_S (amplification) and damping (kappa) beneath the site along with crustal Q(f), especially at larger distances (> about 20 km for small M)(Reference 2.5.2-182); (Reference 2.5.2-183); (Reference 2.5.2-184); (Reference 2.5.2-176)). To approximately accommodate the effects of the K2 antialias filter in the response spectral shapes, a low-pass filter with a 7-pole rolloff was included in the model calculation. Figure 2.5.2-103 shows an example of response spectral shapes calculated with the point-source model (Reference 2.5.2-156); (Reference 2.5.2-142)) at a rock site for **M** 2 at a hypocentral distance of 20 km and unity amplification. The magnitude and distance were selected to be similar to the processed earthquake data at Tellico Dam used for the kappa analyses (Table 2.5.2-31). In this example, kappa was varied by a factor of 2 from 0.005, 0.010 to 0.020s (Figure 2.5.2-103). The peak frequency and shape of the response spectra clearly shift to lower frequency as kappa increases.

Spectral shapes also show a strong magnitude dependence with smaller earthquakes (Figure 2.5.2-103) having a narrower bandwidth and higher frequency peaks than larger earthquakes (Figure 2.5.2-104). This is a consequence of lower corner frequencies for smaller magnitude earthquakes (Reference 2.5.2-156); (Reference 2.5.2-184); (Reference 2.5.2-185); (Reference 2.5.2-176)). Spectral shapes from multiple recordings at similar distances and magnitudes are

averaged to reduce the frequency-to-frequency variability and provide additional stability in kappa estimates (Reference 2.5.2-184); (Reference 2.5.2-176)). These factors allow estimates of kappa to be made from response spectral shapes by visual comparison with spectrum computed using the point-source model (Reference 2.5.2-156), as validated in Reference 2.5.2-142.

2.5.2.5.2.2.2 Direct Measurement from the Slope of the FAS

Direct measurement of the high-frequency decay of the slope of the FAS computed for the S-wave portion of the recorded ground motion was proposed by Anderson and Hough (Reference 2.5.2-175). This original method to estimate kappa was first used on the as-recorded FAS of the S-wave portion of the ground motion. In these analyses, additional estimates of kappa are made on FAS that have been corrected for either crustal attenuation (Q[f]) or crustal amplification, or both. These additional estimates were used to ascertain the uncertainty (range) in the estimate of kappa.

2.5.2.5.2.3 Estimates of Kappa

The results from the two methods used to provide estimates of kappa at Tellico Dam for application to the CRN Site are presented in the following sections.

2.5.2.5.2.3.1 Response Spectral Shape

The analyses of response spectral shape for kappa are shown in Figures 2.5.4-22 through 2.5.4-25. On each figure, three curves show the average, maximum and minimum of the recorded 5% damped acceleration response spectral shape for several earthquakes with similar magnitude and hypocentral distance (Table 2.5.2-31). The fourth curve shows the point-source model fit to these data resulting from a best estimate for kappa.

The magnitude and distance parameters for the point-source model were taken as the average from the recorded data at Tellico Dam. The linear-elastic crustal transfer function used in the model has been discussed in Subsection 2.5.2.5.2.1.2. The attenuation model used $Q(f) = 630\ f^{0.5}$, was developed from the inversion of FAS by Darragh et al. (Reference 2.5.2-186) using 1133 recordings from 53 earthquakes recorded at 241 unique sites in central and eastern North America. As such the Q(f) model is appropriate for the CEUS and assumed consistent with those reflected in the ground motion prediction equations (GMPEs) used for developing the hard rock hazard.

Figure 2.5.4-22 shows the average, maximum, and minimum of the recorded 5%-damped acceleration response spectral shapes computed for three earthquakes with magnitude between **M** 0.9 and **M** 1.3 and hypocentral distances between 17.6 and 24.5 km (Table 2.5.2-31). A kappa of 0.009s in the point-source model provided the best fit with an average **M** of 1.1 and average hypocentral distance of 20 km. In general, the overall fit is good over a wide bandwidth with particular emphasis on the frequency of the peak. At lower frequencies (about 30 Hz and below) there is evidence of deeper amplification not accommodated in the simple shallow V_S profile (Figure 2.5.2-101).

Figure 2.5.4-23 shows the average, maximum, and minimum of the recorded 5%-damped acceleration response spectral shapes computed for seven earthquakes with magnitude between **M** 0.9 and **M** 1.6 and hypocentral distance between 16.4 and 24.5 km (Table 2.5.2-31). In this case four slightly larger earthquakes were added to the previous case, illustrating both the stability of the peak frequency (kappa) but also showing increased excitation of lower frequency amplification. As in Figure 2.5.4-22, the best fit kappa was 0.009s and the point-

source model used an average **M** of 1.3, and an average hypocentral distance of 20 km. Also the inclusion of the additional larger magnitude earthquakes broadens the peak as expected (Figure 2.5.2-103) and slightly improves the fit of the point-source model to the data.

Figure 2.5.4-24 shows the average, maximum, and minimum of the recorded 5% damped acceleration response spectral shapes computed for seven earthquakes with magnitude between **M** 1.4 and **M** 2.2 and hypocentral distance between 15.3 and 28.1 km (Table 2.5.2-31, note the **M** 2.1 earthquake at 37.6 km was not included due to significantly greater distance than the average). Average values of **M** 1.7 and hypocentral distance of 19 km were used in the point-source model. Figure 2.5.2-24 includes larger magnitudes than in Figure 2.5.4-23. In this case, a lower kappa estimate of 0.006s provided a better fit around the peak frequency than the 0.009s for the smaller magnitude earthquakes (Figures 2.5.4-22 and 2.5.4-23). Additionally, the larger magnitudes with higher source amplitudes at lower frequency result in larger motions at the site for frequencies below about 30 Hz. As was indicated with Figure 2.5.4-22, this effect may be due to un-modeled amplification at depth and/or too low of a magnitude assigned by the network (Table 2.5.2-31).

Figure 2.5.4-25 shows the average, maximum, and minimum of the recorded 5%-damped acceleration response spectral shapes computed for six earthquakes with magnitude between **M** 2.4 and **M** 3.2 and hypocentral distance between 33.2 and 54.2 km. The point-source model used an average **M** 2.8 and an average hypocentral distance of 43 km. This Figure includes both larger magnitudes and greater distances than in the other figures. As with the previous suite of earthquakes (Figure 2.5.4-24), these larger magnitude shapes reflect the lower kappa estimate with a best fit estimate of about 0.006s.

The response spectral shape analyses reflected analyses of 14 sets of recordings at the Tellico Dam recording site over the magnitude and hypocentral distance ranges of **M** 0.9 to **M** 3.2 and 15.3 to 54.2 km, respectively (Tables 2.5.2-31 and 2.5.4-32). The spectral shape analyses assumed a Q(f) model, based on inversions of central and eastern North America recordings, and a site-specific amplification factor based on a shallow suspension log survey. Based on these analyses, the best fit kappa values were 0.006s and 0.009s and are summarized on Table 2.5.2-32.

In all the comparisons with spectral shapes between recorded motions and model predictions, the model predicts the location and width of the peak well but consistently underpredicts the amplitude. This general underprediction is likely the result of too low a peak in the amplification factor (Figure 2.5.2-102) suggesting too much smoothing and/or too small of an impedance contrast in the shallow profile (Figure 2.5.2-101). Since the amplification of the peak is not strongly affected by kappa (Figures 2.5.2-103 and 2.5.2-104), the mismatch of the peak amplitude is not considered a significant issue.

2.5.2.5.2.3.2 Direct Measurement from the Slope of the FAS

The Anderson and Hough (Reference 2.5.2-175) method to estimate kappa was used on the as-recorded S-wave FAS for the 20 Tellico Dam earthquakes (Tables 2.5.2-31 and 2.5.4-32). In these analyses, the vector average (orientation independent) of the FAS was used. The vector average was also corrected for crustal amplification (Subsection 2.5.2.5.2.1.2) in order to avoid the site amplification from affecting kappa estimation (i.e., by distorting the slope of the spectrum). To avoid fitting the distant dependent kappa to estimate κ_0 at zero distance, the FAS were corrected for crustal Q(f) (Reference 2.5.2-176). The identical Q(f) model used for the response spectral shapes 630 $f^{0.5}$ (Reference 2.5.2-186) was used for the FAS correction to yield κ_0 directly from the slope of the FAS.

The main steps in applying this method have been summarized in Kishida et al. (Reference 2.5.2-187). The main considerations include using:

1) Frequencies above the earthquake source corner frequency,

2) Frequencies below the instrument anti-alias filter (high frequency limit of 80 Hz) for the Tellico Dam instrument (Subsection 2.5.2.5.2.1.1),

3) Frequencies with an acceptable signal to noise ratio (SNR) (greater than about 3). Table 2.5.2-31 lists the low-frequency limit where the SNR fell below 3 on either horizontal component while the high-frequency limit was 80 Hz for all the recordings,

4) An adequate frequency bandwidth (6 Hz or greater) to estimate the slope. This requirement led to the exclusion of several entries [denoted by (b) and (c)] in Table 2.5.4-32 from further analyses. The earthquake on 23 December 2004 was only recorded on a single horizontal component (Table 2.5.2-31) and this instrument at Tellico Dam was replaced before the next recording in March 2006. Also, the estimate of kappa from the single horizontal component is significantly larger than the other kappa estimates (Table 2.5.4-32). For these reasons this recording was also excluded from further analyses [denoted by (a) in Table 2.5.4-32].

5) Frequencies away from any strong site resonance (near 60 Hz) as discussed in Subsection 2.5.2.5.2.1.2 (Figure 2.5.2-102). Examination of each spectrum was conducted and the bandwidth (Table 2.5.4-32) was selected to ensure that the resonance was not significantly affecting the linear portion of the spectrum where the slope was estimated.

Following these considerations, the spectra were smoothed with a triangular window using a 2.0 Hz bandwidth. Kappa was then estimated from as the straight-line over the bandwidth where attenuation is controlling the spectrum (Reference 2.5.2-175). The bandwidth was subjectively chosen on visual inspection of the smoothed spectrum. The lower limit was chosen to be above the resonance peak (near 60 Hz) and/or an estimate of the corner frequency of the source spectrum. The upper limit was selected where a change in slope indicated that noise is dominant, with an upper limit of 80 Hz set from the characteristics of the instrumentation at the Tellico Dam site. Once the frequency bandwidth (Table 2.5.4-32) was selected, the unsmoothed spectrum was subjected to a least-square fit routine which produced estimates of kappa as well as standard errors. The unsmoothed spectra were used in the fitting process, since the standard error would vary with the bandwidth chosen for smoothing.

To examine the FAS, Figure 2.5.2-105 shows the as-recorded vector sum FAS along with the spectra corrected for both Q(f) ($630\ f^{0.5}$) as well as shallow amplification (Figure 2.5.2-102). The FAS clearly shows the stable effects of the shallow structure with resonance near 60 Hz. For these small earthquakes with high corner frequencies, the FAS increases with increasing frequency with source corner frequencies likely exceeding 30 to 40 Hz in many cases. At lower frequencies there do not appear to be stable broadband resonances that may be expected from dipping structures such as basin edges (Reference 2.5.2-169). Figure 2.5.2-99 shows steeply dipping beds of sedimentary rock extending up to about 9,000 ft beneath the instrument. Provided the dipping interfaces are continuous with depth and of sufficient impedance contrast, such as basin edges, broadband resonances at low frequency (≤ 10 Hz) may be expected from such structures. In this case, stable broadband resonances do not appear to be present in the

recordings suggesting impedance contrasts between the dipping structures may not be large enough to generate significant 2D effects (Reference 2.5.2-169).

The least-squares fits (Reference 2.5.2-188) to the twelve earthquakes meeting the criteria outlined in Subsection 2.5.2.5.2.3.2 are shown in Figure Set 2.5.2-106. The spectra shown reflect vector average (orientation independent) FAS with the fits shown over the frequency range judged to reflect where the FAS is controlled by kappa (Table 2.5.4-32). On these plots the FAS has been smoothed with a 1.0 Hz window so that the linear fit at high frequencies (kappa) can be seen. The slope method of estimating kappa, as with spectral shapes, is associated with uncertainty and judgement, particularly for small magnitude earthquakes and low kappa values (Figure Set 2.5.2-106) (Reference 2.5.2-176); (Reference 2.5.2-141); (Reference 2.5.2-177); (Reference 2.5.2-179)).

Using the base case Q(f) correction, 630 $f^{0.5}$ (Reference 2.5.2-186) and the shallow amplification factors (Figure 2.5.2-102) the best estimate of kappa was a median 0.0098s with an aleatory variability of σ_{ln} = 0.8 over the 12 earthquakes listed in Table 2.5.4-32. For comparison, including the five earthquakes with limited bandwidth (but excluding the two earthquakes with negative kappa estimates) increases the estimate slightly to 0.011s , σ_{ln} = 0.5.

As a refinement, small earthquakes with **M** < 1.6 were excluded from additional analyses due to concerns about estimating kappa below the source corner frequency (consideration 1, above). Again using the base case Q(f) correction, 630 $f^{0.5}$ (Reference 2.5.2-186) and the shallow amplification factors (Figure 2.5.2-102), the best estimate of kappa was a median of 0.0095s with an aleatory variability of σ_{ln} = 0.8 over these 8 earthquakes (Table 2.5.4-32).

To provide an estimate of epistemic uncertainty in kappa, additional slope analyses were performed for the alternative Q(f) model (410 $f^{0.5)}$, (Reference 2.5.2-189)) as well as with and without the shallow amplification (Figure 2.5.2-102). The results are tabulated in Table 2.5.4-32 and show a general bimodal distribution at about 0.010s and 0.016s depending primarily on the presence or absence of shallow amplification. The range in kappa is also from about 0.010s to 0.016s from the 8 larger magnitude earthquakes that range from **M** 1.8 to **M** 3.0 (Table 2.5.4-32).

Certainly a limitation in the FAS slope analyses is the narrow bandwidth over which kappa was assumed to control the FAS. The narrow bandwidth is a consequence of the low magnitudes, shallow amplification, and anti-alias filters. Reasonable steps were taken to mitigate potential effects of the limited bandwidth on the results. While not ideal, the slope analyses for kappa are considered to reflect a positive contribution to characterizing kappa and its range at the site.

2.5.2.5.2.3.3 Kappa Based on V_S30

Since kappa at rock sites $V_S30 \geq 500$ m/s appears to be related in some manner to rock quality with poorer rock quality (softer) sites generally associated with larger kappa values than higher quality (stiffer) rock (Reference 2.5.2-176), attempts have been made to relate kappa to stiffness for cases where ground motion recordings are unavailable (Reference 2.5.2-190); (Reference 2.5.2-141); (Reference 2.5.2-177)). While the contributions to kappa are considered to occur over the top several kilometers, shallow shear-wave velocities in the context of V_S30 are correlated with broadband site amplification (Reference 2.5.2-191); (Reference 2.5.2-192)) which in turn correlates well with deeper velocities (Reference 2.5.2-193). Since shallow stiffness can be an indicator of deeper rock quality through stiffness, the correlation of rock site kappa with V_S30 has resulted in stable mean predictive relations, albeit with significant variation. Applying the kappa V_S30 relation from Silva et al. (Reference 2.5.2-190) using the simple profile (Figure 2.5.2-101) based on the suspension log (Figure 2.5.2-100) with a V_S30 of 2,416 m/s

(8,000 ft/sec) results in a kappa estimate of 0.009s. This estimate is well within the range of the site-specific estimates of 0.006s to 0.016s and close to the median of 0.010s, suggesting at least consistency with the spectral shape and FAS slope analyses of the recordings.

2.5.2.5.2.3.4 Summary

Kappa values ranging from 0.006 to 0.016s are supported for the CRN Site based on the analyses of response spectral shapes (5% damped) as well as slopes of the FAS at high frequency. Analyses of spectral shapes showed kappa values of 0.006s, as well as 0.009s with the larger magnitude shapes favoring the lower kappa estimate. For the FAS slope analyses the best estimate of kappa was 0.010s using the regional Q(f) model (630 $f^{0.5}$) and shallow crustal amplification. Alternative Q(f) model (410 $f^{0.5}$) and no shallow crustal amplification resulted in an increase in kappa to about 0.016s with the greatest dependence on the difference in shallow crustal amplification. The analyses support a range in kappa estimates for the CRN site from 0.006s to 0.016s with a best-estimate value taken as the median at 0.010s, as summarized in Table 2.5.2-32.

2.5.2.5.3 Dynamic Material Nonlinearity

Potential nonlinearity of rock materials ranging from soft to hard has a long history (Reference 2.5.2-167). Dynamic material properties of rock are as sensitive to strains as soils but, because of the much higher stiffness, loading levels must be very high to induce cyclic shear strains which result in discernable changes in V_S and material damping (Reference 2.5.2-190). As a result little (if any) effects of nonlinearity have been observed due to earthquake loading at stiff sites (e.g., $\overline{V_S}$ (30m)) ≥ 760 m/sec, Abrahamson and Silva, 2008 (Reference 2.5.2-166); (Reference 2.5.2-194)). Additionally, results of laboratory testing are few, especially at cyclic shear strains exceeding about 2 x 10^{-2}%, due to material stiffness and loading capability, particularly at higher confining pressures. As such, nonlinearity of rock materials is poorly quantified but is known to exist in laboratory conditions (Reference 2.5.2-167) at shear strains exceeding about 10^{-2}%.

At high loading levels at low exceedance frequencies, which may exceed cyclic shear strains of about 10^{-2}%, potential nonlinearity in rock response was accommodated in developing amplification factors. The consideration of nonlinear response within rock units, at least at shallow depths, is especially important in the context of hazard analyses using Approach 3 where each site-specific exceedance frequency is based on an integration of the reference site (hard rock) hazard across all exceedance frequencies, reflecting very low to very high loading levels.

For the CRN Site, neither site-specific modulus reduction and hysteretic damping curves nor dynamic testing results for similar materials of comparable stiffness were available. Additionally, because the uncertainty in degree of nonlinearity in rock materials is high, with very limited cyclic strain levels achieved in laboratory dynamic testing, particularly for stiff rock samples as well as high confining stresses, the epistemic uncertainty in the degree of nonlinearity was captured with a range of both nonlinear (M1) as well as linear (M2) models (Table 2.5.2-20).

To accommodate potential loading level dependencies on shear-wave velocities and hysteretic damping within the shallow sedimentary rock column at the CRN Site, a modified subset of the EPRI rock modulus reduction and hysteretic damping curves (Reference 2.5.2-142) was used (Figure 2.5.2-56) along with equivalent-linear site response analyses. The curves were

implemented to characterize consideration for upper-range, highly nonlinear, rock response with a lower range nonlinearity defined by linear analyses.

The subset of the EPRI rock curves reflect the original depth-dependent suite but with the 51 ft to 120 ft and 2,001 ft to 5,000 ft curves taken over revised depths of 0 to 20 ft and 21 ft to 500 ft, respectively. The revised depth distributions were based on modeling recorded motions at sites classified as rock (Reference 2.5.2-142). Below a depth of 500 ft linear analyses were assumed with low strain damping (in terms of Q) taken as proportional to shear-wave velocity with the kappa budget constrained by the total effective kappa defined at the profile surface. The 500 ft potential nonlinear zone was based on validation exercises with recorded motions that showed an unconservative bias (underprediction) at high frequency at soil sites when nonlinearity was extended to a depth beyond 500 ft (Reference 2.5.2-142). The depth limitation was assumed to occur at rock sites as well.

An additional revision to the curves used involved reducing the low-strain hysteretic damping from about 3% to 2% ($Q \approx 25$) to be more consistent with in-situ observations of shear-wave damping at shallow depths (< 500 m) (Reference 2.5.2-195).

2.5.2.5.3.1 Linear Analyses

For the linear analyses (M2), shear-wave damping was not based on laboratory tests of similar materials as hysteretic damping determined from laboratory dynamic testing (e.g., resonant column, torsional shear, direct simple shear, cyclic triaxial, etc.) is typically based on "undisturbed" samples and performed at varying confining pressures from atmospheric to at or above estimates of in situ stresses at sample depths. Laboratory dynamic tests, sometimes employing approximate corrections for sample disturbance, measure predominately intrinsic damping as damping is not measured through a change in amplitude in wave propagation, for example, but rather through the width of a resonant peak or the phase delay between an applied force and a reaction. As such laboratory dynamic testing may underestimate the effective damping which occurs in situ.

In-situ measurements of total effective damping within the frequency range of interest (1 to 50 Hz) is typically done with earthquake recordings from vertical arrays in soft to hard rock materials at low loading levels (Reference 2.5.2-196); (Reference 2.5.2-157); (Reference 2.5.2-197); (Reference 2.5.2-195); (Reference 2.5.2-198)). Typical damping ranges, in terms of Q ($Q \approx 50/D$ where D is percent critical damping), are about 10 to 100 with most values well below 50, even at significant depths (≈ 300 to 3,000 ft), as summarized by Campbell (Reference 2.5.2-155). The general trend with depth from in- situ analyses shows damping decreasing (Q increasing) with increasing depth, likely as a result of decreased friction due to crack closure as confining pressure increases. Typically V_S also increases with increasing confining pressure leading some to correlate Q with V_S at both rock (Reference 2.5.2-176) and soil sites (Reference 2.5.2-155). It is likely that the primary causal mechanism affecting the depth dependency of damping is confining pressure (Reference 2.5.2-167) rather than shear-wave velocity and suggests damping may be quite high at shallow depth (hundreds of feet) perhaps decreasing significantly at great depth. The overall levels of damping along with its trends with depth are consistent with the primary contributions to kappa over the top several km of the crust (Reference 2.5.2-175); (Reference 2.5.2-176)).

Observationally this indeed appears to be the case where in situ measurements of damping generally exceeds laboratory based measurements of damping (Reference 2.5.2-155). Differences between in-situ measurements of damping and laboratory-based damping either directly (Reference 2.5.2-199); (Reference 2.5.2-200); (Reference 2.5.2-136); (Reference 2.5.2-201); (Reference 2.5.2-202)) or inferred by generic material specific damping curves (Reference

2.5.2-203); (Reference 2.5.2-204)), reflect 50% to 100% higher damping occurring in-situ than measured in the laboratory (Reference 2.5.2-205). While nearly all comparisons are for soil or soft rock conditions, it is reasonable to assume scattering mechanisms existing in wave propagation through soils may also be active in stiffer (higher velocity) materials such as firm and hard rock.

The differences between laboratory and in situ damping for stiff materials may not be as great as in soils due to the longer wavelengths, conditional on frequency and depending on fracture size and density. Reflecting this difference, there are laboratory measurements of damping for firm rock materials at the Comanche Peak nuclear power plant and the Los Alamos National Laboratory and these show a range in low-strain damping from about 0.5% to about 5.0% with a mean damping of 3% (Reference 2.5.2-142), similar to the low-strain value of the (Reference 2.5.2-136) rock curves. Conversely there are also laboratory dynamic measurements in rock materials which are much more consistent and average about 1% (Q = 50) ((Reference 2.5.2-206); (Reference 2.5.2-207)). These measurements suggest that low-strain laboratory dynamic material testing show wide variability, perhaps strongly conditional on material type and fracturing, both related to shear-wave velocity. In-situ hysteretic damping measurements in rock materials depend weakly on rock type, with an average Q of about 10 in the top 100 m, increasing with depth to about 30 at a depth of about 500 m (Reference 2.5.2-195). At deeper depths, well beyond 500m, *Q* increases rapidly, likely contributing to the frequency-dependent crustal damping (Reference 2.5.2-156); (Reference 2.5.2-176)).

The apparent stability of in situ damping, albeit with few measurements, compared to the more variable laboratory-based measurements, suggest the laboratory measurements incorporate varying degrees of scattering damping with the lower range values perhaps principally measuring intrinsic damping.

Based on the observations of in- situ low strain damping at rock sites with a range in shear-wave velocity from about 1,500 m/s to 3,000 m/s and rock type from sedimentary to crystalline, Q ranged from about 10 to about 60 (Reference 2.5.2-155) with most estimates well below 60 and an average value of about 30 over the upper 500 m (Reference 2.5.2-195). As a reasonable conservative estimate, a value of 40 (damping 1.25%) was adopted for total effective damping at the CRN site over the top 500 ft. Below a depth of 500 ft, to accommodate the observational trends of decreasing damping with increasing depth, Q was taken proportional to V_S (Reference 2.5.2-176). As with the nonlinear analyses, below 500 ft kappa was used to constrain the shear-wave damping.

2.5.2.5.3.2 Total Effective Kappa (note - text revised from existing Subsection 2.5.2.5.1)

To distribute damping throughout profiles P1, P2, and P3, the total effective kappa was used as a constraint for the sum of damping throughout the profiles. Low-strain damping for each profile was also constrained over the top 500 ft by revised EPRI rock curves for the nonlinear case (M1) at 2 percent and 1.25 percent for the linear case (M2), in keeping with the assumption damping is higher over the shallower portions of profiles, leaving the damping over the remaining profile to be defined. It is important to note the details of how the damping is distributed through the profiles, conditional on the total effective kappa, has a minor effect on the amplification (Reference 2.5.2-164). As such the damping (in terms of Q) may be made either constant with depth, increasing with depth due perhaps to increasing confining pressure (e.g. typical damping curves and Reference 2.5.2-167), or proportional to V_S. Lacking a physical basis for preference, proportional to V_S was used (References 2.5.2-168 and 2.5.2-155) as it accommodates confining pressure dependencies in a consistent manner.

The kappa budget, separating site-specific profile and crustal model (Table 2.5.2-21), would typically include 0.006 s nominally for the crustal model, with the remaining kappa (damping) distributed through the profile including low-strain damping from the damping curves. In this case, however, the site profiles to basement depths (Figures 2.5.4-20 and 2.5.4-21) were taken to replace the top 1 km thick layer in the Midcontinent crust (Table 2.5.2-21) and, as such, characterize the damping contributing to the total effective kappa. For Locations A and B, the fixed low-strain damping over the top 500 ft (150 m) is 2.00 percent and 1.25 percent for the nonlinear (M1) and linear (M2) cases, respectively. At depths greater than 500 ft, the damping is inversely proportional to V_S. This results in decreasing damping with depth due to the V_S increasing with depth. For Locations A and B, the sedimentary rock sections extending to depths of nearly 4 km, damping is assumed to occur throughout the profiles relatively high at shallow depths with relatively low damping for the deeper materials. However, because kappa is affected by travel time, the major contribution to the total effective kappa comes from the deeper part of the profiles, below 500 ft. Profile damping is listed in Tables 2.5.4-30 and 2.5.4-31 for Locations A and B, respectively. Table 2.5.2-20 shows the profile kappa estimates and relative weights for Locations A and B.

~~2.5.2.5.2~~2.5.2.5.4 Capturing Site-Specific Geologic Column Properties, Uncertainties, and Correlations

To provide an objective means of smoothing resonances which tend to be overpredicted by the vertically propagating shear-wave model in a one-dimensional profile (Reference 2.5.2-136) and, to a far lesser extent, account for the aleatory variability in dynamic material properties that is expected to occur across a site at the scale of a typical nuclear facility, variability in the basecase V_S profiles has been incorporated in the site response calculations. For the CRN Site, random V_S profiles were developed about t~~he smoothed~~each basecase profile~~s~~ shown in Figures 2.5.4-20 and 2.5.4-21. Sixty random velocity profiles were generated for each of the best-estimate, upper-range, and lower-range profiles for each of Locations A (Figures 2.5.2-57 and 2.5.2-58) and B (Figures 2.5.2-59 and 2.5.2-60). In order to randomly vary the V_S in each base-case profile ~~(best-estimate, upper-range, and lower range)~~, a profile randomization scheme ~~has~~was ~~been developed~~implemented which varies both layer velocity and thickness. However, in this case layer thickness was not varied ~~in this study~~ as it is: (1) generally equivalent to varying layer velocities, (2) tends to increase contributions to scattering kappa, and (3) can result in increased site variability which is already accommodated in the hard rock hazard. Rather layer thickness variation was accommodated in the variation of the total profile depth. The depth randomization to the effective basement, at a depth of about 12,000 ft, was taken as 15 percent of the depth at ± 1800 ft using a uniform distribution. The percentage was based on the rock unit thickness variability of about 10 percent across the site determined from boreholes and increased by 50 percent to reflect likely increases in unit thickness variability within the deep structure as well as provide a realistic broadening of the fundamental resonance for deep sites.

The random velocity profiles were generated using a natural log standard deviation of 0.25 over the upper 50 ft and 0.15 below that depth using the footprint correlation model (Reference 2.5.2-134). The correlation model was developed from an analysis of variance on about 500 measured V_S velocity profiles (References 2.5.2-136 and 2.5.2-142). In the correlation model, a limit of ± 2 standard deviations about the median value in each layer was considered for the limits on random velocity fluctuations. For the upper-range profiles, the high V_S depths where the velocity was limited to 3.52 km/s (Figures 2.5.4-20 and 2.5.4-21), bounds were necessarily placed on the random velocities of 3.4 to 3.6 km/s. The correlation model selected reflects a minimum variability while providing for a realistic variation across footprint dimensions (several hundred feet) resulting in an objective smoothing of narrow resonances while preserving broad

resonances, yet not developing deep low velocity zones which introduce artificial damping through wave scattering (scattering kappa).

An example of the kappa budget to assess potential contributions from scattering in the randomization process is shown on Figure 2.5.2-55, which compares median amplification with that of a single analysis using the basecase profile. The example shows results for Location A, the P1 basecase profile, along with the basecase kappa (Table 2.5.2-20), with the median estimate closely matching the amplification of the basecase profile across frequency. The median estimate smoothes through narrow-band resonances and shows no bias, not falling below the basecase amplification at high frequency (≥ 10 Hz) suggesting little contribution to kappa due to scattering. The similarity between the median estimate and the basecase amplification across frequency also indicates the median profile adequately replicates the basecase profile throughout its depth with the checks routinely performed for each profile. ~~Additionally, with little contribution to scattering kappa resulting from the relatively thin layering used in the site response analyses over the top 500 ft (Figures 2.5.2-57 and 2.5.2-59), any contribution to scattering kappa from the smoothed basecase profiles (Figures 2.5.4-20 and 2.5.4-21) would be even smaller. As a result, not correcting for amplification of the entire profile in the kappa analysis is not considered to bias the estimates of kappa.~~

While the effects on hazard of site variability through profile randomization are small (References 2.5.2-132 and 2.5.2-144), the full ergodic variability (References 2.5.2-158 and 2.5.2-159), which includes the site component, was used in developing the hard rock hazard. As such the ~~use of a correlation model with larger variability increases the potential for double counting site variability.~~ inclusion of the variability about the median amplification in the site-specific Approach 3 analyses implies a conservative inclusion of site variability in development of the GMRS.

Associated with each of the 60 randomized profiles was also a set of randomized strain strain-dependent shear modulus and hysteretic damping curves. To accommodate aleatory variability in the modulus reduction and hysteretic damping curves on a generic basis, the curves were independently randomized about the basecase values (Figure 2.5.2-61) ~~using the program RANPAR~~. A log normal distribution was assumed with a logarithmic standard deviation (σ_{ln}) of 0.15 and 0.30 at a cyclic shear strain of 3×10^{-2} percent for modulus reduction and hysteretic damping, respectively (Reference 2.5.2-142) with upper and lower bounds of $2\sigma_{ln}$. The truncation was necessary to prevent modulus reduction or damping models that are not physically realizable. The distribution was based on an analysis of variance of measured G/G_{max} and hysteretic damping curves and is considered appropriate for applications to generic (material type specific) nonlinear properties (Reference 2.5.2-142). The random curves were generated by sampling a transformed normal distribution with a σ_{ln} of 0.15 and 0.30 as appropriate, computing the change in normalized modulus reduction or percent damping at 3×10^{-2} percent cyclic shear strain, and applying this factor at all strains. The random perturbation factor was reduced or tapered near the ends of the strain range to preserve the general shape of the basecase curves (References 2.5.2-160 and 2.5.2-136). Also, damping was limited to a maximum value of 15 percent. For linear analyses, damping was not randomized as it is equivalent to randomizing kappa, the variability of which is included in the hard rock kappa. ~~The program RANPAR was used to randomize the dynamic material properties as well as profile depth.~~

~~2.5.2.5.3~~2.5.2.5.5 Site Response Analysis

Traditionally in the estimation of site-specific probabilistic ground motions for a soil site, a rock ground motion is calculated and modified by deterministic site response analyses derived for the soil column to arrive at the ground motions at the soil surface. This process can also be

followed to obtain the ground motions at the ground surface atop firm rock. In doing so, the annual exceedance probability of that surface (either rock or soil) motion is generally unknown, varies with period, and may be of a higher probability than the control (rock) motion. If a risk analysis is desired, the surface motions (either rock or soil) must be hazard consistent, i.e., the annual exceedance probability of the surface ground motion should be the same as the input rock ground motion.

In NUREG/CR-6728 (Reference 2.5.2-132), several site response approaches are described that produce surface motions consistent with the rock outcrop hazard. The approaches also incorporate the aleatory variabilities in the site properties into the surface motions. The NUREG identifies four basic approaches for determining the ground motions at a site. They are in order of increasing accuracy.

- Approach 1: Rock UHRS used as control motions
- Approach 2A: Develop transfer functions for 1 Hz and 10 Hz design earthquakes using a single magnitude for each frequency.
- Approach 2B: Develop transfer functions for 1 Hz and 10 Hz design earthquakes accommodating magnitude distributions
- Approach 3: Approximations to UHRS integrations
- Approach 4: UHRS computed using site-specific ground motion prediction models

The approaches range from a PSHA using ground motion prediction models for the specific site or location of interest (Approach 4) to scaling the rock motion on the basis of a site response analysis using a broadband input motion (Approach 1).

To compute the ground motions at the top of unweathered rock for the CRN Site, Approach 3 was implemented. Approach 3 is a fully probabilistic analysis procedure which moves the site response, in an approximate way, into the hazard integral. The approach is described by Bazzurro and Cornell (Reference 2.5.2-143) and NUREG/CR-6769 (Reference 2.5.2-144). In this approach, the hazard at the surface is computed by integrating the site-specific hazard curve at generic rock level with the probability distribution of the transfer functions, i.e., amplification factors (References 2.5.2-145 and 2.5.2-146). The site-specific amplification, relative to a reference rock, in this case hard rock, is characterized by a suite of frequency-dependent amplification factors that can account for nonlinearity in soil/rock response. Approach 3 involves approximations to the hazard integration using suites of transfer functions, which result in complete hazard curves at the ground surface for specific ground motion parameters (e.g., spectral accelerations) and a range of frequencies.

The basis for Approach 3 is a modification of the standard PSHA integration:

$$P[A_S>z]=\iiint P\left[AF>\frac{z}{a}|m,r,a\right] f_{M,R|A}(m,r;a)f_A(a)\,dmdrda \qquad \text{Equation 2.5.2-8}$$

where A_S is the random ground-motion amplitude at the ground surface at a certain natural frequency; z is a specific level of A_S; m is earthquake magnitude; r is distance; a is an amplitude level of the random rock ground motion, A, at the same frequency as A_S; $f_A(a)$ is derived from

the rock hazard curve for this same frequency (it is the absolute value of its derivative); and $f_{M,R|A}$ is the deaggregated hazard (i.e., the joint distribution of M and R, given that the rock amplitude is level a). AF is an amplification factor defined as:

$$AF = A_S/a \qquad \text{Equation 2.5.2-9}$$

where AF is a random variable with a distribution that can be a function of m, r, and a. To accommodate epistemic uncertainties in site dynamic material properties, multiple suites of AF may be used and the resulting hazard curves combined with weights to properly reflect mean hazard and fractiles.

The ground surface response is controlled primarily by the level of rock motion and m, so Equation 2.5.2-8 can be approximated by:

$$P[A_S>z] = \iint P\left[AF>\frac{z}{a}|m,a\right] f_{M|A}(m;a) f_A(a)\, dm da \qquad \text{Equation 2.5.2-10}$$

where r is dropped because it has an insignificant effect in most applications (Reference 2.5.2-132). To implement Equation 2.5.2-10, only the conditional magnitude distribution for relevant amplitudes of a is needed. $f_{M|A}(m;a)$ can be represented (with successively less accuracy) by a continuous function, with three discrete values or with a single point, (e.g., $m^1(a)$, the mean magnitude given a). With the latter, Equation 2.5.2-10 can be simplified to:

$$P[A_S>z] = \int P\left[AF>\frac{z}{a}|a,m^1(a)\right] f_A(a)\, da \qquad \text{Equation 2.5.2-11}$$

where, $f_{M|A}(m;a)$ has been replaced with m^1 derived from deaggregation. With this equation, one can integrate over the rock acceleration, a, to calculate $P[A_S>z]$ for a range of surface amplitudes, z.

~~2.5.2.5.3.1~~2.5.2.5.5.1 Implementation of Approach 3

In Approach 3, the following steps are performed:

- Randomization of basecase site-dynamic material properties to produce a suite of velocity profiles as well as G/G_{max} and hysteretic damping curves that incorporate site randomness.

- Computation of site amplification factors as characterized by a mean (log) and distribution for each set of basecase site properties using the random vibration theory (RVT) based equivalent-linear site response model.

- Full integration of the fractile and mean hazard curves for the generic site condition in this case hard rock and amplification factors to arrive at a distribution of site-specific hazard curves.

The computation of the amplification factors is the first phase of the calculations and is similar to what is done in other site-response approaches.

~~2.5.2.5.3.2~~2.5.2.5.5.2 RVT-Based Equivalent-Linear Site Response Approach

To compute the horizontal ground motions at the ground surface, the results of the PSHA are modified using a site-response model. The conventional site response approach in quantifying the effects of soil and other unconsolidated sediments on strong ground motions involves the use of time histories compatible with the specified outcrop response spectra to serve as control (input) motions. The control motions are then used to drive a nonlinear computational formulation to transmit the motions through the profile.

The computational formulation that has been most widely employed to evaluate 1D site response assumes vertically-propagating plane S-waves. Departures of soil response from a linear constitutive relation are treated in an approximate manner through the use of the equivalent-linear formulation. The equivalent-linear formulation, in its present form, was introduced by Idriss and Seed (Reference 2.5.2-147). A stepwise analysis approach was formalized into a 1D, vertically propagating S-wave code called SHAKE (Reference 2.5.2-148). Subsequently, this code has become the most widely used and validated analysis package for 1D site response calculations.

The computational scheme employed to compute the amplification factors in this study uses an alternative approach employing RVT (References 2.5.2-156, 2.5.2-149, and 2.5.2-136). In this approach, as embodied in the computer program RASCALS, the control motion power spectrum is propagated through the 1D profile using the plane-wave propagators of Silva (Reference 2.5.2-150). In this formulation only shear waves (S-waves) polarized in the horizontal plane (SH-waves) are considered. Arbitrary angles of incidence may be specified. In this analysis, the standard approach of vertical incidence was used. Cyclic shear-strain iterated properties were developed using a constant effective strain ratio of 0.65, based on an extensive suite of validations (References 2.5.2-136 and 2.5.2-142).

Inputs to RASCALS are as follows:

- Location of input and output motions within the site profile.
- Input (control) motions characterized by earthquake power spectra.
- Incidence angles of input motion.
- A vertical profile consisting of uniform plane-layer layers with specified thickness, seismic velocity, low strain damping, and density as a function of depth.
- Nonlinear ~~D~~dynamic properties of the material at the site, consisting of strain-dependent shear modulus and damping curves for each layer.

Control motions (power spectral density) must be calculated for input into the site response analysis that are representative of the earthquake magnitude and distance dominating the hazard at the desired rate of exceedance. The basis for the control motions are the magnitude and distances specified by the hazard deaggregation.

Evaluation of site-response using the equivalent-linear model is based on convolution of appropriate control motions through randomized velocity profiles combined with randomized

G/G_{max} and hysteretic damping curves. The randomized profiles and curves are generated from basecase velocity and nonlinear dynamic properties. The convolutions yield transfer functions for 5 percent-damped response spectra and peak ground velocity (PGV).
~~RASCALS was used to generate control motions, acceleration, power, and response spectra for two earthquakes, M 5.5 and 7.5, which dominate the high- and low-frequency hard rock hazard. For the M 5.5, a single-corner source spectral shape was considered. For the M 7.5, both single and double-corner source spectral shapes were used. The events were placed at a suite of distances to produce expected median rock peak accelerations of 0.01, 0.05, 0.10, 0.20, 0.30, 0.40, 0.50, 0.75, 1.00, 1.25 and 1.50 g.~~

Consistent with the deaggregation of the hard rock hazard at the CRN Site, which showed contributions from events in the range of **M** 5.5 at short distances and at high frequency as well as contributions from larger magnitude earthquakes, **M** 7.5, at larger distances and low frequency, control motion Fourier amplitude spectra, as well as reference site response spectra (5 percent-damped PS~~a~~A) were defined for representative earthquake magnitudes of **M** 5.5 and 7.5 and were generated with the point-source model for the Midcontinent crustal model listed in Table 2.5.2-21. This approach is similar to that used in adjusting ground motion prediction equations (GMPEs) for different regions having different crustal models, kappa, and crustal Q(f) (Reference 2.5.2-141). Modal magnitudes **M** 5.5 and 7.5 (single- and double-corner source models) were used to accommodate potential effects of control motion spectral shape on nonlinear response. Although differences in amplification factors due to control motion spectral shapes is expected to be ~~quite~~ small, the multiple shapes were used for completeness to accommodate random velocity excursions to lower velocities. Frequency-dependent weights for the relative contribution from the control motions (**M** 5.5 and 7.5), based on the deaggregation, are shown in Table 2.5.2-22. Two different assumptions regarding the shape of the seismic source spectrum (single-corner and double-corner, Reference 2.5.2-161) were used for **M** 7.5 while only the single-corner was used for **M** 5.5. Equal weights were given to the single- and double-corner control motions. A range of 11 different reference site input amplitudes (median PGAs ranging from 0.01 to 1.5 g) with point-sources placed at a suite of hypocentral distances to produce expected median rock peak accelerations of 0.01, 0.05, 0.10, 0.20, 0.30, 0.40, 0.50, 0.75, 1.00, 1.25 and 1.50 g were used in the site response analyses. The characteristics of the seismic source and upper crustal attenuation properties used for the analysis of the CRN Site were typical values for hard rock sites in the Central and Eastern North America (CENA): stress parameter of 110 bars, Q(f) of 670 $f^{0.33}$, a kappa value of 0.006 s, crustal model (Table 2.5.2-21), and source depth of 8 km. Because the reference motions were developed for a suite of median peak acceleration values by varying hypocentral distances, apart from kappa, the reference motions are not very sensitive to either the stress parameter or Q(f) model.

~~The deaggregation showed contributions from events in the range of **M** 5.5 at short distances and at high frequency. Contributions from larger magnitude earthquakes **M** 7.5 are seen in the hard reference rock deaggragation as summarized in Table 2.5.2-22.~~

~~2.5.2.5.3.3~~2.5.2.5.5.3 Horizontal Amplification Factors

Based on the RASCALS runs for the randomized V_S profiles from each of the ~~three~~ basecase profiles, ~~a~~ probability distributions ~~of~~for horizontal amplification factors ~~was~~were calculated. RASCALS ~~is~~was used for horizontal spectra using normally-incident plane SH-waves. For each control motion, mean (log) and standard deviations ~~are~~were computed from each of the 60 response spectra. The mean (log) response spectrum from the 60 convolutions ~~is~~was divided by the mean (log) hard rock spectrum to produce the amplification factors. The amplification factors include the effects of the inherent aleatory variability (randomness) of the site properties about each basecase and any possible effects of source spectral shape (e.g. magnitude) of the control motions. Epistemic variability (uncertainty) ~~is~~was captured in consideration of alternate

basecase (mean) profiles and properties. The horizontal amplification factors are a function of the reference (hard rock) peak acceleration, spectral frequency, and linear as well as nonlinear rock response.

The ~~results of the site response analysis consist of~~ horizontal amplification factors (5 percent-damped PSA) are computed from the source layer to the surface for both the site profiles and reference rock crustal model (Table 2.5.2-21), which describe the amplification (or de-amplification) of hard reference rock motion as a function of frequency and input reference rock amplitude. Site specific motions (5 percent-damped PS~~a~~A) were computed with the point-source model using the same source parameters as in generating reference rock motions with the randomly generated site profiles replacing the first layer of the reference site crustal model (Table 2.5.2-21). The modeling approach is consistent with that used in validating the point source model (References 2.5.2-136, 2.5.2-142, and 2.5.2-156), developing amplification factors for generic site conditions (References 2.5.2-162 and 2.5.2-163), assessing crustal amplification (Reference 2.5.2-164), and in hazard analyses calculating V_S-kappa corrections to translate ground motion prediction equations (GMPEs) backbone curves from one region to another (Reference 2.5.2-165).

The amplification factors are represented in terms of a median amplification value and an associated standard deviation (sigma) for each oscillator frequency (100 points per decade beginning at 0.1 Hz) and input rock amplitude. A minimum median amplification value of 0.5 was employed to accommodate potential limitations in equivalent-linear analyses at high loading levels due to overdamping.

Figures 2.5.2-62 and 2.5.2-63 illustrate, for **M** 5.5 single-corner control motion spectra, the median and ± 1 standard deviation in the predicted amplification factors developed for the eleven loading levels parameterized by the median reference (hard rock) peak acceleration (0.01 to 1.50 g) for profile P1 of Location A and revised EPRI (Subsection 2.5.2.5.1) rock G/G_{max} and hysteretic damping curves (M1). The variability in the amplification factors results from variability in V_S and depth to hard rock. To illustrate the effects of nonlinearity at the CRN Site, Figures 2.5.2-64 and 2.5.2-65 show the corresponding amplification factors developed assuming a linear analysis (M2). Little difference is seen over all loading levels for structural frequencies less than about 20 Hz. The amplification factors for Location B are similar to those developed for Location A as shown in Figures 2.5.2-66 and 2.5.2-67 for revised EPRI rock G/G_{max} and hysteretic damping curves (M1). The results for **M** 7.5 single-corner control motion spectra are similar to those for **M** 5.5 as shown in Figures 2.5.2-68 and 2.5.2-69 for Location A and M1 curves.

For **M** 5.5 single-corner control motion spectra and the basecase P2 profile of Location A, Figures 2.5.2-70 and 2.5.2-71 illustrate, the median and ± 1 standard deviation of the amplification factors for revised EPRI rock G/G_{max} and hysteretic damping curves (M1). Similarly, Figures 2.5.2-72 and 2.5.2-73 show the amplification factors developed for the basecase P3 profile of Location A.

~~2.5.2.5.4~~2.5.2.5.6 Development of V/H Ratios

Given the firm to hard rock conditions at the CRN Site, with V_S30 of 2351 m/s (7713 ft/s) and 2336 m/s (7664 ft/s) at Locations A and B, respectively, NUREG/CR-6728 (Reference 2.5.2-132) presents an appropriate suite of design vertical-to-horizontal (V/H) ratios. The NUREG/CR-6728 V/H ratios conservatively accommodate potential magnitude and distance dependencies that have been observed in recent empirical V/H ratios (References 2.5.2-151 and 2.5.2-137) using three intervals of horizontal peak ground acceleration (PGA) on rock as a proxy for the magnitude and distance dependence: < 0.2g, 0.2 to 0.5g, > 0.5g.

The methodology implemented to develop the vertical ground motions follows analogously to Approach 3 used to develop fully probabilistic site-specific horizontal motions. For application to the development of site-specific vertical hazard, the same fully probabilistic approach was used with V/H ratios (median and uncertainty estimates) substituted for horizontal amplification factors. In this case, the distributions of V/H ratios were applied to the site-specific horizontal hazard curves. As with the development of the site-specific horizontal hazard, epistemic uncertainty in median V/H ratios was incorporated in this case by including σ_μ, epistemic uncertainty about the median V/H ratio.

Since V/H ratios for firm to hard rock site conditions are not well constrained due to a lack of recordings at design magnitudes and distances, epistemic uncertainty (σ_μ) was accommodated in the V/H Approach 3 analyses. Epistemic uncertainty in V/H ratios was assessed by examining the range in available models for V/H ratios appropriate for firm to hard rock site conditions (Reference 2.5.2-138). The models considered include Bozorgnia and Campbell (Reference 2.5.2-151), Bommer et al. (Reference 2.5.2-152), Edwards et al. (Reference 2.5.2-153), and Gülerce and Abrahamson (Reference 2.5.2-137), with the range in models spanning a V/H factor of 1.5 to 1.8 depending on frequency. The range was taken to reflect $2\sigma_\mu$ estimates with $\sigma_{\mu ln}$ taken as the average at 0.25 and used for epistemic uncertainty in the V/H ratios. In the Approach 3 analyses for the vertical component the three PGA dependent V/H ratios from NUREG/CR-6728 along with the $\sigma_{\mu ln}$ of 0.25 were implemented based on the site-specific horizontal hazard for peak acceleration with the bin boundaries preserved.

For the aleatory variability about the mean (log) V/H ratio, resulting in increased aleatory variability for the vertical component compared to the horizontal component, some attention is required as the contribution of site-specific aleatory variability to the hazard has already been accommodated in developing the site-specific horizontal component hazard. The site component of aleatory variability was included in developing the hard rock hazard in the variability about the hard rock ~~ground motion prediction equations (~~GMPEs~~)~~. Additionally, in the Approach 3 analyses to develop the site-specific horizontal hazard, the variability about the median amplification factors, treated as aleatory variability, was included as well. As a result there is some double-counting of site aleatory variability but, because the variability of the amplification factors is small, with σ_{ln} ranging from 0.05 to 0.20 across structural frequency, the potential impacts on the site-specific hazard are not considered significant. However in the application of Approach 3 in developing the vertical hazard, care must be exercised in contributing additional unnecessary aleatory variability in the vertical component, with the implication that vertical motions reflect higher variability than horizontal motions. The recent development of NGA-West 2 vertical GMPEs (Reference 2.5.2-154) using the same suite of recordings as in the development of the horizontal GMPEs permits a straightforward assessment of the relative degrees of aleatory variability between horizontal and vertical components. The recent vertical GMPEs (Reference 2.5.2-154) indicate estimates of aleatory variability comparable to the corresponding horizontal GMPEs, suggesting adequate aleatory variability for the vertical component has been already accommodated in developing the horizontal hazard. As a result only epistemic uncertainty in firm to hard rock V/H ratios was incorporated in developing the vertical hazard.

~~2.5.2.5.5~~2.5.2.5.7 Site-Specific Horizontal and Vertical UHRS

Implementing Approach 3, the hard rock hazard curves derived from the PSHA and the horizontal amplification factors relative to hard rock were integrated to produce a site-specific amplified horizontal hazard curves. The hazard curves calculated using the amplification factors from the **M** 5.5 and 7.5 controlling earthquakes were weighted based on their contributions to the hazard at each spectral frequency and hazard level. The epistemic uncertainty in seismic hazard is typically represented by a set of weighted hazard curves. Using these sets of curves

as discrete probability distributions, they can be sorted by the frequency of exceedance at each ground-motion level and summed into a cumulative probability mass function. When the cumulative probability mass function for a particular exceedance frequency equals or exceeds fractile *y*, then the exceedance frequency represents the y^{th} fractile. The weighted-mean hazard curve is the weighted average of the exceedance frequency values.

Analogously, the horizontal site-specific hazard curves themselves were convolved with the suite of median V/H factors from NUREG/CR-6728 (Reference 2.5.2-132), considering the uncertainties discussed in Subsection 2.5.2.~~5~~6.4, to derive the corresponding vertical site-specific hazard curves.

Horizontal and vertical UHRS for mean annual frequencies of exceedance (MAFE) of 10^{-4}, 10^{-5}, and 10^{-6} computed for Locations A and B are shown in Figures 2.5.2-74 and 2.5.2-75, respectively, and are tabulated in Tables 2.5.2-23 through 2.5.2-26. The spectra were interpolated between the seven frequencies specified in the hard rock reference site hazard curves (0.5, 1.0, 2.5, 5.0, 10.0, 25.0, and 100.0 Hz) by overlying response spectral shapes computed in the development of amplification factors on the UHRS and filling in spectral ordinates.

~~2.5.2.6~~2.5.2.5.8 Site-Specific Ground Motion Response Spectra (GMRS)

The horizontal and vertical ~~design response spectra (DRS)~~ground motion response spectra (GMRS) are developed following the RG 1.208 performance-based procedure for the assessment of a site-specific seismic design ground motion, satisfying the requirements of 10 CFR 100.23, paragraphs (c), (d)(1), and (d)(2), and leading to the establishment of an SSE to satisfy the design requirements of 10 CFR 50, Appendix S. The steps necessary to develop the design ground motions are described in NUREG-0800, Chapter 2, *Site Characteristics and Site Parameters*, and Chapter 3, *Design of Structures, Components, Equipment and Systems*.

The performance-based, site-specific design earthquake ground motion is developed using the method presented in RG 1.208, Section B, which is analogous to the development of the ASCE/SEI Standard 43-05 (Reference 2.5.2-135). The ~~DRS~~GMRS that achieves the annual first onset of significant inelastic deformation (FOSID) target performance goal with a performance factor (P_F) of 10^{-5}, and hazard exceedance probability (H_D) of 10^{-4}, is described in ASCE/SEI Standard 43-05, Chapters 1 and 2. To meet the performance goal, the performance-based methodology specifies the two parameters A_R and DF:

$$A_R(f) = \mathrm{UHRS}\left(f|10^{-5}\right)/\mathrm{UHRS}\left(f|10^{-4}\right) \qquad \text{Equation 2.5.2-12}$$

where $A_R(f)$ represents the slope of the site-specific hazard curve for a given spectral frequency *f* between hazard levels of mean annual frequencies of exceedance (MAFE) of 10^{-4} and 10^{-5}, presented in Subsection 2.5.2.5; and

$$\mathrm{DF}(f) = \mathrm{Max}\left\{1.0,\ 0.6[A_R(f)]^{0.8}\right\} \qquad \text{Equation 2.5.2-13}$$

where the design factor DF(*f*) was developed to meet the performance goal, as presented in ASCE/SEI Standard 43-05.

Given $A_R(f)$ and $DF(f)$, the horizontal ~~DRS~~GMRS(f) is given in RG 1.208 by:

$$DRS(f) = DF(f) \times UHRS\left(f|10^{-4}\right) \text{ for } A_R(f) \leq 4.2 \quad \text{Equation 2.5.2-14a}$$

$$DRS(f) = 0.45 \times UHRS\left(f|10^{-5}\right) \text{ for } A_R(f) > 4.2 \quad \text{Equation 2.5.2-14b}$$

Equation 2.5.2-14a is based on the assumption that the hazard curves are approximated by a power law equation (i.e., linear on a log-log plot) in the range of 10^{-4} and 10^{-5}. As presented in RG 1.208, if A_R is greater than 4.2, then this assumption is not valid and in these cases, it is acceptable to use a value equal to 45 percent of the mean 10^{-5} UHRS, given in Equation 2.5.2-14b. ~~Following RG 1.208, the formulation for the DRS, above, gives the GMRS.~~

The implementation of Approach 3 to develop the vertical GMRS consistent with the performance goals of the horizontal GMRS assumes the performance-based methodology is also appropriate for the vertical component.

All response spectra were extended between 2.0 and 10.0 s. The corner period (T) for constant displacement is magnitude dependent and given by (Reference 2.5.2-166):

$$Log(T) = -1.25 + 0.3 \times \mathbf{M} \quad \text{Equation 2.5.2-15}$$

The modal magnitude at 2.0 s was used to define the **M** and the corner period (T). For MAFE 10^{-4}, 10^{-5}, and 10^{-6} the modal magnitude is between **M** 7.5 and 8.0 giving a cornerperiod (T) between 10.0 and 14.1 s. Figures 2.5.2-76 and 2.5.2-77 show the 10^{-4} and 10^{-5} MAFE horizontal and vertical UHRS and the GMRS for Locations A and B, respectively. The spectra is extended using a slope of 1 beyond 2.0 s to extrapolate to 10.0 s for MAFE 10^{-4}, 10^{-5}, and 10^{-6} since the corner period is beyond 10.0 s. Figure 2.5.2-78 shows the horizontal and vertical GMRS and the envelope spectra for Locations A and B. As can be seen, the GMRS are similar for Locations A and B. The horizontal and vertical GMRS and the envelope spectra are tabulated in Tables 2.5.2-27 and 2.5.2-28, respectively.

To examine the effects of accommodating increased confining pressure due to soil overburden on the free-surface outcrop GMRS, the distribution of firm rock shear modulus and hysteretic damping curves with depth was revised. Since the generic G/G_{max} and hysteretic damping curves reflect confining pressure effects in an approximate manner through depth, the estimate of an soil overburden thickness of 42 ft was added to the depth of the nonlinear profiles with nonlinear zones extending in depth to 458 ft with the 21 to 500 ft suite of shear modulus and hysteretic damping curves implemented over the top 458 ft of the nonlinear profiles.

The final confining pressure adjusted GMRS reflects the hazard weighting of the original linear analyses along with the confining pressure adjusted nonlinear analyses, enveloped over the hazard developed for Locations A and B. The resulting GMRS is compared to the original GMRS on Figure 2.5.2-79 (Table 2.5.2-29) at the seven frequencies defined by the hard rock hazard. As Table 2.5.2-29 and Figure 2.5.2-79 indicate the effects of increased confining

pressure due to overburden material on the firm to hard rock nonlinear properties are insignificant.

SSAR Subsection 2.5.2.6 is revised as indicated: (Note - deletions are shown as "strike-through" text and additions are shown as "underlined" text.)

~~2.5.2.6.1~~2.5.2.6 2D Sensitivity Analysis

Due to the dipping nature of the underlying stratigraphy beneath the CRN Site (approximately 33 degrees) (Figure 2.5.4-12), potential 2D effects on earthquake ground motions were evaluated. In the development of the GMRS using Approach 3 from NUREG/CR-6728, a 1D equivalent-linear site response approach was used, and potential 2D effects were initially addressed by evaluating the epistemic uncertainty in V_S beneath the CRN Site.

The objectives of the 2D sensitivity analysis were to: (1) evaluate how simplifying the dipping stratigraphy beneath the CRN Site to a 1D model for site response impacts the GMRS, and (2) assess whether sufficient epistemic uncertainty had been incorporated into the 1D analysis to address potential 2D effects. A 2D model of the site was developed which included both Locations A and B (Figure 2.5.4-13). The amplification between Precambrian basement rock (where V_S exceeds about 11,500 ft/s) and the surface of the model was then computed. The influence of the dipping stratigraphy was evaluated by comparing the amplification computed by the 2D analysis with that from the 1D analysis. The 2D effects were analyzed at three points across Locations A and B to allow averaging across both locations. The three points at each location that were analyzed were center, left (updip of center), and right (downdip of center).

The computational zone for the 2D modeling, defined as the area shown in the geologic cross-section (Figure 2.5.4-12), and was approximately 20,000 ft wide by 14,800 ft deep and consisted of multiple layers having interfaces at various dip angles (Figure 2.5.2-80). The depth of the mesh to the top of the basement hardrock is about 12,600 ft with 2200 ft of basement rock included in the mesh. All properties of the rock layers were assumed to be linear-viscoelastic using the same hysteretic damping model in the 2D calculations used in the 1D site response calculations. The computational zone was represented by a 2D finite element (FE) mesh, having the capability to transmit 50 Hz frequency response (Figure 2.5.2-81). This 50 Hz frequency requirement is consistent with the NRC recommendations provided in NUREG-0800 for site response analysis. The element sizes were determined using the standard criterion of $f = V_S/5d$, where V_S is the material shear-wave velocity, d is the largest dimension of the element and f is the passing frequency.

The 2D mesh included the Precambrian basement with a V_S of about 11,500 ft/s, consistent with the V_S used in the GMRS (Figure 2.5.2-82; Subsection 2.5.2.6). The V_S values for the geologic formations represented in the mesh were adopted from the 1D V_S profiles used in calculating the GMRS presented in Section 2.5.2.5.1. The damping was taken as the average of the six sets of profiles used in the calculation of the GMRS (Figure 2.5.2-82).

The 2D analyses were performed using SDE-SASSI Version 2.0. 1D analyses were performed to compare against the 2D model. The 1D analysis used the validated equivalent-linear site response analysis program CARES Version 2.0. SDE-SASSI is an expanded and fully validated version of the SASSI computer code, which includes a transmitting boundary at the base (Figure 2.5.2-80). The model also includes transmitting boundary elements on both vertical sides of the finite element mesh. The side transmitting boundary elements were located at each node of the mesh boundary and are defined by spring/dashpot elements for both normal and shear motions at the boundary node. The purpose of these boundary elements is to minimize the effects of the numerical boundaries on the computed response in the central region of the mesh. The input motion was assumed to be located at the top of the basement rock and is an outcrop motion (Figure 2.5.2-80).

Other pertinent data on rock properties (Poisson's ratio, unit weight, and hysteretic material damping ratio) used in the 2D computational zone were also adopted from the GMRS analysis. Poisson's ratio was required in the 2D analysis. A value of 0.25 was used, which is a typical value for hard rock, and was measured in dynamic laboratory tests of rock samples from the same formation located approximately 30 mi southwest of the CRN Site. It was not necessary to run the lower-range and upper-range V_S profiles considered in the GMRS 1D analysis in the 2D analysis because both profiles were developed to accommodate 2D effects.

A basement outcrop horizontal time history, spectrally-matched to the enveloped GMRS, was used as input to both the 1D and 2D calculations. Because the 2D analysis was a linear analysis, the results are not sensitive to control motion spectral shapes provided it has sufficient amplitude across spectral frequency to excite the 5 percent-damped oscillators. The smooth GMRS reflects design levels of motion over a wide bandwidth and was selected to reflect control motions for the 2D analyses. The seed time history was the Pacoima Kagel Canyon record of the 1994 **M** 6.7 Northridge, California earthquake (Figure 2.5.2-83). The spectral matching meets the applicable criteria from NUREG-0800. The 5-95 percent Arias intensity was 21.79 m/s. The 5 percent-damped response spectra for this time history record as computed by both the CARES and RASCALS programs are very similar (Figure 2.5.2-84).

The 1D site profiles (velocity and hysteric material damping) used in the 1D CARES calculations were then used in the 2D/1D spectral comparisons. The response calculations, 1D and 2D, were performed using linear properties, with no strain iteration considered in the computations.

Figure 2.5.2-80 presents a schematic diagram of the 2D SASSI model used to evaluate site effects. The CRN Site is represented by 2D triangular and quadrilateral finite elements generated throughout the zone of influence, considered from the surface down to and into the basement rock and from the left to right boundary (Figure 2.5.2-82). As previously stated, results were calculated at three points for both Locations A and B.

For the 2D calculations, the input horizontal time history is defined at the top of basement as a normally (vertical) incident outcrop motion applied in the plane of the figure; that is, the problem considered is SV wave (vertically-polarized shear-wave) transmission (Figure 2.5.2-80). Vertical input and corresponding surface output motions were not considered in the 2D analysis because potential effects on the vertical component are expected to be less than the horizontal as the compressional-wave velocities are significantly greater than the shear-wave velocities. No horizontal wave passage effects are considered in the calculations. Transmitting boundary conditions are assumed along the two vertical side boundaries in the form of both horizontal and vertical dashpots applied at each node along the vertical boundaries, which accommodate approximate normal wave incidence. The purpose of these boundary elements is to minimize the energy feedback off these computational boundaries back into the large 2D mesh. The lack of usage of such elements may lead to significant increase in mesh response, particularly at relative low frequency (between 1 and 5 Hz for such a site profile). The transmitting boundary formulation used in these calculations is based on the simple viscous Lysmer-Kuhlemeyer (References 2.5.2-170 and 2.5.2-171) model, and has been long used in such wave transmission calculations ~~(References 2.5.2-170 and 2.5.2-171)~~ in both finite-element and finite-difference wave propagation.

The semi-infinite half-space at the base of the 2D SASSI model consists of two parts: (1) the addition of 20 layers having a total depth of 1.5 V_Sb / f (where 'V_Sb' is the V_S of the basement half-space and 'f' is the frequency of the analysis) and (2) the addition of horizontal and vertical dashpots applied at the base of the extended layered site model. This modeling approach is inherent within the SASSI code and is intended to minimize any reflections off the bottom

boundary of the model. The transmitting boundary models have been found to be an important component of these large half-space problems.

For the CRN Site calculations, two finite element meshes were developed for the 2D calculations, a fine and coarse mesh, established throughout the computational zone (20,000 ft wide by 14,800 ft deep) (Figure 2.5.2-80). The fine mesh described earlier with a 50 Hz transmission capability is computationally very large, resulting in a mesh having about 500,000 finite elements (with over 1,000,000 degrees-of-freedom, two at each node) and requires large computer capacity along with modern matrix solvers. Figure 2.5.2-81 presents a snapshot of the fine mesh in the CRN Site. For the firm and hard rocks in the fine mesh, the resulting element dimensions are on average about 28 ft.

A coarse mesh model was developed to have a transmission capability limited to about 10 Hz. The average element size for the coarse mesh is about five times larger than those of the fine mesh, or about 125 ft. The coarse mesh model results in a much smaller (as compared to the fine model) complex dynamic matrix to be solved at each frequency of interest, and allows the solutions to be obtained much more efficiently. The comparisons of results at low frequency (less than 10 Hz) are used to provide support and verification to the fine mesh solutions. This coarse mesh calculation is especially appropriate where the most significant 2D effects are expected to be most pronounced at low frequencies (below 10 Hz).

Figures 2.5.2-85 and 2.5.2-86 present the results of the horizontal surface response spectra for Locations A and B, respectively, from the 2D calculations for the fine mesh. The 2D spectra generated at the sites in Locations A and B span a distance of about 400 ft from the left to the right side. The lognormal mean of the three spectra for each site was also computed and is plotted in the figures. The three 2D spectral results show the scatter expected for three different locations in each area.

Figures 2.5.2-87 and 2.5.2-88 present the lognormal-mean horizontal 2D surface spectra for Locations A and B, respectively, as compared to the resulting 1D surface spectra. The 2D effect of the rock layering essentially eliminates the higher frequencies (above about 5 to 6 Hz) from the response; that is, the 2D response spectra fall off rapidly from the 1D response spectra at the higher frequencies. This is primarily due to the scattering of the high-frequency responses caused by the non-horizontal layer interfaces. Figures 2.5.2-89 and 2.5.2-90 present the same spectra as in Figures 2.5.2-87 and 2.5.2-88, but after smoothing with a seven-point averaging window. To achieve statistical stability of the spectral ratios, both the numerator (2D) and denominator (1D) were smoothed separately prior to taking the ratios.

Figure 2.5.2-91 presents the corresponding 2D/1D effect on smoothed surface spectral response for Locations A and B, in terms of response spectral ratios. The spectral ratios are all below 1 except for ~~two~~ one small exceedance~~s~~ at Location B (less than 10 percent). The 2D scattering effect removes the higher frequency responses (above about 5 to 6 Hz). At lower frequencies, the 2D scattering effect can cause the response to increase but the ratios are still below 1 (Figure 2.5.2-91).

In summary, in this sensitivity analysis, the resulting 2D response for the ~~best~~ best-estimate profile properties indicates no significant exceedance of the 1D response. This is due to the site V_S being high for this site and the differences in velocities between rock layers not being significant, reducing the magnitude of the 2D effects at lower frequencies of interest. As stated in Section 2.5.2.5.1, the use of multiple basescase velocity profiles in calculating the GMRS is expected to accommodate potential 2D effects from dipping layers. Also in examining the FAS of the small earthquakes recorded at Tellico Dam as part of the kappa evaluation, no broadband resonances were observed suggesting that 2D effects are not present at the site. Tellico Dam

has a similar dipping structure beneath it as does the CRN Site. ~~No~~ Hence no adjustment of the GMRS for 2D effects is required based on the implementation of multiple basecase V_S profiles in the site response analysis and the results of the 2D sensitivity analysis.

As a result of the replaced text in Subsection 2.5.2.5 the following references are added at the end of SSAR Subsection 2.5.2.7:

2.5.2-171. Lysmer, J. and R.L. Kuhlemeyer, Finite-dynamic model for infinite media: ASCE, JEM Div., Vol. 95, p. 859, 1969.

2.5.2-172. URS Corporation, Site-specific probabilistic seismic hazard analysis and development of ground motion response spectra for Watts Bar Nuclear Plant Unit 2: unpublished report prepared for Tennessee Valley Authority, 2014.

2.5.2-173 Hatcher, R.D., Jr., Report to accompany cross-sections through the proposed CRN Nuclear site, unpublished report prepared for TVA, 2015.

2.5.2-174 Boore, D.M. and Joyner, W.B., Site amplifications for generic rock sites: Bulletin of the Seismological Society of America, Vol. 87, p. 327-341, 1997.

2.5.2-175 Anderson, J.G. and S.E. Hough, A model for the shape of the Fourier amplitude spectrum of acceleration at high frequencies: Bulletin of the Seismological Society of America, Vol. 74, p. 1969–1993, 1984.

2.5.2-176 Silva, W.J. and R. Darragh, Engineering characterization of strong ground motion recorded at rock sites: Electric Power Research Institute, EPRI TR-102262, 1995.

2.5.2-177 Laurendeau, A., F. Cotton, O.-J. Ktenidou, L.–F. Bonilla, and F. Hollender, Rock and stiff-soil site amplification: Dependency on V_S30 and kappa: Bulletin of Seismological Society of America, Vol. 103(6), p. 3131-3148, 2013.

2.5.2-178 Hatcher, R. D., Lemiszki, P. J., and Whisner, J. B., Character of rigid boundaries and internal deformation of the southern Appalachian foreland fold-thrust belt: Geological Society of America Special Papers 2007, Vol. 433, p. 243-276, 2007.

2.5.2-179 Ktenidou O.-J., Cotton F., Abrahamson N.A., and Anderson J.G., Taxonomy of kappa: a review of definitions and estimation methods targeted to applications: Seismological Research Letters, Vol. 85(1), p. 135-146, 2014.

2.5.2-180 Ancheta, T.D., Darragh, R.B., Stewart, J.P., Seyhan, E., Silva, W.J., Chiou, B.S.J., Woodell, K.E., Graves, R.W., Kottke, A.R., Boore, D.M., Kishida, T. and Donahue, J.L., PEER NGA-West2 Database: PEER Report 2013/03, Pacific Earthquake Engineering Research Center, Berkeley, CA, 2013.

2.5.2-181 Goulet, C. A., Kishida, T., Ancheta, T.D., Cramer, C. H. Darragh, R.B., Silva, W.J., Hashash, Y. M. A., Harmon, J., Stewart, J.P., Woodell, K.E., and Youngs, R. R., PEER NGA-East Database: PEER Report 2014/17, Pacific Earthquake Engineering Research Center, Berkeley, CA., 2014

2.5.2-182 Boore, D.M. and Atkinson, G. M., Point-source prediction of ground motion and spectral response parameters at hard-rock sites in eastern North America: Bulletin of Seismological Society of America, Vol. 77(2), p. 440-467, 1987.

2.5.2-183 Toro, G.R. and McGuire, R.K., An investigation into earthquake ground motion characteristics in eastern North America: Bulletin of Seismological Society of America, Vol. 77(2), p. 468-489, 1987.

2.5.2-184 Silva, W.J., and Green, R.K., Magnitude and distance scaling of response spectral shapes for rock sites with applications to North American tectonic environment: Earthquake Spectra, Vol. 5(3), p. 591-624, 1989.

2.5.2-185 Silva, W.J., Global characteristics and site geometry: Chapter 6 in Proceedings NSF/EPRI Workshop of Dynamic Soil Properties and Site Characterization. Palo Alto, CA. Electric Power Research Institute, EPRI NP-7337, 1991.

2.5.2-186 Darragh, B. Abrahamson, N.A., Silva, W.J. and Gregor, N., Development of hard rock ground-motion models for Region 2 of Central and Eastern North America: in Goulet, C. A., Kishida, T., Ancheta, T.D., Cramer, C. H. Darragh, R.B., Silva, W.J., Hashash, Y. M. A., Harmon, J., Stewart, J.P., Woodell, K.E., and Youngs, R. R. (2014). PEER NGA-East Database, PEER Report 2014/17, Pacific Earthquake Engineering Research Center, Berkeley, CA, 2014.

2.5.2-187 Kishida, T., Kayen, R. E., Ktenidou, O-J., Silva, W.J., Darragh, R.B., and Watson-Lamprey, J., PEER Arizona Strong-Motion Database and GMPEs Evaluation: PEER Report 2014/09, Pacific Earthquake Engineering Research Center, Berkeley, CA, 2014.

2.5.2-188 Press, W.H., Flannery, B.P., Teukolsky, S.A., Vetterling, W.T., Numerical Recipes: Cambridge University Press, Cambridge, 1986.

2.5.2-189 Boatwright, J and L. Seekins, Regional spectral analysis of three moderate earthquakes in northeastern North America: Bulletin of Seismological Society of America, Vol. 101(4), p. 1769-1782, 2011.

2.5.2-190 Silva, W.J., R. Darragh, N. Gregor, G. Martin, C. Kircher, N. Abrahamson, Reassessment of site coefficients and near-fault factors for building code provisions: Final Report USGS Grant award #98-HQ-GR-1010., 1999.

2.5.2-191 Power, M., B. Chiou, N. Abrahamson, Y. Bozorgnia, T. Shantz, C. Roblee, An overview of the NGA project: Earthquake Spectra, Vol. 24(1), p. 3-21., 2008.

2.5.2-192 Bozorgnia et al., NGA-West2 Research Project: Earthquake Spectra, Vol. 30(3), p. 973-988., 2014.

2.5.2-193 Boore, D.M., Thompson, E.M., and Cadet, H., Regional correlations of Vs30 and velocities averaged over depths less than and greater than 30 m: Bulletin of the Seismological Society of America, Vol. 101, p. 3046-3059, 2011.

2.5.2-194 Abrahamson, N.A., Silva, W.J., and Kamai, R., Summary of the ASK14 ground-motion relation for active crustal regions: Earthquake Spectra, Vol. 30, p. 1025-1055, 2014.

2.5.2-195 Abercrombie, R.E., A summary of attenuation measurements from borehole recordings of earthquakes: the 10 Hz transition problem: Pure and Applied Geophysics, Vol. 153, p. 475-487, 1998.

2.5.2-196 Hauksson, E., Teng, T.L., and Henyey, T.L., Results from a 1500m deep, three level downhole seismometer array: site response, low Q values, and fmax: Bulletin of the Seismological Society of America, Vol. 77, p. 1883-1904, 1987.

2.5.2-197 Fukushima, Y., J-Chris. Gariel, and R. Tanaka, Site-dependent attenuation relations of seismic motion parameters at depth using borehole data: Bulletin of the Seismological Society of America, Vol. 85(6), p. 1790-1804, 1995.

2.5.2-198 Bonilla, L. F., J. H. Steidl, J.C. Gariel, and R. J. Archuleta, Borehole response studies at the Garner Valley downhole array, southern California: Bulletin of the Seismological Society of America, Vol. 92, p. 3165-3179, 2002.

2.5.2-199 Redpath, B.B., R.B. Edwards, R.J. Hale, F.C. Kintzer, Development of field techniques to measure damping values for near-surface rocks and soils: Report prepared for the NSF earthquake hazards mitigation. Grant No. PFR-7900192: URS/John A. Blume & Associates, 1982.

2.5.2-200 Redpath, B.B., and C. Lee, In-situ measurements of shear-wave attenuation at a strong motion recording site: Report prepared for U.S.G.S. contract No. 14-08—001-21823: John A. Blume and Associates, 1986.

2.5.2-201 Field, E. H. and K. H. Jacob, Monte-Carlo simulation of the theoretical site response variability at Turkey Flat, California, given the uncertainty in the geotechnically derived input parameters: Earthquake Spectra, Vol. 9(4), 1993.

2.5.2-202 Rix, G., C. Lai, and A. Spang Jr., In-situ measurement of damping ratio using surface waves: Journal of Geotechnical and Geoenvironmental Engineering, Vol. 126(5), p. 472-480, 2000.

2.5.2-203 Assimaki, D., W. Li, J. H. Steidl, and K. Tsuda, Site amplification and attenuation via downhole array seismogram inversion: A comparative study of the 2003 Miyagi-oki aftershock sequence: Bulletin of the Seismological Society of America, Vol. 98, p. 301-330, 2005.

2.5.2-204 Zalachoris, G. Dipl., M.S.E., Evaluation of one-dimensional site response methodologies using borehole arrays: Dissertation Presented to the faculty of the graduate school of The University of Texas at Austin in Partial Fulfillment of the Requirements for the Degree of Doctor of Philosophy, The University of Texas at Austin, 2014.

2.5.2-205 Assimaki, D., W. Li, J. H. Steidl, and K. Tsuda, Site amplification and attenuation via downhole array seismogram inversion: A comparative study of the 2003 Miyagi-oki aftershock sequence: Bulletin of the Seismological Society of America, Vol. 98, p. 301-330, 2008.

2.5.2-206 Choi, W. K., Dynamic properties of ash-flow tuffs: Dissertation Presented to the faculty of the graduate school of The University of Texas at Austin in Partial Fulfillment of the Requirements for the Degree of Doctor of Philosophy, The University of Texas at Austin, 2008.

2.5.2-207 Jeon, S.Y., Dynamic and cyclic properties in shear of tuff specimens from Yucca Mountain, Nevada: Dissertation Presented to the faculty of the graduate school of The University of Texas at Austin in Partial Fulfillment of the Requirements for the Degree of Doctor of Philosophy, The University of Texas at Austin, 2008.

2.5.2-208 Mavko, G., Mukerji, T., and Dvorkin, J., The Rock Physics Handbook: Cambridge University Press, 1998.

2.5.2-209 Electric Power Research Institute (EPRI), Seismic Evaluation Guidance: Screening, Prioritization, and Implementation Details (SPID) for the Resolution of Fukishima Near-Term Task For Recommendation 2.1: Seismic, 2013b.

As a result of the revised text in Subsection 2.5.2.5.1, Tables 2.5.2-30, 2.5.2-31, and 2.5.2-32 are added at the end of SSAR Subsection 2.5.2:

Table 2.5.2-30
Unit Weights

Geologic Unit	Unit Weight (pcf)
Benbolt	168
Rockdell	168
Fleanor	168
Eidson	168
Blackford	168
Newala	168
Knox	168
Conasauga	170
Pumpkin Valley	175
Rome	175

Table 2.5.2-31
Processed Earthquake Data Used at Tellico Dam Site

Earthquake Date (YrMoDy)	Time (UTC)	Mag	Latitude	Longitude	Depth (km)	Epicentral Distance (km)	Hypocentral Distance (km)	Comment	Low Frequency Limit SNR ≤ 3
041223	6:54	3.0	35.4293	-84.2042	7.68	39	39.8	Only one horizontal	
060317	15:20	1.0	35.7100	-84.1600	13	12	18.8		5.0
060411	3:29	3.3	35.3600	-84.4800	19.81	50.4	54.2		1.6
060413	6:26:35	2.2	35.6000	-84.3500	12.1	21.3	24.5		1.5
060510	12:17	3.2	35.5330	-84.3960	24.7	30.2	39.0		1.0
061218	8:34	3.0	35.3560	-84.3508	17.69	46.8	49.9		2.5
061226	11:25	1.8	35.7610	-84.3180	14.3	5.4	15.3		7.0
070103	23:06	2.8	35.9080	-83.9420	14.7	32.2	35.4		5.0
070210	18:43	1.3	35.6730	-84.2767	12.07	11.8	17.6		6.0
070221	6:38	1.4	35.6722	-84.2772	11.56	11.6	16.4		15.0
070412	1:37	2.1	35.4700	-84.3800	11.4	35.8	37.6		3.0
070608	9:11	1.6	35.7000	-84.1500	20.0	13.2	24.0		6.0
070614	17:06	2.4	35.5400	-84.1300	7.0	28.9	29.7		3.0
070811	21:24	2.0	35.7200	-84.1000	10.2	15.9	16.4		4.0
070910	18:01	1.6	35.6700	-84.5400	14.6	27.9	28.1		7.0
070916	13:10	1.4	35.7900	-84.1700	15.1	8.3	17.2		8.0
071023	5:15	2.8	35.5900	-84.1000	21.0	25.3	33.2		2.0
071123	5:48	2.4	35.5300	-84.3000	17.0	27.7	32.5		4.0
071209	6:58	2.4	36.2500	-84.3700	21.0	53.5	57.5		6.0
080111	2:11	0.9	35.6200	-84.3300	15.99	18.5	24.5		15.0

Table 2.5.2-32
Kappa Estimates (Range) for the CRN Site

Method	Lower Kappa Values (s)	Upper Kappa Values (s)
Response Spectral Shape (Reference 2.5.2-176)	0.006	0.009
Anderson and Hough (Reference 2.5.2-175)	0.010	0.016

As a result of the revised text in Subsection 2.5.2.5.1, the following Figures are added at the end of SSAR Subsection 2.5.2:

Figure 2.5.2-56. Shear Modulus Reduction and Damping Curves for Firm Rock

Figure 2.5.2.66. Horizontal Amplification Factors, 5 Percent-Damped Pseudo-Absolute Spectra, Profile P1, EPRI Rock Curves M1, M 5.5, 0.01 to 0.40 g for Location B

Figure 2.5.2-67. Horizontal Amplification Factors, 5 Percent-Damped Pseudo-Absolute Spectra, Profile P1, EPRI Rock Curves M1, M 5.5, 0.50 to 1.5 g for Location B

Figure 2.5.2-68. Horizontal Amplification Factors, 5 Percent-Damped Pseudo-Absolute Spectra, Profile P1, EPRI Rock Curves M1, Single Corner, M 7.5, 0.01 to 0.40 g for Location A

Figure 2.5.2-69. Horizontal Amplification Factors, 5 Percent-Damped Pseudo-Absolute Spectra, Profile P1, EPRI Rock Curves M1, Single Corner, M 7.5, 0.5 to 1.5 g for Location

Copies of the revised Figures are provided on the following pages.

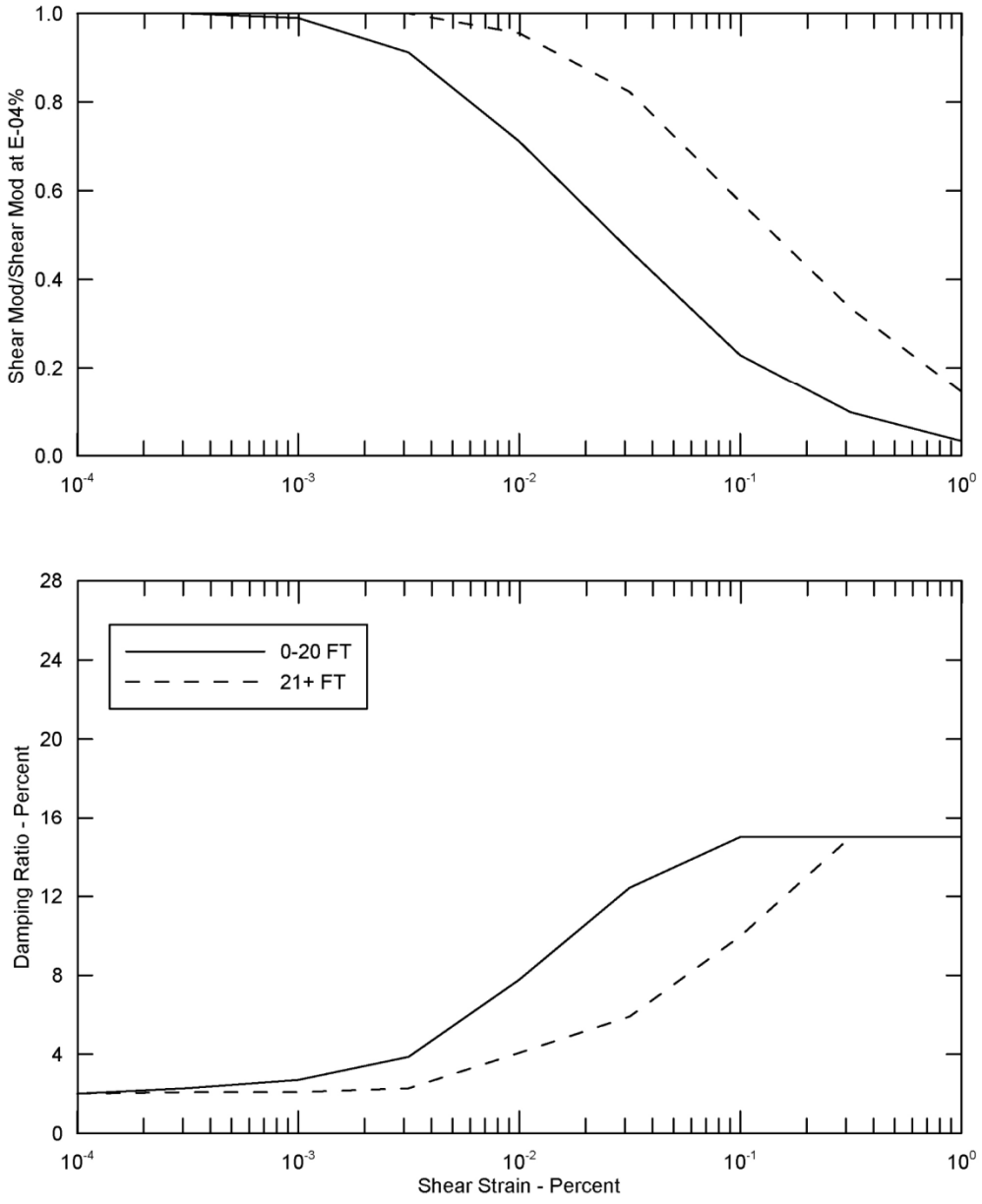

Figure 2.5.2-56. Shear Modulus Reduction and Damping Curves for Firm Rock

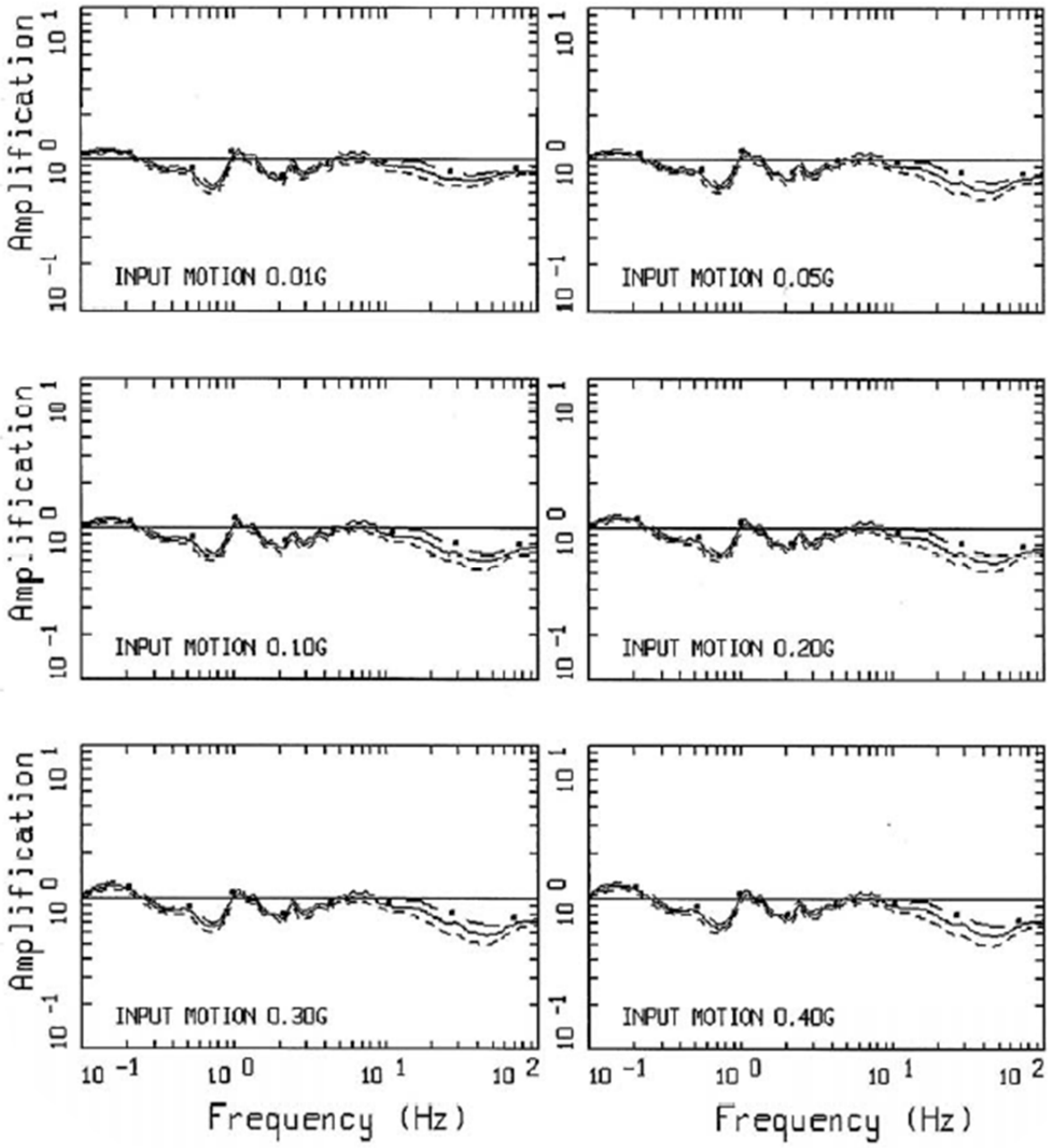

Note: Location shown on Figure 2.5.2-2.

Figure 2.5.2-66. Horizontal Amplification Factors, 5 Percent-Damped Pseudo-Absolute Spectra, Profile P1, EPRI Rock Curves M1, M 5.5, 0.01 to 0.40 g for Location B

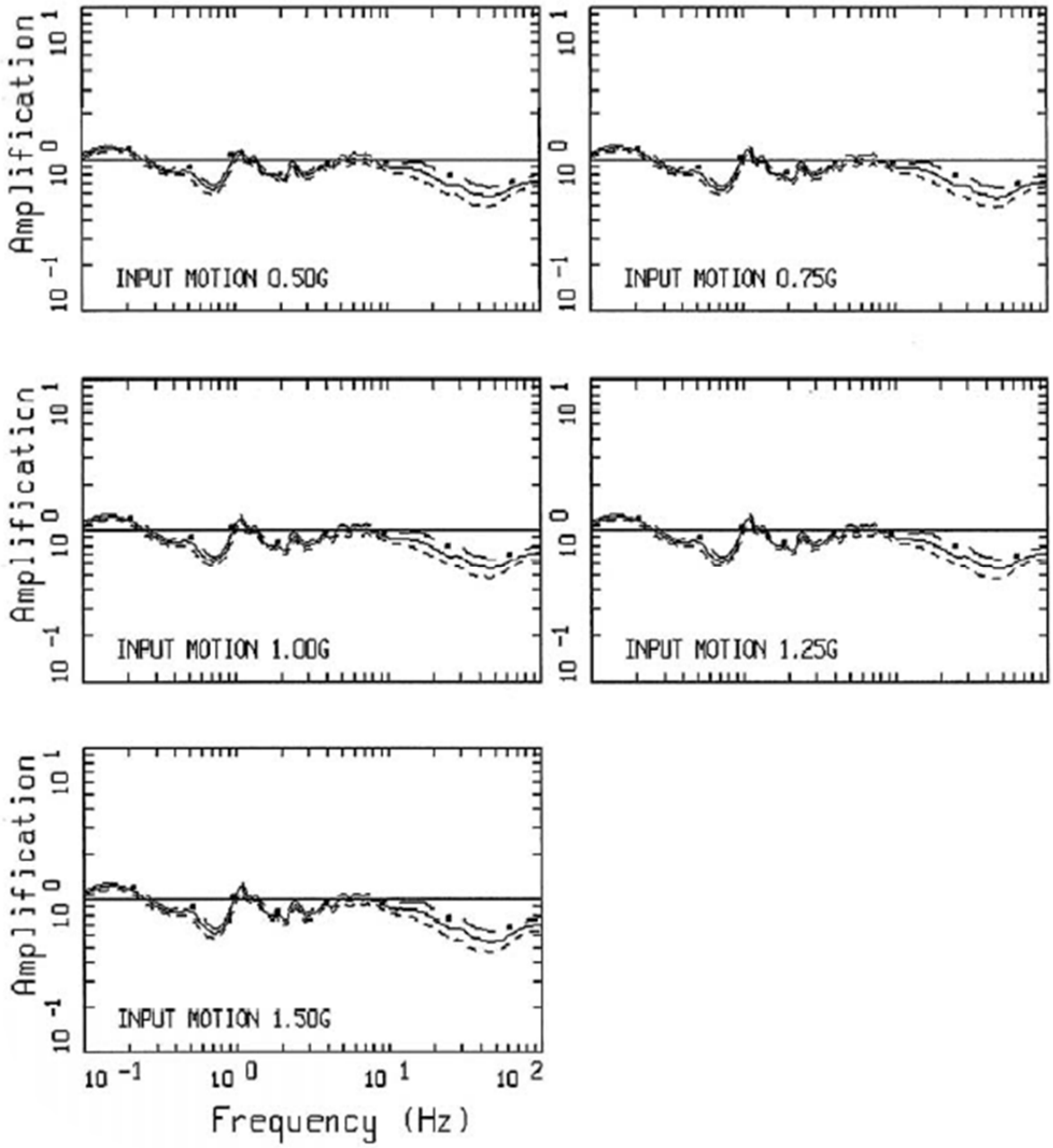

Note: Location shown on Figure 2.5.2-2.

Figure 2.5.2-67. Horizontal Amplification Factors, 5 Percent-Damped Pseudo-Absolute Spectra, Profile P1, EPRI Rock Curves M1, M 5.5, 0.50 to 1.5 g for Location B

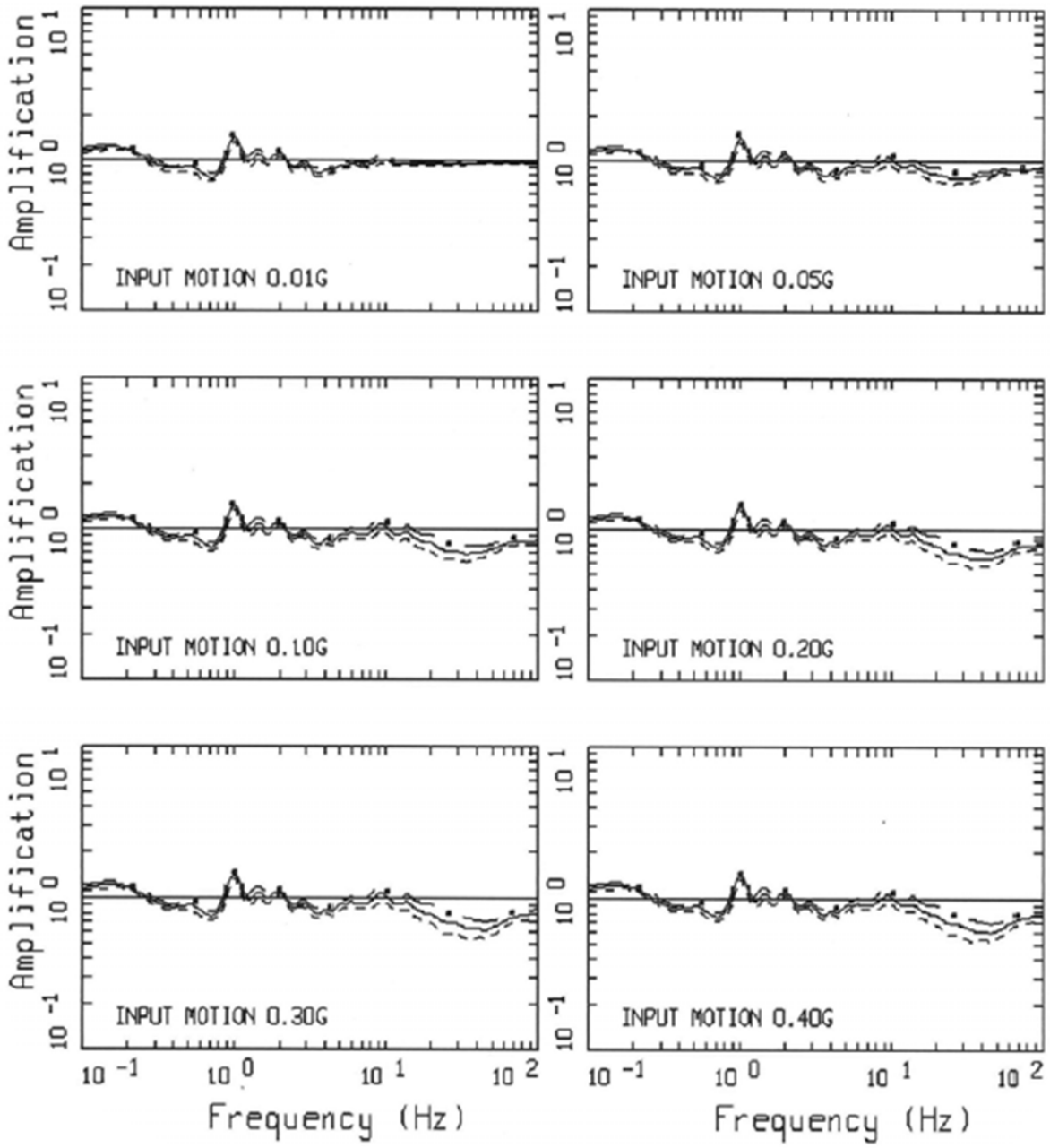

Note: Location shown on Figure 2.5.2-2.

Figure 2.5.2-68. Horizontal Amplification Factors, 5 Percent-Damped Pseudo-Absolute Spectra, Profile P1, EPRI Rock Curves M1, Single Corner, M 7.5, 0.01 to 0.40 g for Location A

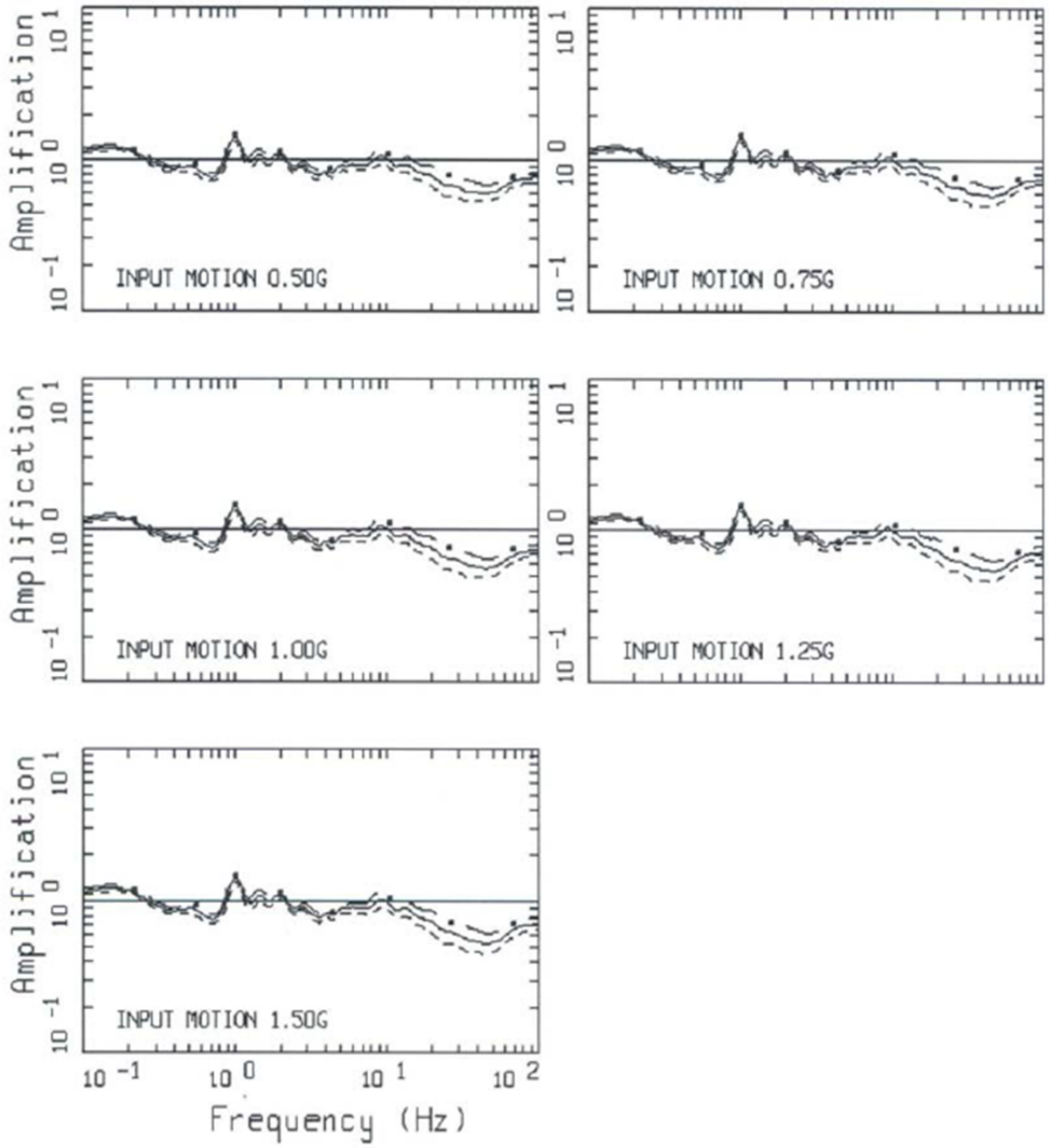

Note: Location shown on Figure 2.5.2-2.

Figure 2.5.2-69. Horizontal Amplification Factors, 5 Percent-Damped Pseudo-Absolute Spectra, Profile P1, EPRI Rock Curves M1, Single Corner, M 7.5, 0.5 to 1.5 g for Location A

As a result of the revised text in Subsection 2.5.2.5.1, the following Figures are added at the end of SSAR Subsection 2.5.2:

Figure 2.5.2-92. Clinch River V_s Profile Sigma for Each Chickamauga Subunit and Newala

Figure 2.5.2-93. Clinch River V_s Profile Cov for Each Chickamauga Subunit and Newala

Figure 2.5.2-94. TVA Damsite V_s Profile Sigma for Each Rock Type

Figure 2.5.2-95. TVA Damsite V_s Profile COV for Each For Type

Figure 2.5.2-96. Clinch River and TVA Damsite V_s Profile Sigmas

Figure 2.5.2-97. Clinch River and TVA Damsite V_s Profile COVS

Figure 2.5.2-98. Location of Tellico Dam

Figure 2.5.2-99. Geological sections through Tellico Dam and Vicinity

Figure 2.5.2-100. Tellico Dam Suspension PS log.

Figure 2.5.2-101. Interpreted shear-wave velocity at Tellico Dam. Velocity from suspension log in Boring TLH-4.

Figure 2.5.2-102. Smoothed Tellico Dam crustal transfer functions for local crustal model with a surface shear-wave velocity of 1,524m/s in the top 6.1m (20 ft) over hard rock (2,830m/s).

Figure 2.5.2-103. Response spectral shapes (5% damping) computed for M 2.0 at 20 km with kappa values of 0.005, 0.010 and 0.020s.

Figure 2.5.2-104. Response spectral shapes (5% damping) computed for M 6.5 at 20 km with kappa values of 0.005, 0.010 and 0.020s.

Figure 2.5.2.105. (Sheet 1 of 2) Vector average FAS computed from windowed shear-wave recordings of the twenty earthquakes analyzed at Tellico Dam: solid line as recorded, dashed line corrected for amplification (Figure 2.5.2-102) and Q(f) (630 $f^{0.5}$, Table 2.5.4-32).

Figure 2.5.2-105. (Sheet 2 of 2) Vector average FAS computed from windowed shear-wave recordings of the twenty earthquakes analyzed at Tellico Dam: solid line as recorded, dashed line corrected for amplification (Figure 2.5.2-102) and Q(f) (630 $f^{0.5}$, Table 2.5.4-32).

Figure 2.5.2-106. (Sheet 1 of 12) Vector average Fourier amplitude spectra for the twelve earthquakes analyzed corrected for amplification (Figure 2.5.2-102) and Q(f) (630 f^{05},Table 2.5.4-32) along with kappa fits over the bandwidths considered reliable (Section 2.5.2.5.2.3.2).

Figure 2.5.2.106. (Sheet 2 of 12) Vector average Fourier amplitude spectra for the twelve earthquakes analyzed corrected for amplification (Figure 2.5.2-102) and Q(f) (630 f^{05},Table 2.5.4-32) along with kappa fits over the bandwidths considered reliable (Section 2.5.2.5.2.3.2).

Figure 2.5.2.106. (Sheet 3 of 12) Vector average Fourier amplitude spectra for the twelve earthquakes analyzed corrected for amplification (Figure 2.5.2-102) and Q(f) (630 f^{05},Table 2.5.4-32) along with kappa fits over the bandwidths considered reliable (Section 2.5.2.5.2.3.2).

Figure 2.5.2.106. (Sheet 4 of 12) Vector average Fourier amplitude spectra for the twelve earthquakes analyzed corrected for amplification (Figure 2.5.2-102) and Q(f) (630 f^{05},Table 2.5.4-32) along with kappa fits over the bandwidths considered reliable (Section 2.5.2.5.2.3.2).

Figure 2.5.2.106. (Sheet 5 of 12) Vector average Fourier amplitude spectra for the twelve earthquakes analyzed corrected for amplification (Figure 2.5.2-102) and Q(f) (630 f05,Table 2.5.4-32) along with kappa fits over the bandwidths considered reliable (Section 2.5.2.5.2.3.2).

Figure 2.5.2.106. (Sheet 6 of 12) Vector average Fourier amplitude spectra for the twelve earthquakes analyzed corrected for amplification (Figure 2.5.2-102) and Q(f) (630 f^{05},Table 2.5.4-32) along with kappa fits over the bandwidths considered reliable (Section 2.5.2.5.2.3.2).

Figure 2.5.2.106. (Sheet 7 of 12) Vector average Fourier amplitude spectra for the twelve earthquakes analyzed corrected for amplification (Figure 2.5.2-102) and Q(f) (630 f^{05},Table 2.5.4-32) along with kappa fits over the bandwidths considered reliable (Section 2.5.2.5.2.3.2).

Figure 2.5.2.106. (Sheet 8 of 12) Vector average Fourier amplitude spectra for the twelve earthquakes analyzed corrected for amplification (Figure A-6) and Q(f) (630 f^{05},Table 2.5.4-32) along with kappa fits over the bandwidt2.5.2-102hs considered reliable (Section 2.5.2.5.2.3.2).

Figure 2.5.2.106. (Sheet 9 of 12) Vector average Fourier amplitude spectra for the twelve earthquakes analyzed corrected for amplification (Figure 2.5.2-102) and Q(f) (630 f^{05},Table 2.5.4-32) along with kappa fits over the bandwidths considered reliable (Section 2.5.2.5.2.3.2).

Figure 2.5.2.106. (Sheet 10 of 12) Vector average Fourier amplitude spectra for the twelve earthquakes analyzed corrected for amplification (Figure 2.5.2-102) and Q(f) (630 f^{05},Table 2.5.4-32) along with kappa fits over the bandwidths considered reliable (Section 2.5.2.5.2.3.2).

Figure 2.5.2.106. (Sheet 11 of 12) Vector average Fourier amplitude spectra for the twelve earthquakes analyzed corrected for amplification (Figure 2.5.2-102) and Q(f) (630 f^{05},Table 2.5.4-32) along with kappa fits over the bandwidths considered reliable (Section 2.5.2.5.2.3.2).

Figure 2.5.2.106. (Sheet 12 of 12) Vector average Fourier amplitude spectra for the twelve earthquakes analyzed corrected for amplification (Figure 2.5.2-102) and Q(f) (630 f^{05},Table 2.5.4-32) along with kappa fits over the bandwidths considered reliable (Section 2.5.2.5.2.3.2).

Copies of the new Figures are provided on the following pages.

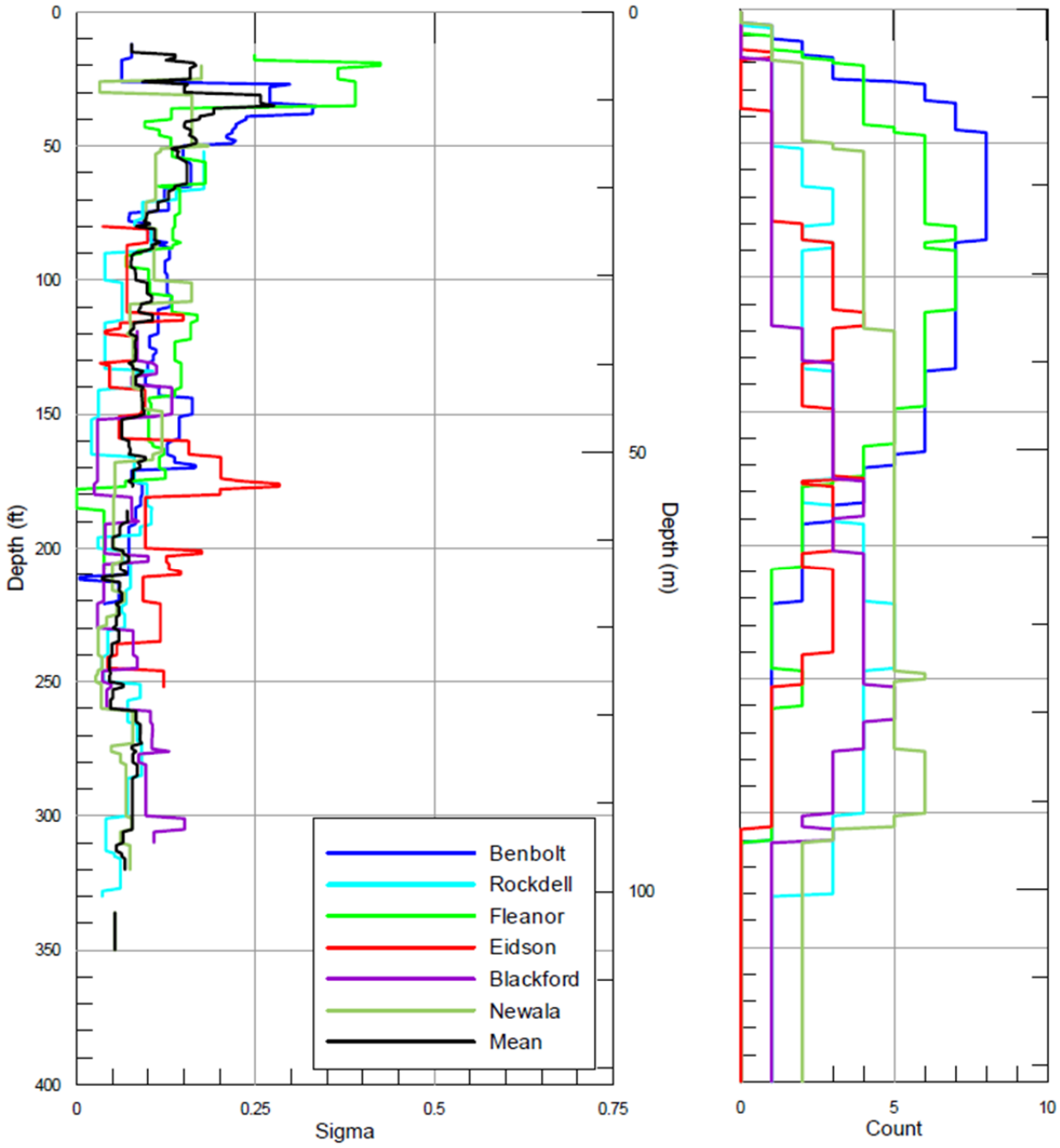

Note: At recorded depths

Figure 2.5.2-92. Clinch River V_S Profile Sigma for Each Chickamauga Subunit and Newala

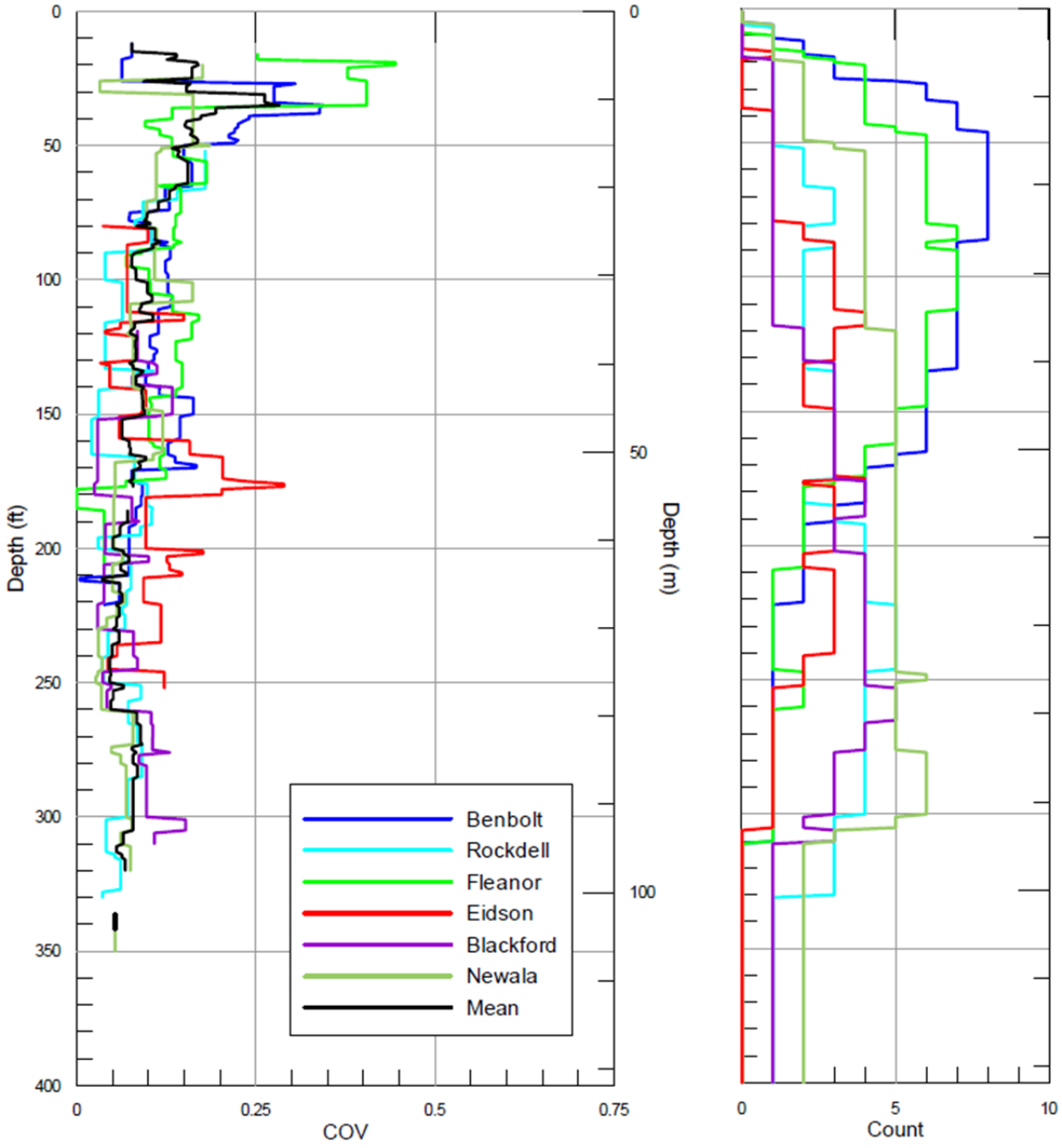

Note: At recorded depths

Figure 2.5.2-93. Clinch River V_S Profile Cov for Each Chickamauga Subunit and Newala

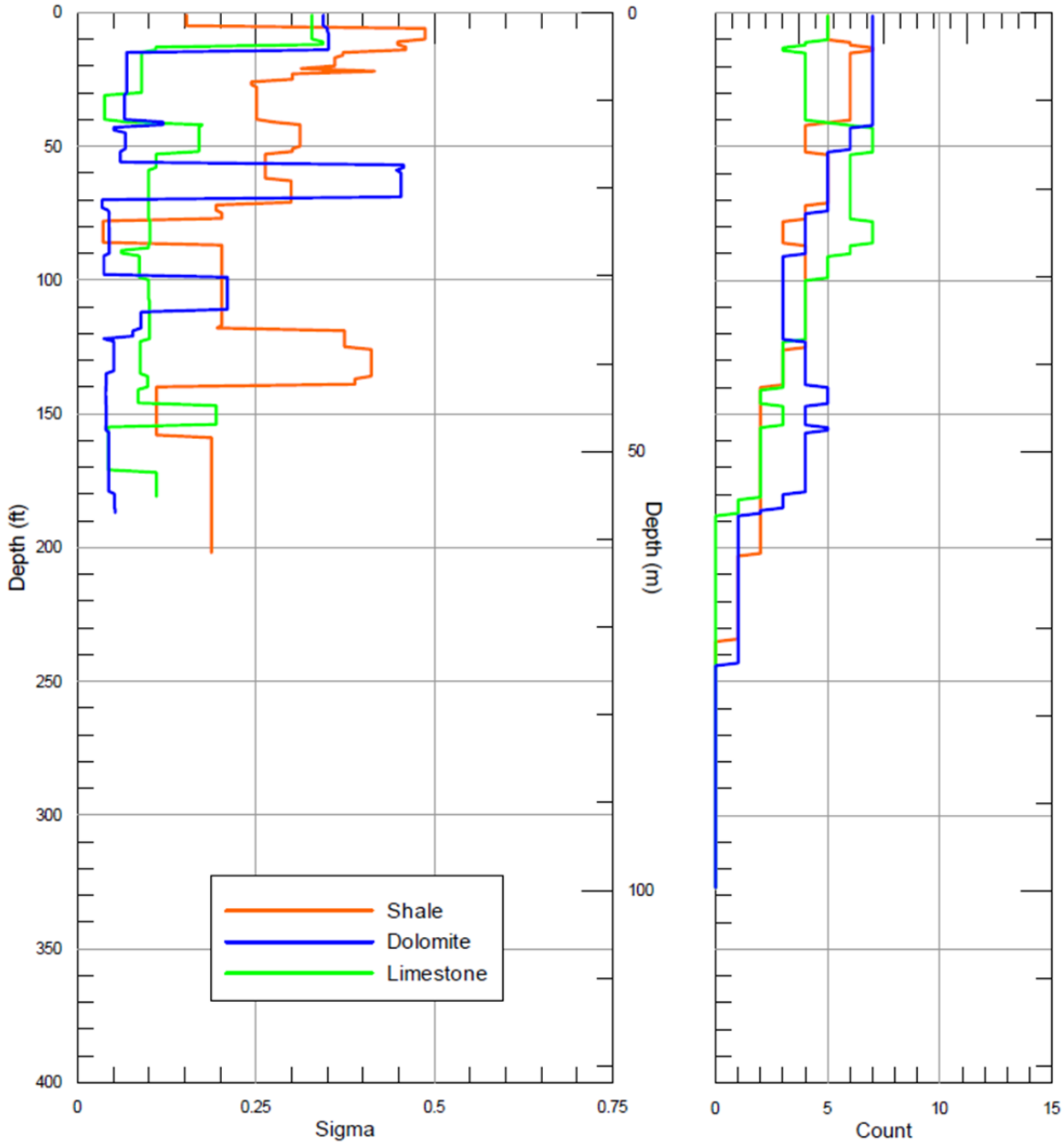

Figure 2.5.2-94. TVA Damsite V_S Profile Sigma for Each Rock Type

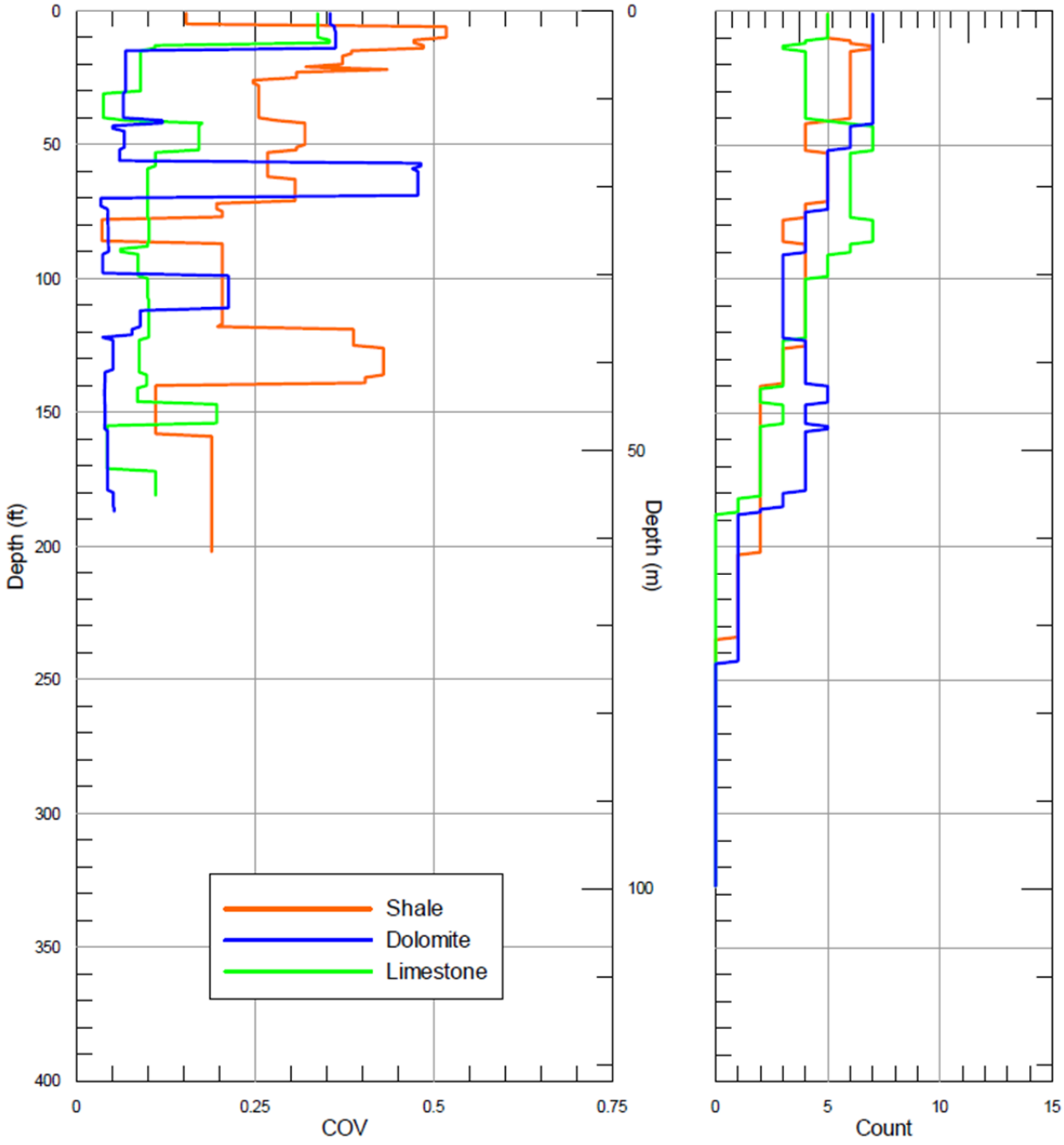

Figure 2.5.2-95. TVA Damsite V_S Profile COV for Each For Type

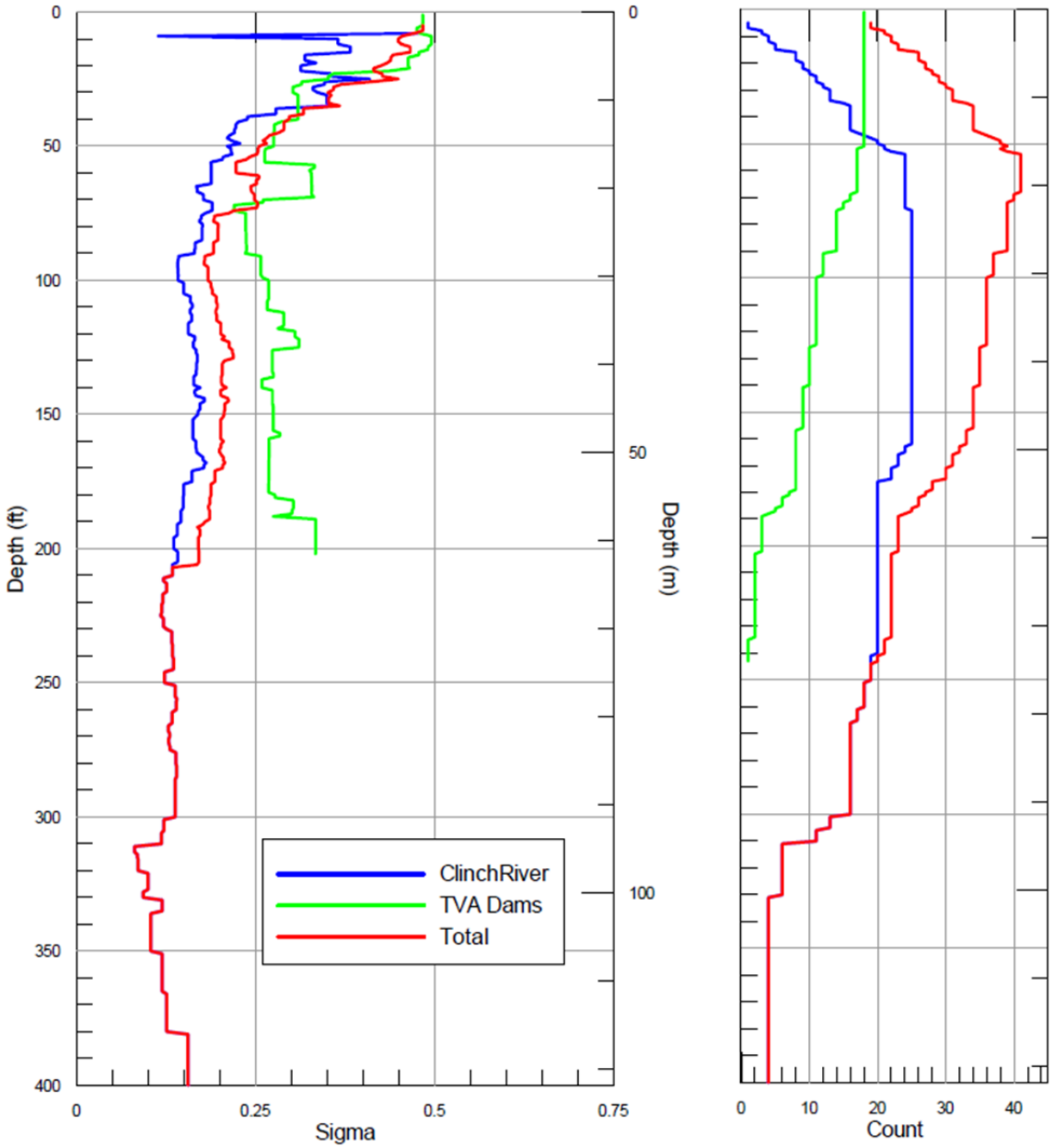

Figure 2.5.2-96. Clinch River and TVA Damsite V_S Profile Sigmas

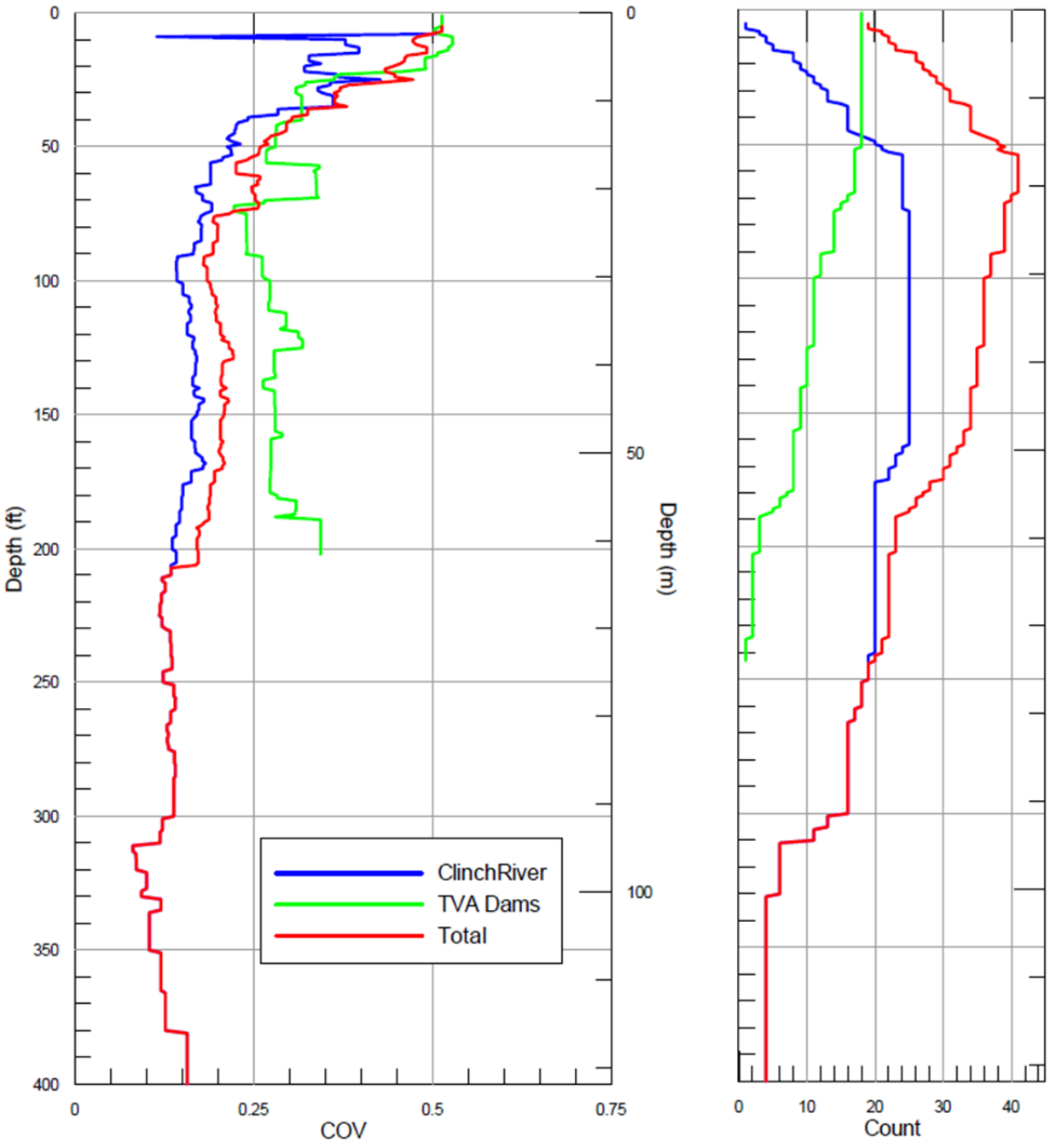

Figure 2.5.2-97. Clinch River and TVA Damsite V_S Profile COVS

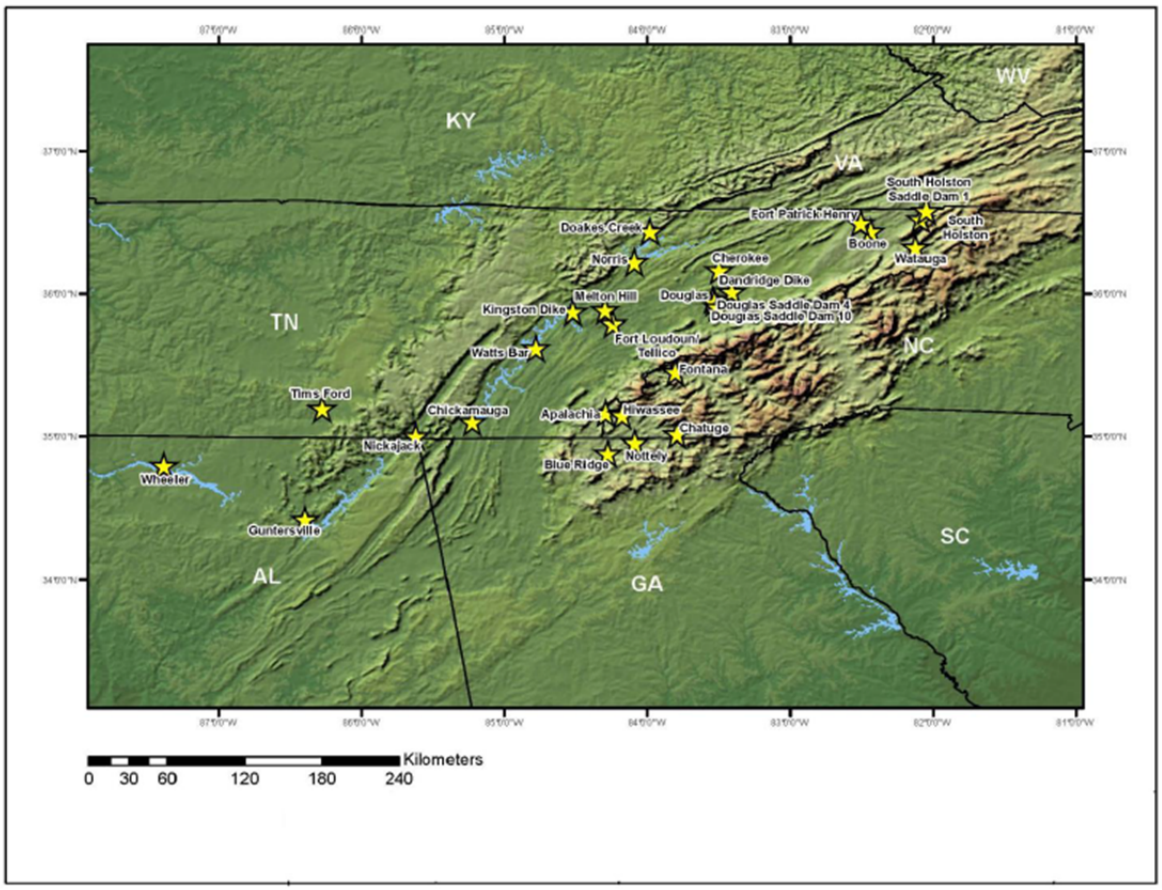

Figure 2.5.2-98. Location of Tellico Dam

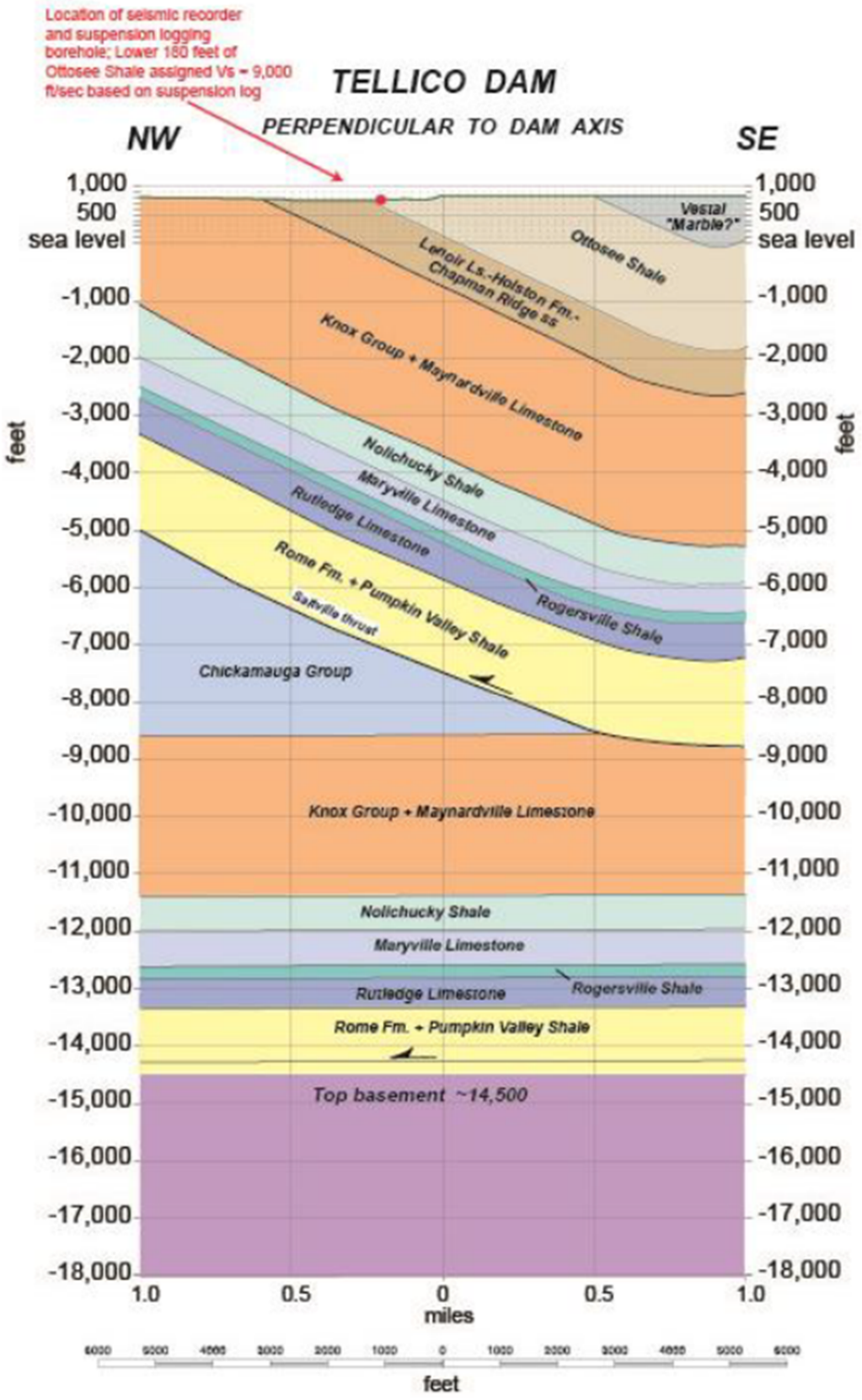

Figure 2.5.2-99. Geological sections through Tellico Dam and Vicinity

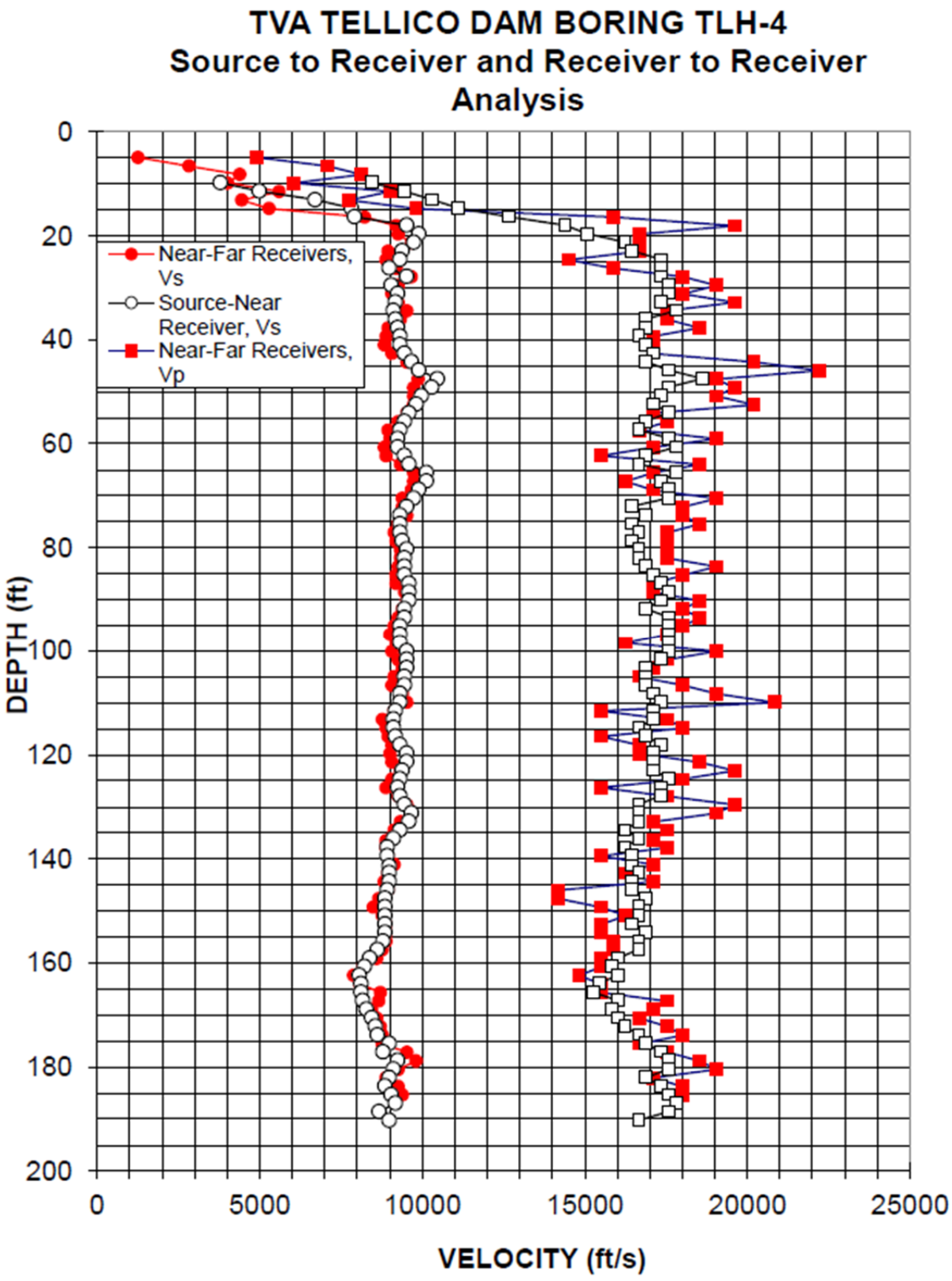

Figure 2.5.2-100. Tellico Dam Suspension PS log

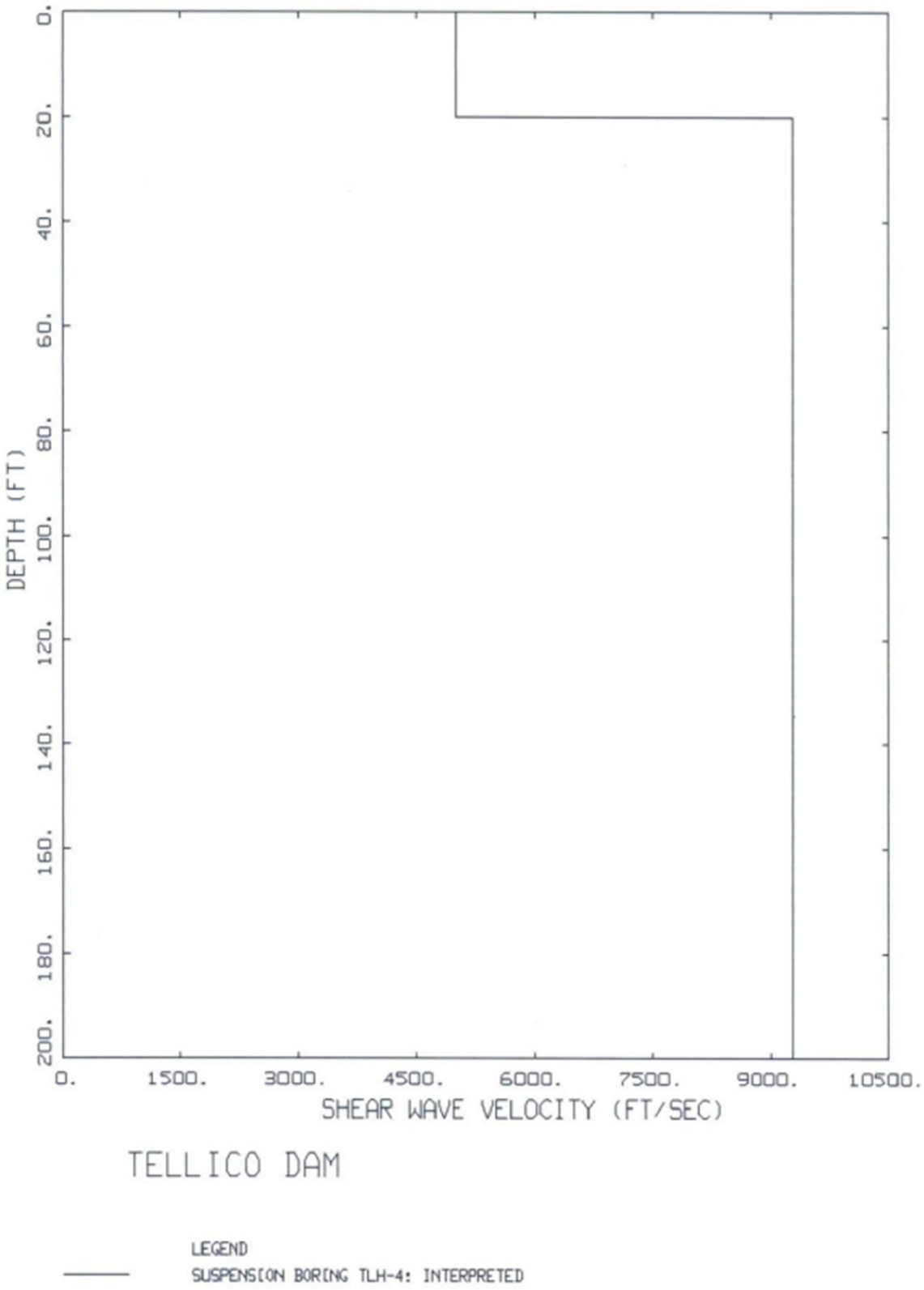

Figure 2.5.2-101. Interpreted shear-wave velocity at Tellico Dam. Velocity from suspension log in Boring TLH-4

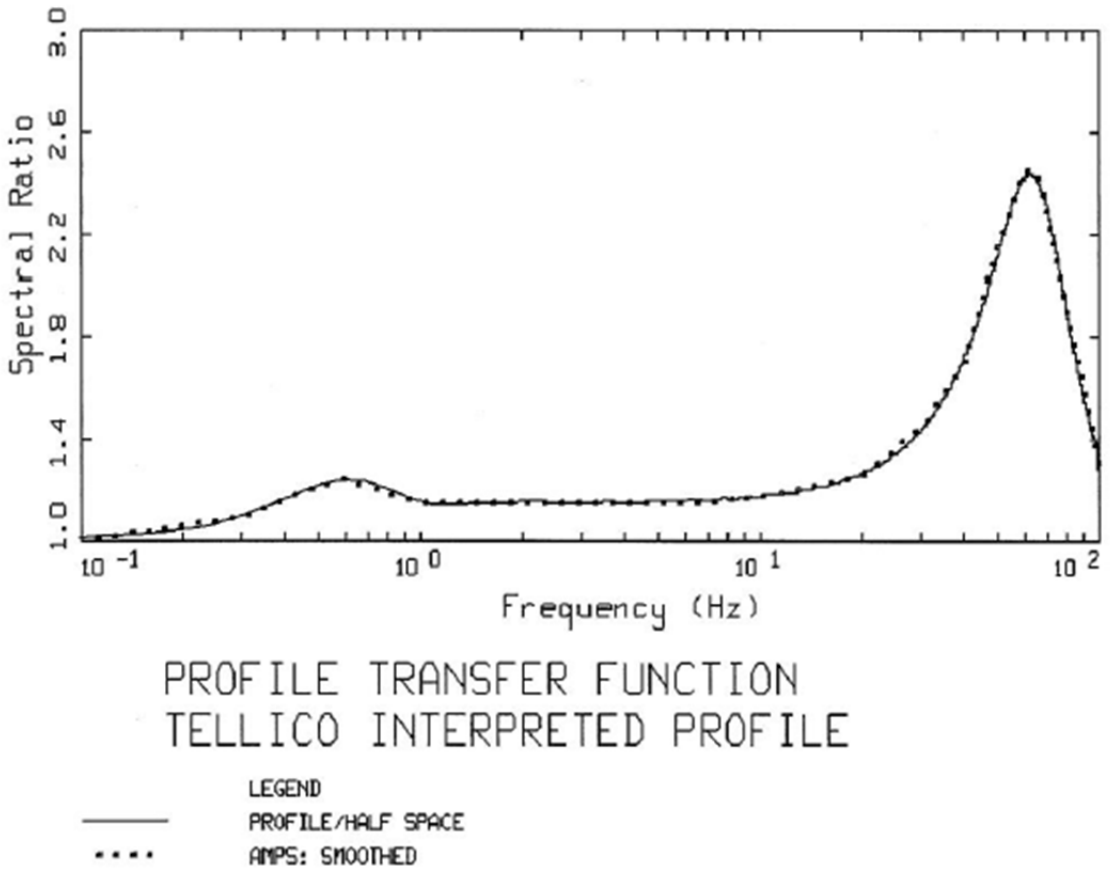

Figure 2.5.2-102. Smoothed Tellico Dam crustal transfer functions for local crustal model with a surface shear-wave velocity of 1,524m/s in the top 6.1m (20 ft) over hard rock (2,830m/s)

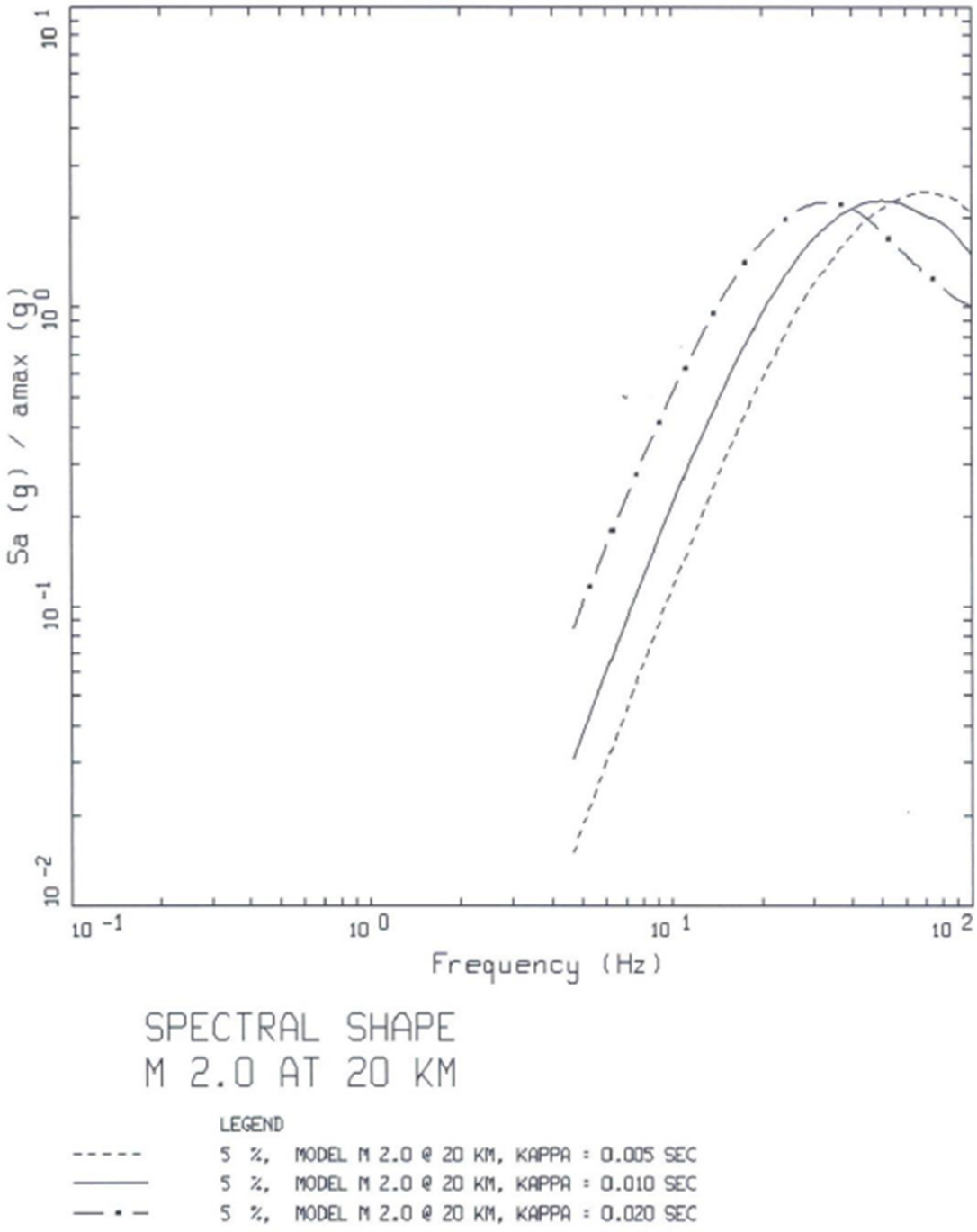

Figure 2.5.2-103. Response spectral shapes (5% damping) computed for M 2.0 at 20 km with kappa values of 0.005, 0.010 and 0.020s

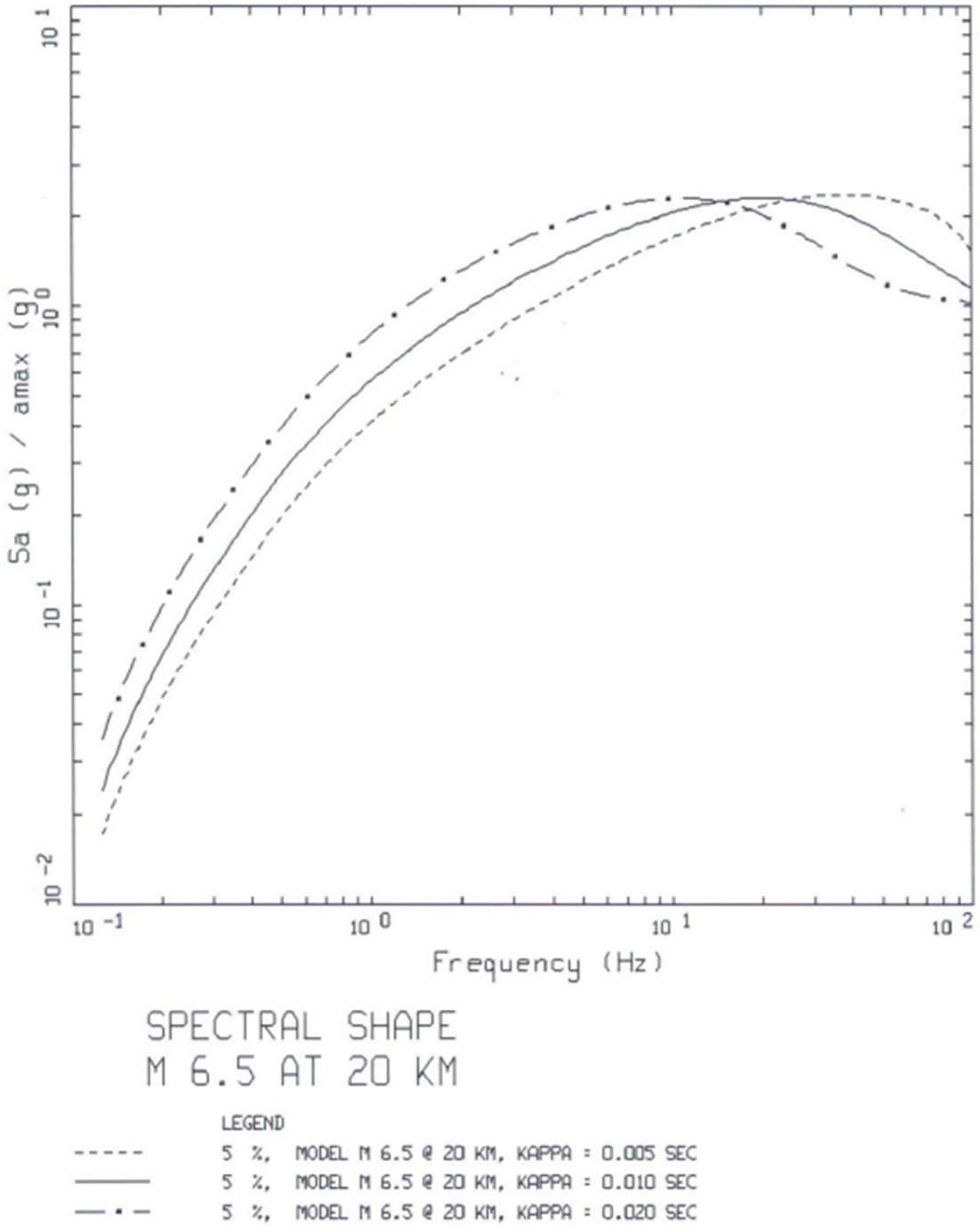

Figure 2.5.2-104. Response spectral shapes (5% damping) computed for M 6.5 at 20 km with kappa values of 0.005, 0.010 and 0.020s

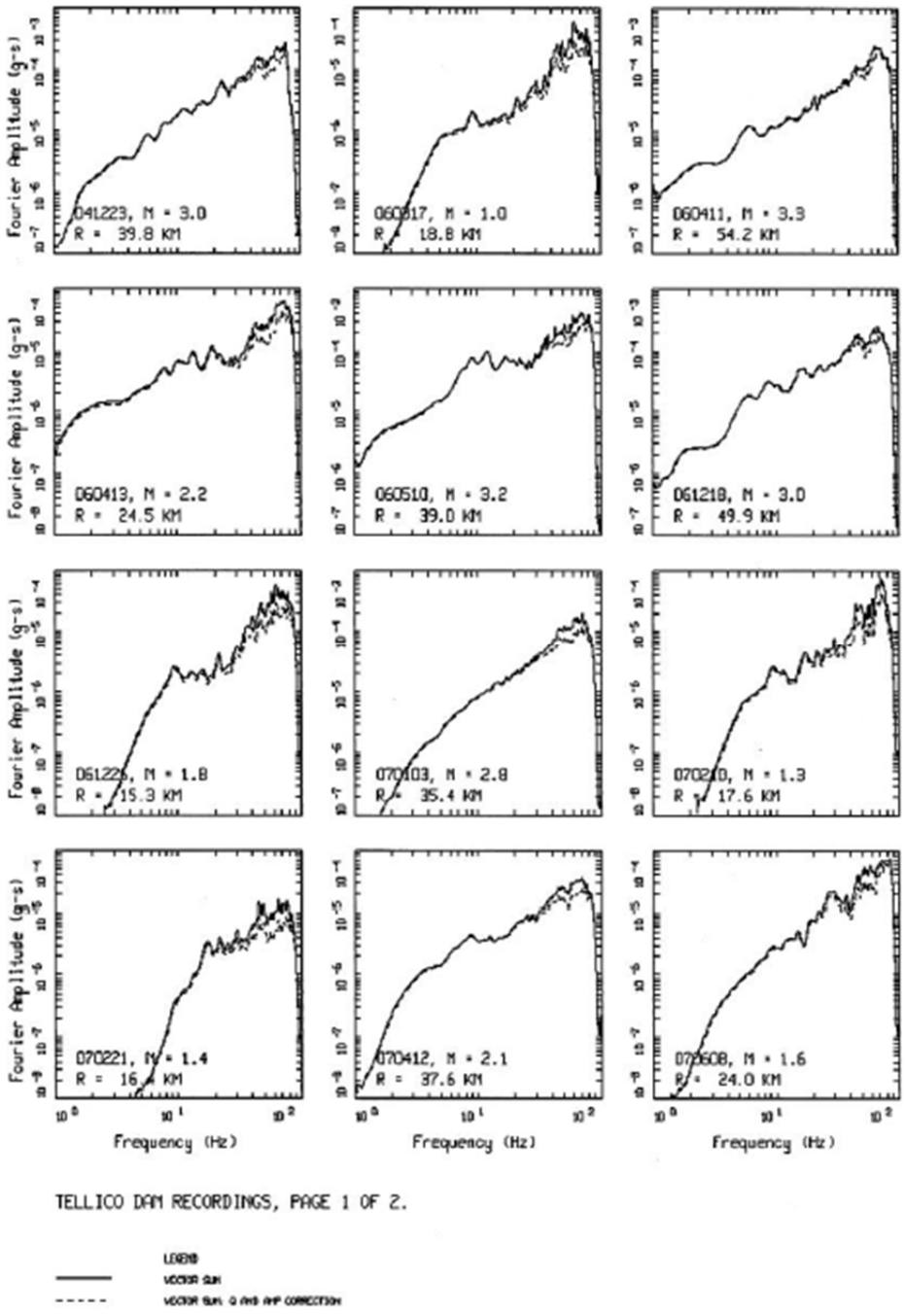

Figure 2.5.2-105. (Sheet 1 of 2), Vector average FAS computed from windowed shear-wave recordings of the twenty earthquakes analyzed at Tellico Dam: solid line as recorded, dashed line corrected for amplification (Figure 2.5.2-102) and Q(f) (630 $f^{0.5}$, Table 2.5.4-32)

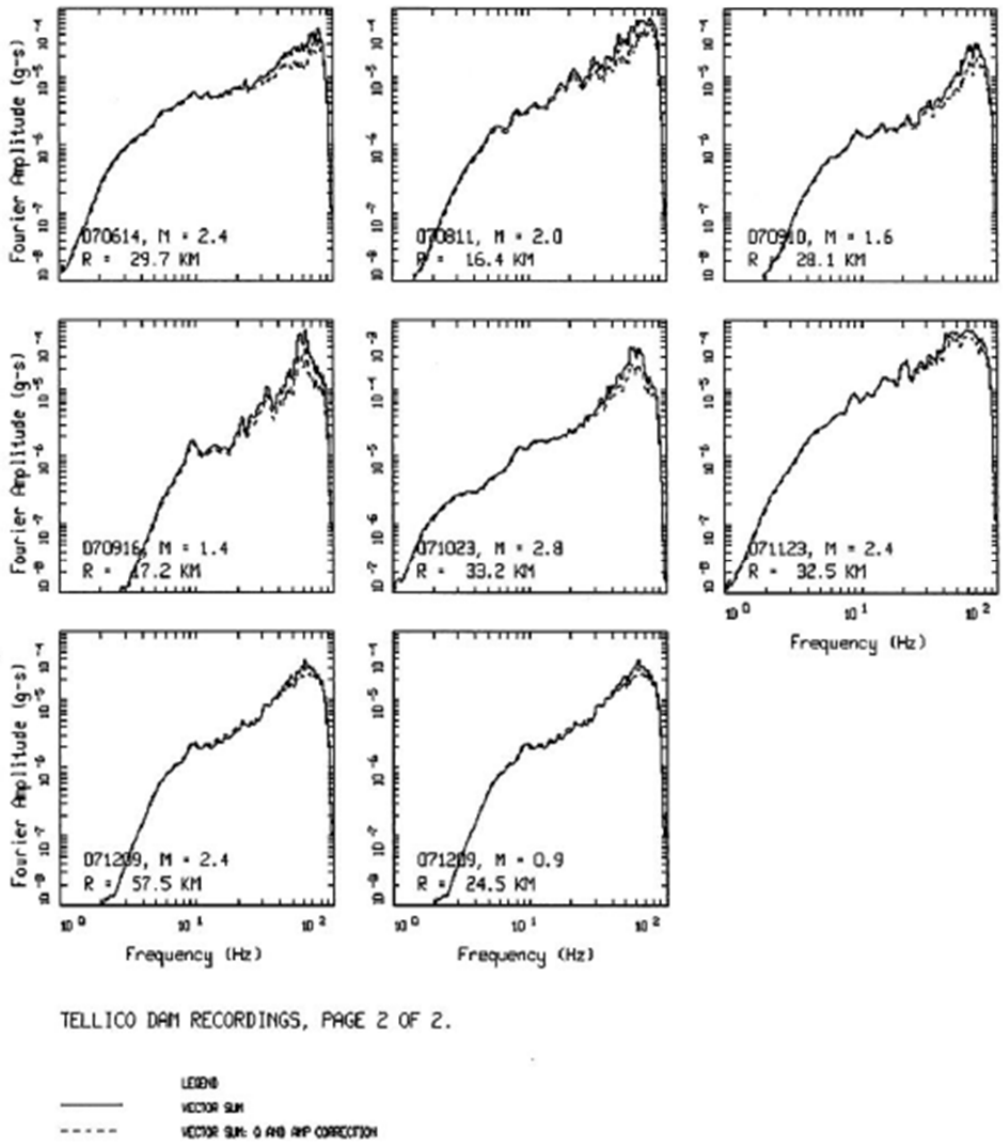

Figure 2.5.2-105. (Sheet 2 of 2), Vector average FAS computed from windowed shear-wave recordings of the twenty earthquakes analyzed at Tellico Dam: solid line as recorded, dashed line corrected for amplification (Figure 2.5.2-102) and Q(f) (630 $f^{0.5}$, Table 2.5.4-32)

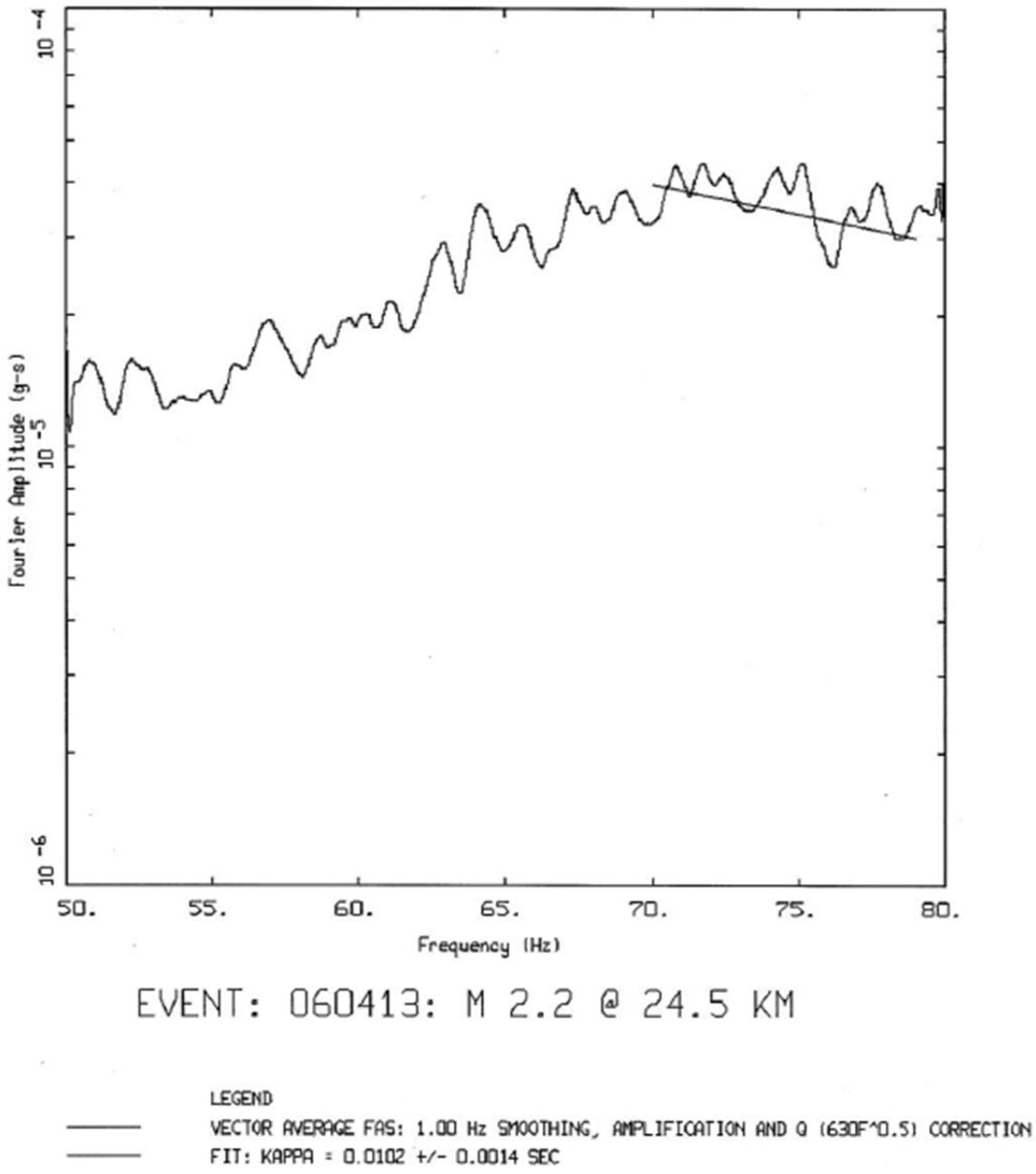

Figure 2.5.2.106- (Sheet 1 of 12), Vector average Fourier amplitude spectra for the twelve earthquakes analyzed corrected for amplification (Figure 2.5.2-102) and Q(f) (630 f^{05},Table 2.5.4-32) along with kappa fits over the bandwidths considered reliable (Section 2.5.2.5.2.3.2)

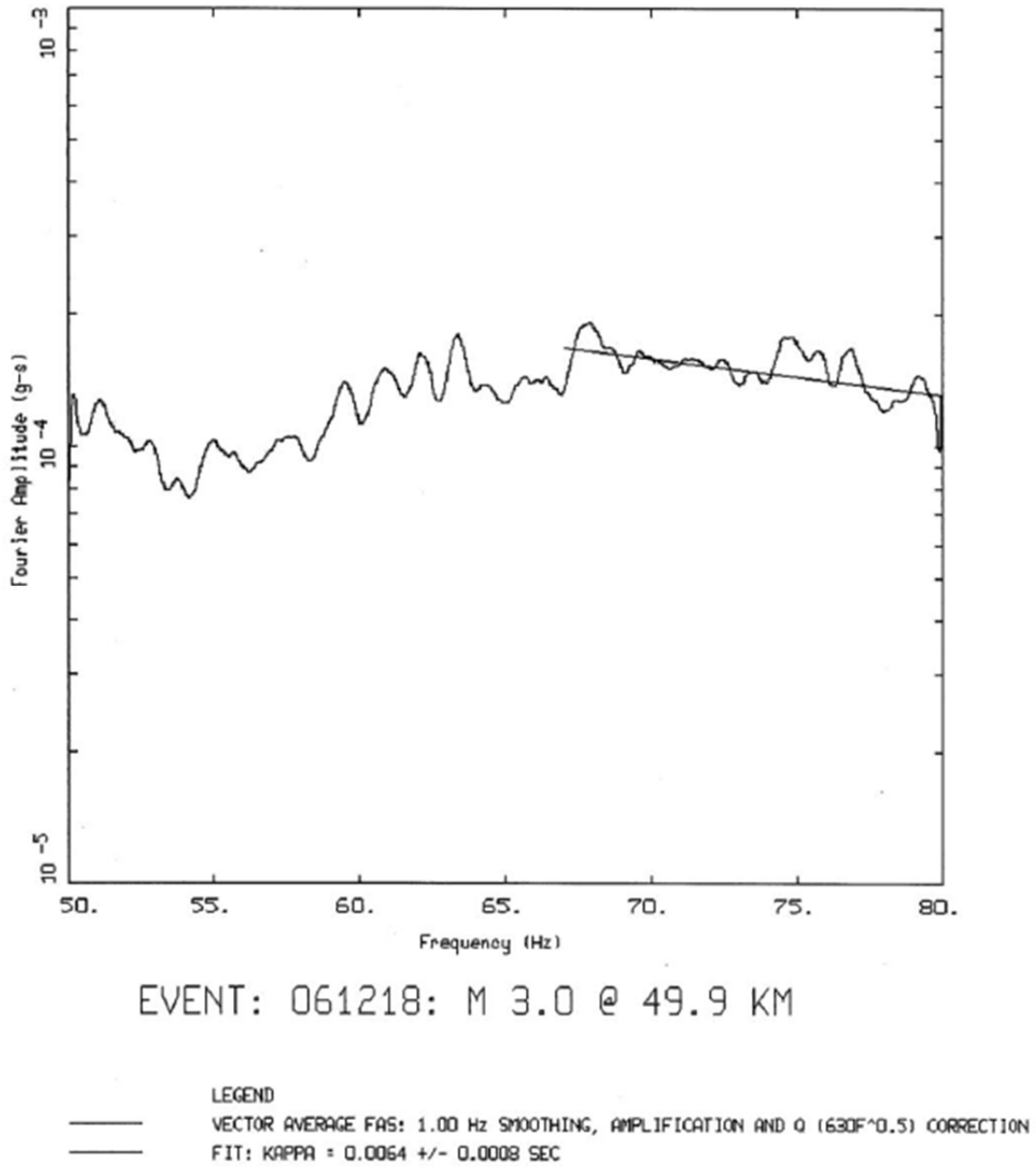

Figure 2.5.2-106. (Sheet 2 of 12), Vector average Fourier amplitude spectra for the twelve earthquakes analyzed corrected for amplification (Figure 2.5.2-102) and Q(f) (630 f^{05},Table 2.5.4-32) along with kappa fits over the bandwidths considered reliable (Section 2.5.2.5.2.3.2)

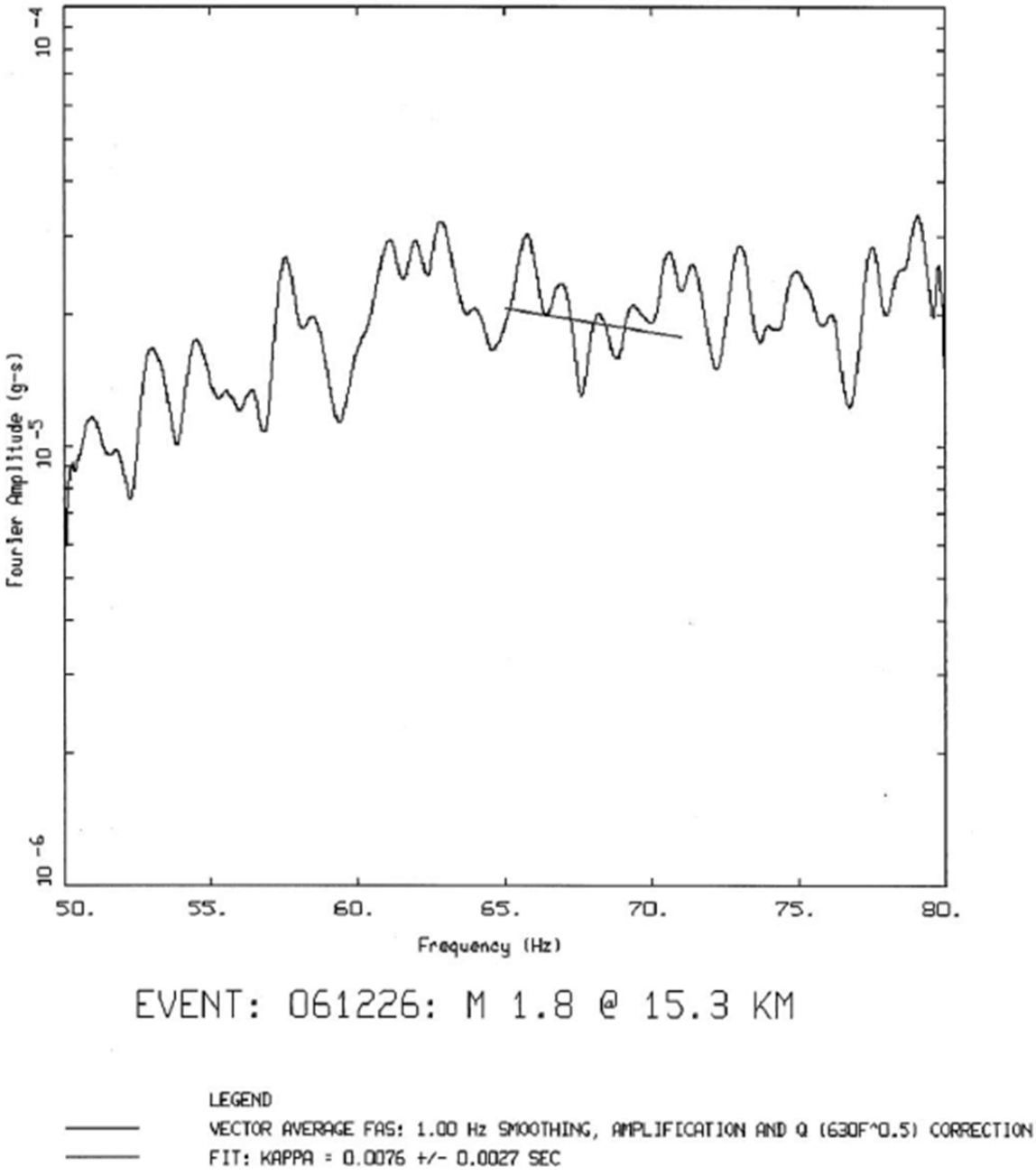

Figure 2.5.2-106. (Sheet 3 of 12), Vector average Fourier amplitude spectra for the twelve earthquakes analyzed corrected for amplification (Figure 2.5.2-102) and Q(f) (630 f^{05},Table 2.5.4-32) along with kappa fits over the bandwidths considered reliable (Section 2.5.2.5.2.3.2)

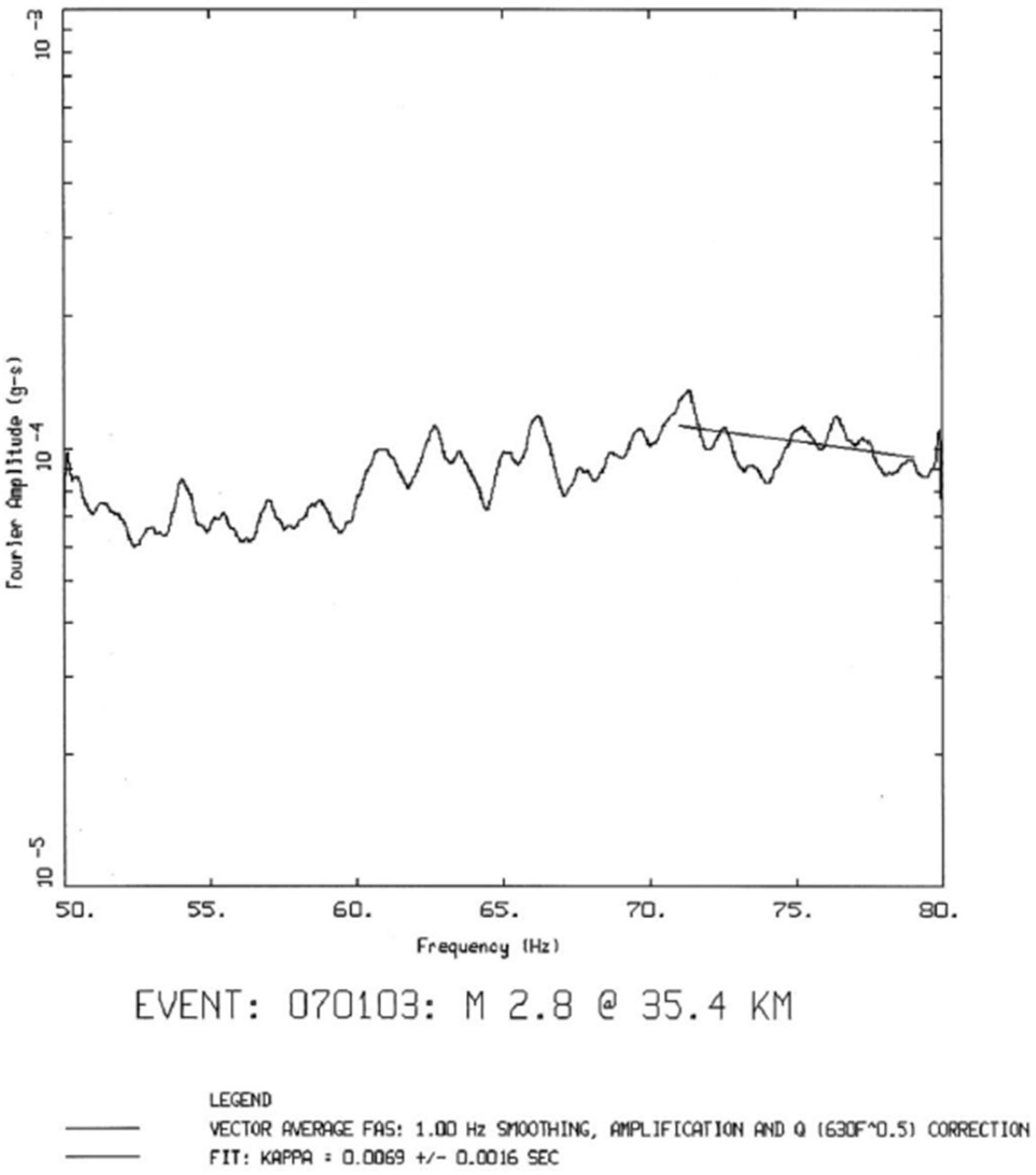

Figure 2.5.2-106. (Sheet 4 of 12), Vector average Fourier amplitude spectra for the twelve earthquakes analyzed corrected for amplification (Figure 2.5.2-102) and Q(f) (630 f^{05},Table 2.5.4-32) along with kappa fits over the bandwidths considered reliable (Section 2.5.2.5.2.3.2)

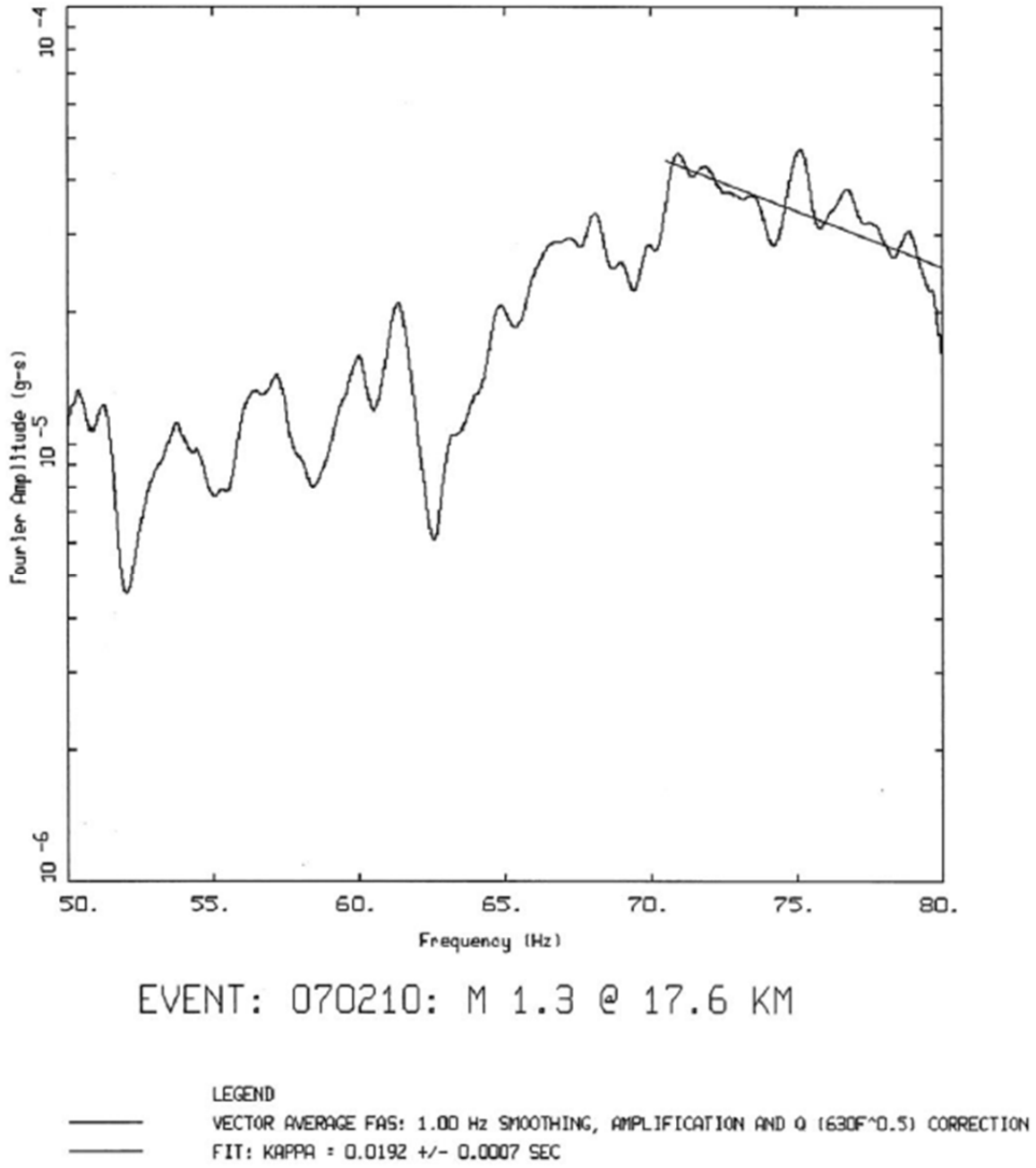

Figure 2.5.2-106. (Sheet 5 of 12), Vector average Fourier amplitude spectra for the twelve earthquakes analyzed corrected for amplification (Figure 2.5.2-102) and Q(f) (630 f^{05},Table 2.5.4-32) along with kappa fits over the bandwidths considered reliable (Section 2.5.2.5.2.3.2)

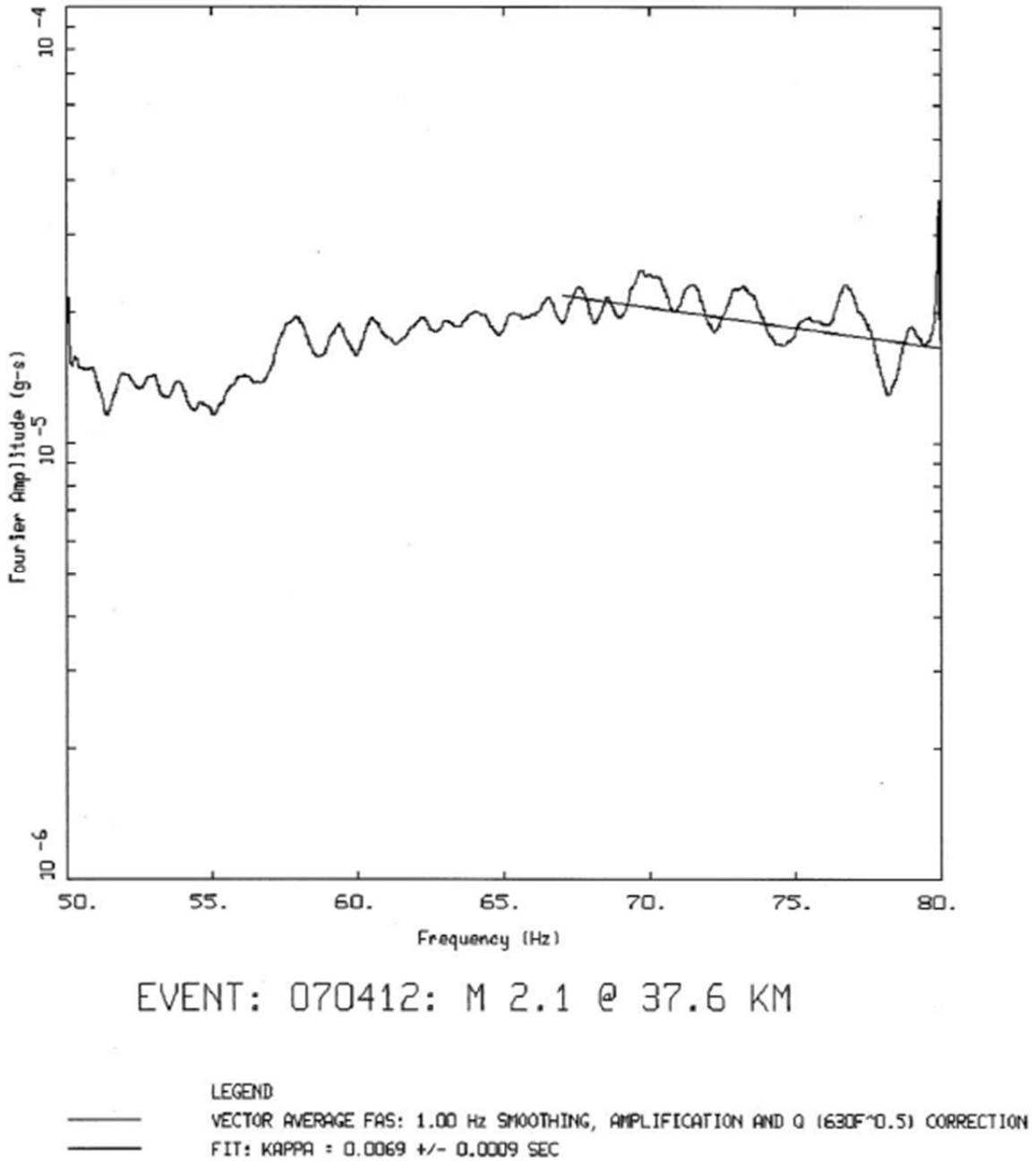

Figure 2.5.2-106. (Sheet 6 of 12), Vector average Fourier amplitude spectra for the twelve earthquakes analyzed corrected for amplification (Figure 2.5.2-102) and Q(f) (630 f^{05},Table 2.5.4-32) along with kappa fits over the bandwidths considered reliable (Section 2.5.2.5.2.3.2)

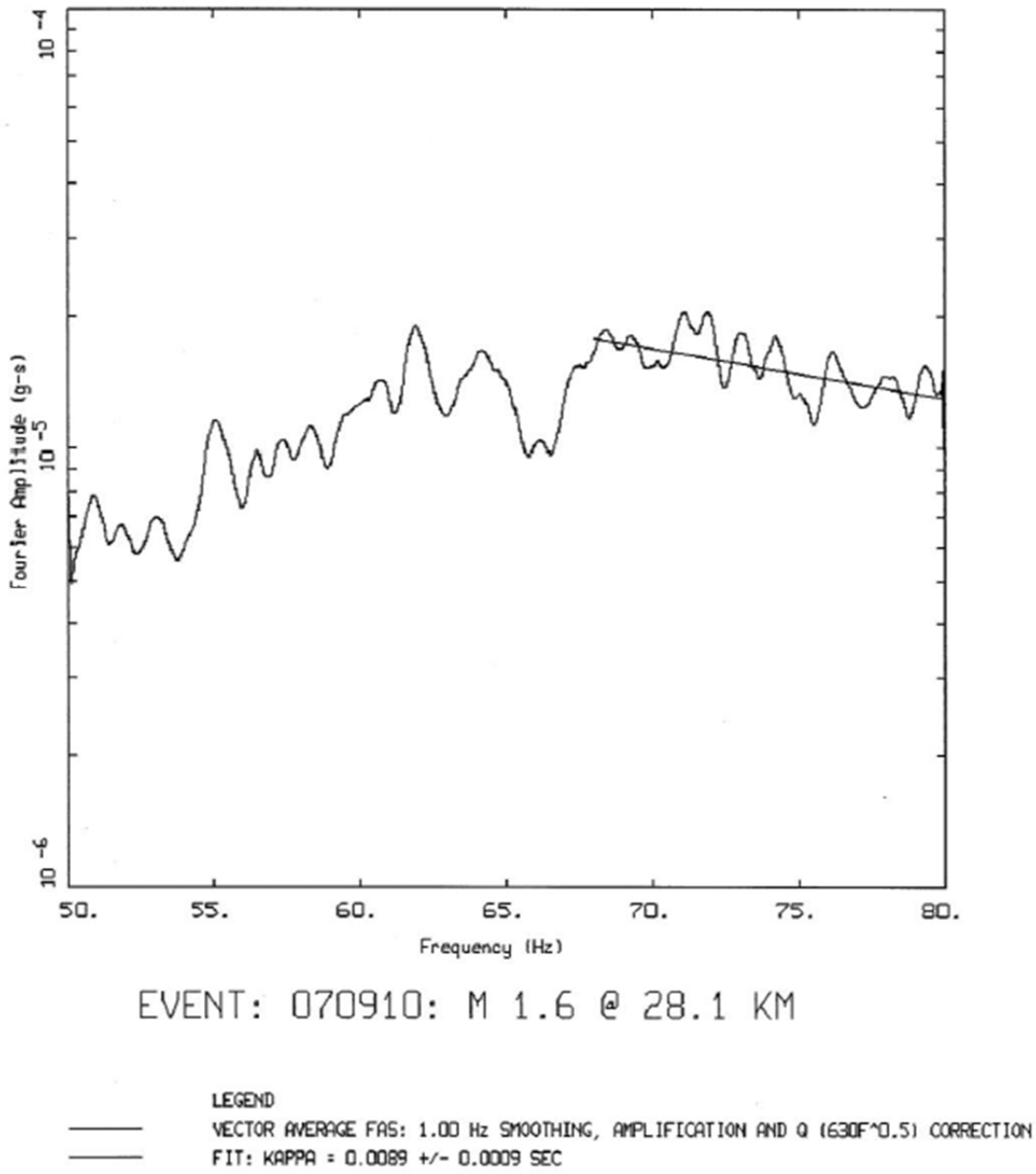

Figure 2.5.2-106. (Sheet 7 of 12), Vector average Fourier amplitude spectra for the twelve earthquakes analyzed corrected for amplification (Figure 2.5.2-102) and Q(f) (630 f^{05},Table 2.5.4-32) along with kappa fits over the bandwidths considered reliable (Section 2.5.2.5.2.3.2)

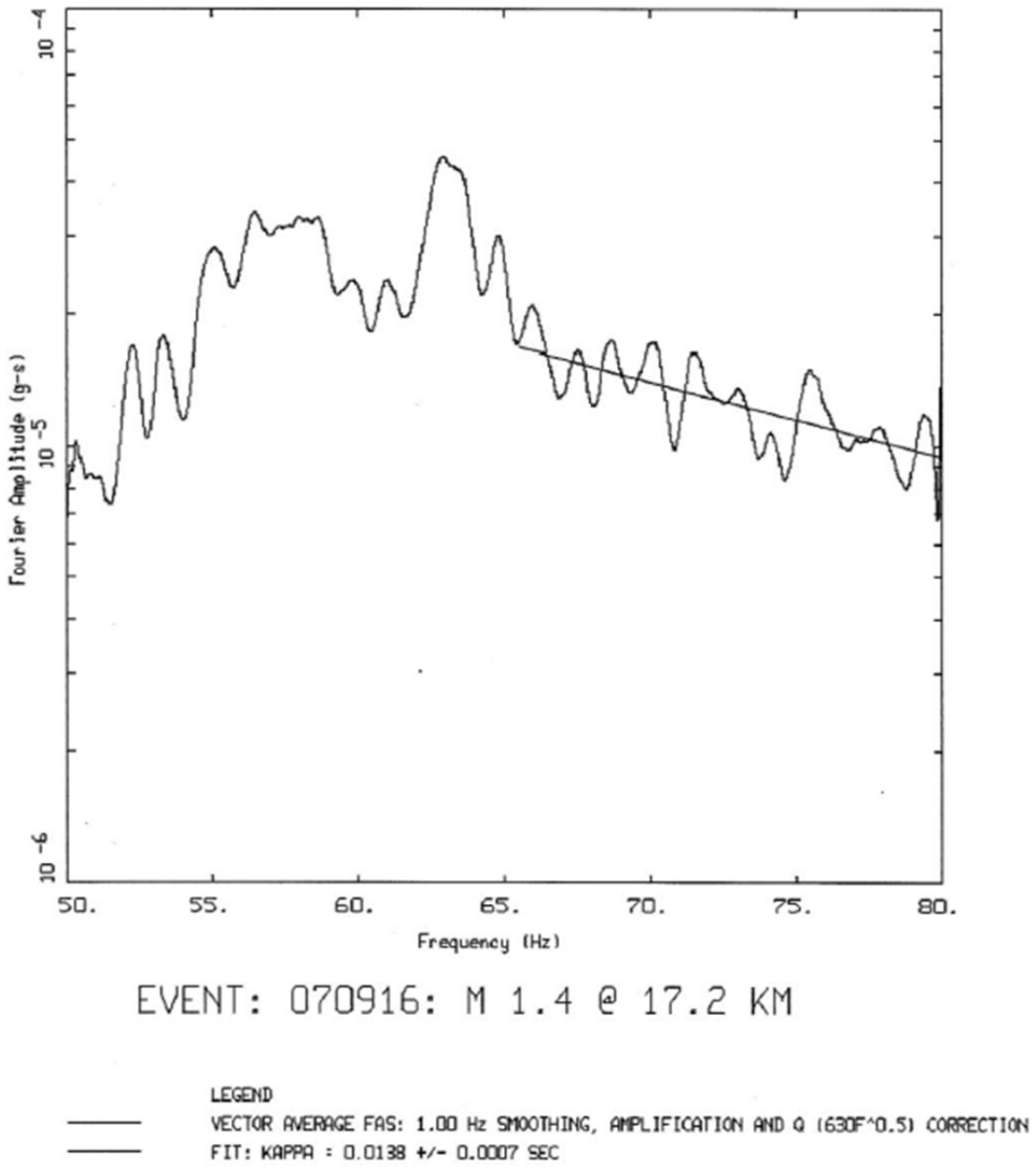

Figure 2.5.2-106. (Sheet 8 of 12), Vector average Fourier amplitude spectra for the twelve earthquakes analyzed corrected for amplification (Figure 2.5.2-102) and Q(f) (630 f^{05},Table 2.5.4-32) along with kappa fits over the bandwidths considered reliable (Section 2.5.2.5.2.3.2)

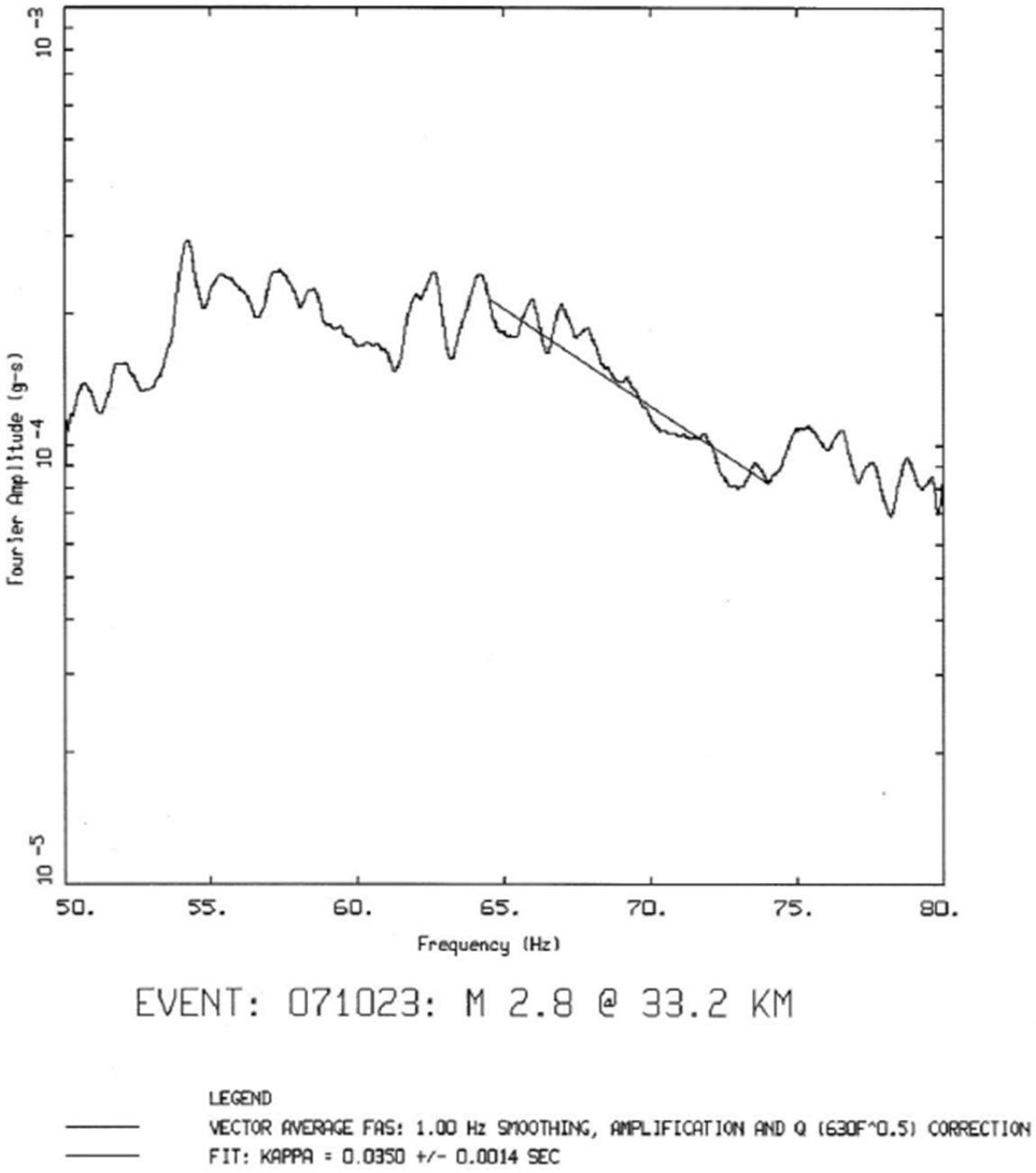

Figure 2.5.2-106. (Sheet 9 of 12), Vector average Fourier amplitude spectra for the twelve earthquakes analyzed corrected for amplification (Figure 2.5.2-102) and Q(f) (630 f^{05},Table 2.5.4-32) along with kappa fits over the bandwidths considered reliable (Section 2.5.2.5.2.3.2)

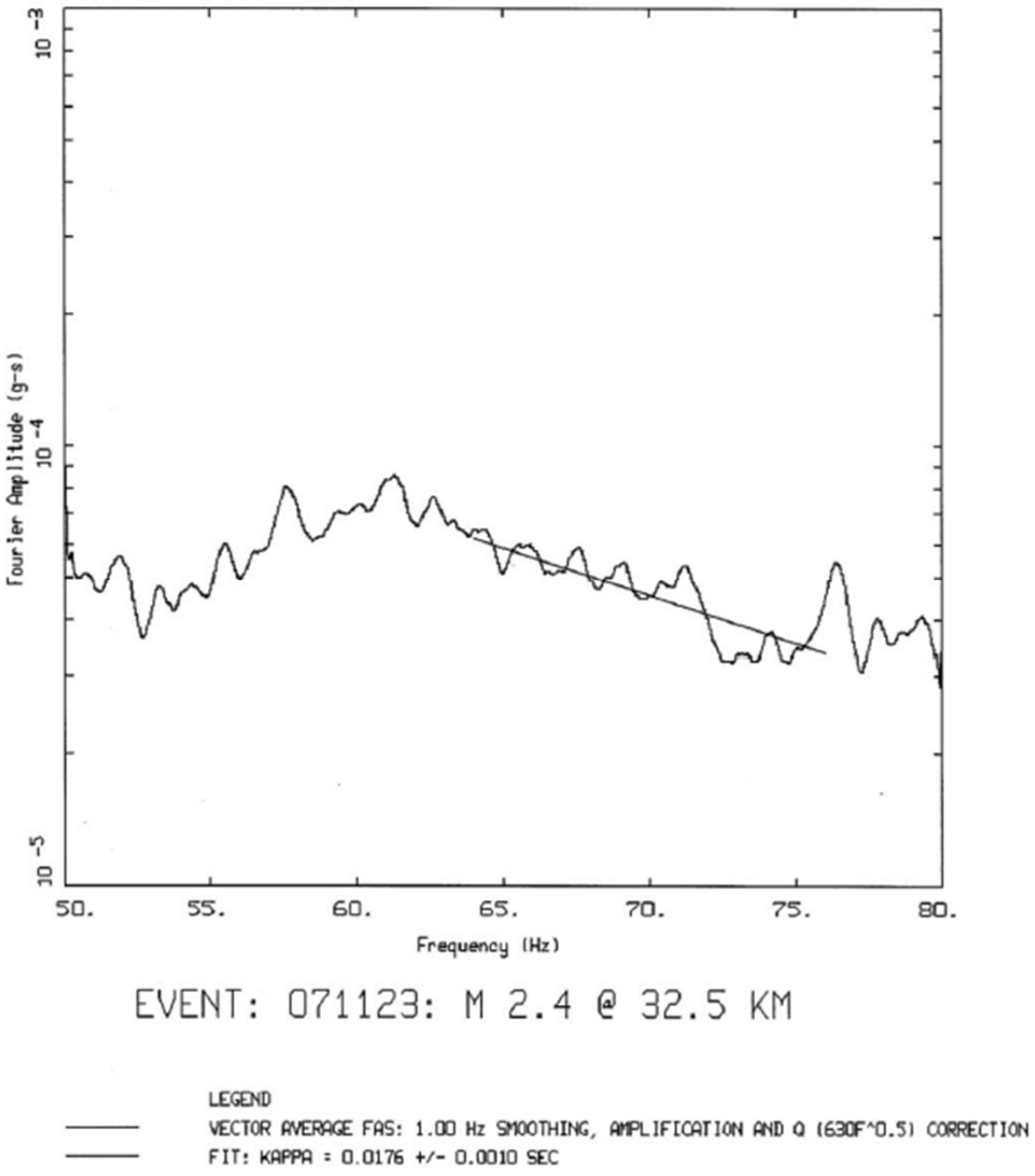

Figure 2.5.2-106. (Sheet 10 of 12), Vector average Fourier amplitude spectra for the twelve earthquakes analyzed corrected for amplification (Figure 2.5.2-102) and Q(f) (630 f^{05},Table 2.5.4-32) along with kappa fits over the bandwidths considered reliable (Section 2.5.2.5.2.3.2)

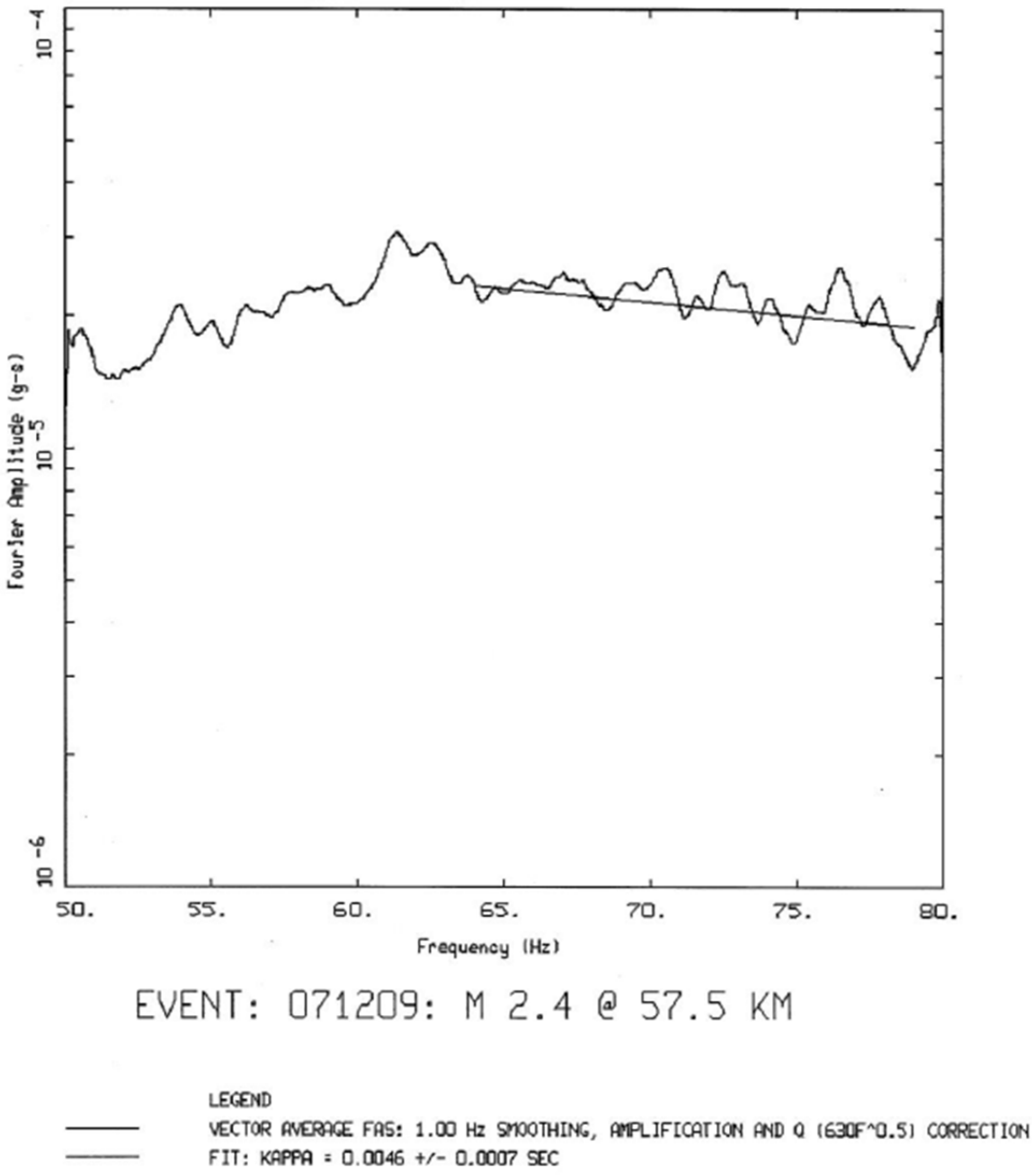

Figure 2.5.2-106. (Sheet 11 of 12), Vector average Fourier amplitude spectra for the twelve earthquakes analyzed corrected for amplification (Figure 2.5.2-102) and Q(f) (630 f^{05},Table 2.5.4-32) along with kappa fits over the bandwidths considered reliable (Section 2.5.2.5.2.3.2)

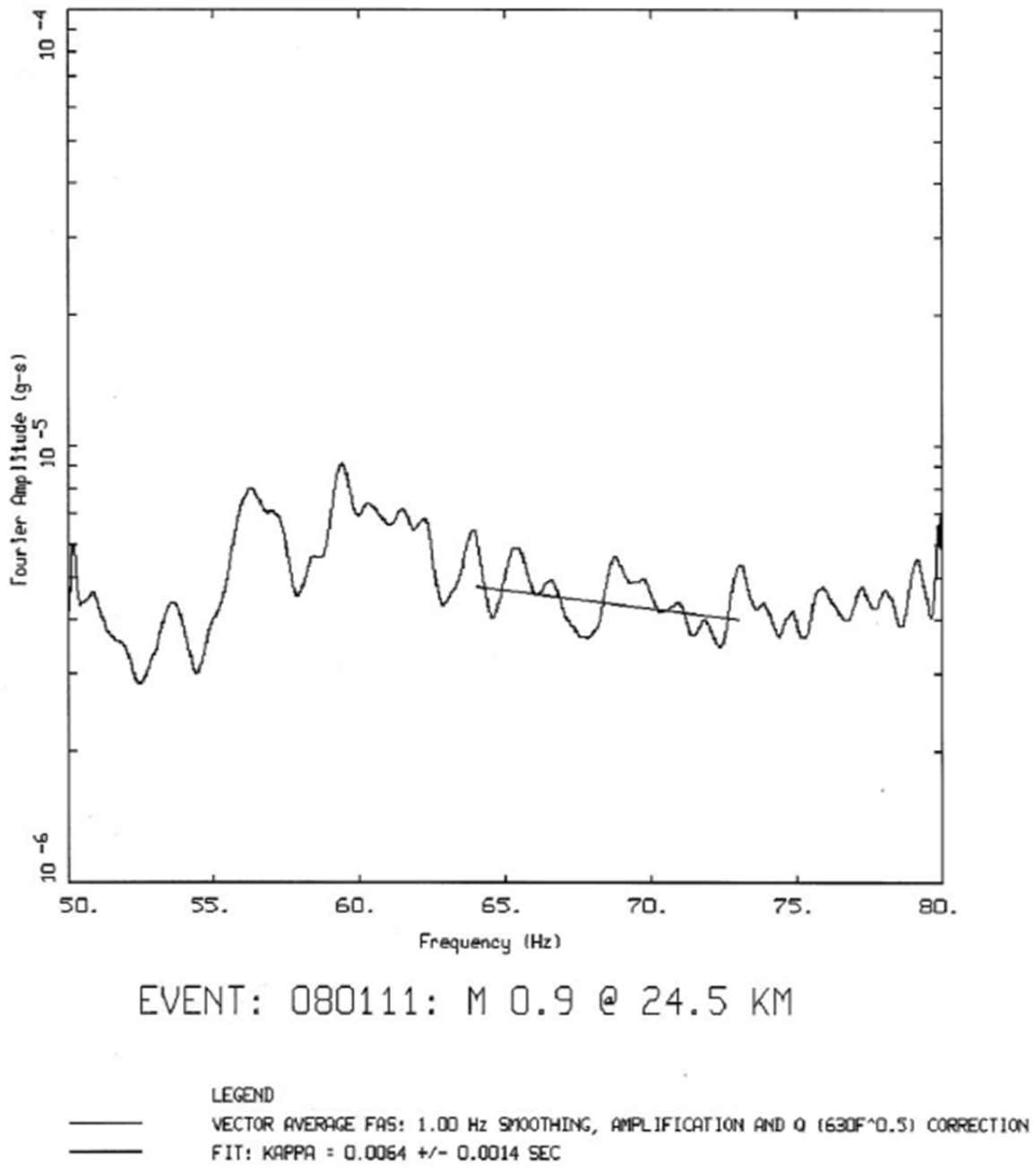

Figure 2.5.2-106. (Sheet 12 of 12), Vector average Fourier amplitude spectra for the twelve earthquakes analyzed corrected for amplification (Figure 2.5.2-102) and Q(f) (630 f^{05},Table 2.5.4-32) along with kappa fits over the bandwidths considered reliable (Section 2.5.2.5.2.3.2)

By letter dated May 12, 2016 (Reference 1), Tennessee Valley Authority (TVA) submitted an application for an early site permit for the Clinch River Nuclear (CRN) Site in Oak Ridge, TN. Subsequent to the submittal of the application, and consistent with interactions with NRC staff, TVA identified certain aspects of the application that it intends to supplement. By letter dated August 11, 2016 (Reference 2), TVA provided a plan for submitting the identified supplemental information.

This enclosure provides supplemental information related to Vibratory Ground Motion to support the NRC staff's review. This enclosure also includes proposed changes to the affected Environmental Report (ER) sections. These changes will be incorporated into a future revision of the Early Site Permit Application (ESPA).

Supplement Item B (From Reference 2)

B. TVA will provide a markup of the applicable ESPA sections to justify the use of input parameters used in the Probabilistic Seismic Hazard Analysis (PSHA), including a description of the SSHAC process used in determining the input parameters.

Supplemental Information B

A Senior Seismic Hazard Analysis Committee (SSHAC) Level 2 study was implemented to evaluate new data, methods, and models developed since publication of the 2012 CEUS SSC model and to assess whether this new information warrants any update or revision to the model. The Technical Integrator (TI) Team consisted of Mr. Scott Lindvall (TI Lead), Mr. Kevin Clahan, Mr. Seth Dee, Ms. Nora Lewandowski, and Dr. Gabriel Toro. Results of the TI Team assessment were reviewed by a Participatory Peer Review Panel (PPRP) consisting of Dr. Robert Youngs and Ms. Kathryn Hanson. Resource and Proponent Experts contacted during the study are listed with their affiliation and expertise in the table below. Dr. Robin McGuire, Dr. Gabriel Toro, and Dr. Arash Zandieh served as the project hazard analysts.

Resource and Proponent Experts Contacted by the TI Team in Support of the SSHAC Level 2 Assessment of the ETSZ

Name	Affiliation	Expertise	Mode of Communication
Anthony Crone (PE)	U.S. Geological Survey	Geomorphology, Neotectonics, and Paleoseismolog	Email Correspondence
Kathryn Hanson (PE)	AMEC	Geology and Neotectonics	Email Correspondence
Robert Hatcher (RE, PE)	University of Tennessee	Tectonics and Structural Geology	TI members K. Clahan, S. Dee, and N. Lewandowski visited selected Douglas Reservoir paleoseismic sites with Robert Hatcher, James Vaughn, and others.
Peter Lemiszki (RE)	Tennessee Geological Survey	Bedrock and Structural Geology	Telephone and in-person correspondence
Jeffrey Munsey (RE, PE)	Tennessee Valley Authority	Seismology	Telephone and in-person correspondence

Name	Affiliation	Expertise	Mode of Communication
Martitia Tuttle (PE)	M. Tuttle & Associate	Geomorphology, Geology, Paleoliquefaction	Email correspondence
James Vaughn (RE, PE)	Keen Geoserve, LLC	Pedology and Geology	TI members K. Clahan, S. Dee, and N. Lewandowski visited selected Douglas Reservoir paleoseismic sites with Robert Hatcher, James Vaughn, and others.
Martin Chapman (RE, PE)	Virginia Tech	Geophysics and Seismology	In-person correspondence
James Marrone (RE)	Bechtel	Seismology	E-mail and in-person correspondence
Robert Youngs (PE)	AMEC	Seismology	Email and in-person correspondence

Notes:
RE - Resource Expert
PE - Proponent Expert

To address the request for supplementary information regarding the SSHAC Level 2 process, ESPA SSAR Subsection 2.5.2.2.5, “Post CEUS SSC Studies,” will be replaced with the new Subsection 2.5.2.2.5, “SSHAC Level 2 Evaluation of the CEUS SSC Model,” text shown below.

To address the request for additional justification of seismic source parameters used in ETSZ hazard sensitivity studies, ESPA SSAR Subsection 2.5.2.2.6.1.3, “ETSZ Mmax Sensitivity Studies,” will be revised as shown below.

References:

1. Letter from TVA to NRC, CNL-16-081, "Application for Early Site Permit for Clinch River Nuclear Site," dated May 12, 2016

2. Letter from TVA to NRC, CNL-16-134, "Schedule for Submittal of Supplemental Information in Support of Early Site Permit Application for Clinch River Nuclear Site," dated August 11, 2016

The following subsection text replaces the existing SSAR Subsection 2.5.2.2.5 in its entirety:

2.5.2.2.5 SSHAC Level 2 Evaluation of the CEUS SSC Model

A Senior Seismic Hazard Analysis Committee (SSHAC) Level 2 study was implemented to evaluate new data, methods, and models developed since publication of the 2012 CEUS SSC model and to assess whether this new information warrants any update or revision to the model. The Technical Integrator (TI) Team reviewed scientific literature published since 2012 (and earlier), contacted experts who have developed data and/or interpretations of seismic sources in the site region, reviewed an updated seismicity catalog developed for this project, and performed site-specific studies, as needed, to assess the quality of data and uncertainty associated with recently published studies. Specifically, the TI Team assessed: (1) recent and ongoing geologic/paleoseismic studies within the Eastern Tennessee Seismic Zone (ETSZ); (2) ongoing investigations of the Mineral, Virginia earthquake that occurred in or near the Central Virginia Seismic Zone (CVSZ); and (3) revisions to the maximum magnitude distributions for seismic zones in the CEUS SSC model.

The published CEUS SSC earthquake catalog extends through 2008 (Chapter 3 of Reference 2.5.2-1). For the CRN Site PSHA, this catalog was updated through mid-September, 2013, as described in Subsection 2.5.2.1. Updating the catalog added 157 events of E(**M**) > 2.2, of which 9 events are E(**M**) > 2.9, to the site region (Table 2.5.2-1). The largest event added to the catalog is the August 23, 2011 **M** 5.8 Mineral, Virginia earthquake (E(**M**) 5.7), which occurred beyond the Site Region but which lies within areal source zones of the CEUS SSC model that extend into the Site Region. The Mineral earthquake is the largest instrumentally recorded earthquake in eastern North America since the 1988 E(**M**) 5.84 Saguenay earthquake.

The TI Team reviewed the updated catalog, evaluated recent studies performed in the ETSZ by Dr. Robert Hatcher at the University of Tennessee and his colleagues, and performed several sensitivity analyses to evaluate the hazard significance of various seismic source parameters. The TI Team conducted interviews with Dr. Hatcher and Mr. James Vaughn regarding their data and interpretations of paleoseismic features in the Douglas Reservoir area (References 2.5.2-88, 2.5.2-92, 2.5.2-93, and 2.5.2-94), and visited several of the Douglas Reservoir paleoseismic sites with Dr. Hatcher and Mr. Vaughn. Selected paleoseismic trenches described in Hatcher et al. (Reference 2.5.2-88) were re-excavated, logged, and analyzed by members of the TI Team. Detailed results of the TI Team assessment are provided in Subsection 2.5.3.2.6 and a summary is given in Subsection 2.5.2.2.5.1 below. A late-stage review of the TI Team assessment of the Douglas Reservoir paleoseismic features was provided by the Participatory Peer Review Panel (PPRP).

Several sensitivity analyses were performed to assist the TI Team in their assessment. These sensitivity analyses are provided in Subsection 2.5.2.2.6 and included evaluating the effect of the updated seismicity catalog on rates and maximum magnitude (Mmax) for areal source zones within 640 km (400 mi) of the CRN site, and the degree of consistency of the Douglas Reservoir paleoseismic features and their postulated rates to the rate and Mmax of earthquakes in the ETSZ.

Results from the TI Team assessment of the Douglas Reservoir paleoseismic features (Subsections 2.5.2.2.5.1 and 2.5.3.2.6) indicate that the features are likely the result of nontectonic processes and, therefore, do not represent paleo-earthquakes. Results from the sensitivity analyses (Subsection 2.5.2.2.6.1.3) show that, even if the Douglas Reservoir features represent paleo-earthquakes, the rate (frequency), general location, and Mmax distribution of

these paleo-earthquakes are captured in the existing CEUS SSC model.

In summary, the SSHAC Level 2 assessment of the CEUS SSC model shows that the existing model adequately and accurately captures new data, methods, and models published since 2012. The only revision to the model is to revise slightly the Mmax distribution for the ECC-AM areal source zone, the host zone for the 2011 Mineral, Virginia earthquake as described in Subsection 2.5.2.2.6.1.2. The TI Team concluded that the recent and ongoing studies of potential paleoseismic features in the Douglas Reservoir area by Dr. Hatcher and his colleagues do not warrant a change in the existing CEUS SSC model.

The following SSAR Subsection 2.5.2.2.6.1.3 is revised as indicated: (Note - deletions are shown as "~~strike-through~~" text and additions are shown as "underlined" text.)

2.5.2.2.6.1.3 ETSZ Mmax Sensitivity Studies

As described in Subsection 2.5.3.1.2, recent work by Hatcher et al. (Reference 2.5.2-88), and Warrell (Reference 2.5.2-89) in the Douglas Reservoir area of Tennessee document potential paleoseismic and paleoliquefaction features interpreted to result from prehistoric, large magnitude earthquakes in the ETSZ. The results of the SSHAC Level 2 study described in Subsection 2.5.2.2.5, which included discussions with the authors, field observations of features, mapping of river terraces, and discussions with other researchers, show that many of these proposed paleoseismic features may have viable alternative origins and that significant uncertainties exist regarding their age. Two sensitivity studies were performed to assess the potential impact of the authors' conclusions that two **M** 6.5 or larger earthquakes occurred in the ETSZ region during the past 73 to 112 thousand years.

The first sensitivity study was designed to test the impact on Mmax distributions by assuming that two **M**~6.5 earthquakes occurred during the prehistorical period and assess the Mmax distributions for all the sources that contain the ETSZ (namely, PEZ-N, PEZ-W, MESE-W, NMESE-N, and STUDY_R). For this sensitivity analysis, it is assumed that the largest paleoseismic observed earthquake (Mmax-observed) in the ETSZ, according to the interpretation by Hatcher et al. (Reference 2.5.2-88) can be represented by a distribution having the following magnitudes and weights: 5.5 (0.1), 6.0 (0.3), 6.5 (0.4), 7.0 (0.1), 7.5 (0.1) and that the associated number of earthquakes is 2.

The weights are assigned to indicate the uncertainty in the assigned Mmax distributions. The majority of features described in Hatcher et al. (Reference 2.5.2-88) are primarily associated with either strong ground shaking (extensional ground surface cracking) or paleoliquefaction. ~~The weights~~ A weight of 0.1 is given for **M** 5.5 because this is the smallest magnitude that may produce localized liquefaction-induced features. Weights of 0.3 and ~~0.3~~0.4 are given for **M** 6.0 and **M** 6.5 respectively, because these reflect magnitudes that are likely to produce ~~these~~ localized liquefaction features. The ~~weight of 0.3 for M 6.0 offsets the overall distribution to signify that the~~ observed Douglas Reservoir features are not widespread throughout a large area and ~~are~~ would likely be produced by a relatively smaller local event. The distribution's lower bound of **M** 5.5 is based on a general magnitude threshold for liquefaction of about **M** 5. The distribution's two upper bound values of **M** 7.0 and **M** 7.5 allow for: (1) the uncertainty in earthquake location, such that a large, distant event might have produced the interpreted paleoseismic features in the Douglas Reservoir area; and (2) the possibility of a more widespread distribution of features beyond the Douglas Reservoir area. The weights ~~or~~ of 0.1 assigned to **M** 7.0 and **M** 7.5 reflect the lack of evidence for widespread distribution of features. The greatest weight assigned to **M** 6.5 partially reflects conclusions proposed by Hatcher et al. (Reference 2.5.2-88) that the paleoearthquakes are **M** 6.5 or larger. These conclusions regarding magnitude from Hatcher et al. (Reference 2.5.2-88) are based on the Wells and Coppersmith (Reference 2.5.2-112) displacement relations for an apparent 1 m reverse fault near Douglas Reservoir. However, the Wells and Coppersmith (Reference 2.5.2-112) rupture length to magnitude regressions are based on slip along the seismogenic fault, and their application to secondary faults or features produced from ground shaking may not be appropriate. This magnitude distribution was developed as part of the SSHAC Level 2 study summarized in Section 2.5.2.2.5.

The Hatcher et al. (Reference 2.5.2-88) interpretation is incorporated by giving 10 percent weight to a Mmax distribution derived from these paleoearthquakes and 90 percent weight to a

distribution derived using the historical- and instrumental-earthquake data used in the CEUS SSC study. Following the procedures described in the CEUS SSC report (Reference 2.5.2-1) a 10 percent weight is given using the potential paleoearthquake data as the largest observed in the PEZ to be used in ~~truncating~~ updating the Mmax prior distribution.

The weight ~~reflects significant uncertainties in~~ of 10 percent was developed as part of the ~~origin of many reported~~ SSHAC Level 2 study. The SSHAC evaluation process was based on reviews of published papers and trench logs; geologic field reconnaissance of sites described in Hatcher et al. (Reference 2.5.2-88) and Warrell (Reference 2.5.2-89), and other areas in eastern Tennessee; conversations with Hatcher and other proponent experts; logging of re-excavated trenches; mapping of river terraces; and discussions with resource experts. Based on ~~field inspection and review~~ this evidence, the SSHAC TI Team concluded that nearly all the features interpreted as paleoseismic in origin can also be explained by other plausible, non-seismic processes. A number of the SSHAC Resource Experts agree with this interpretation. Also, some of the early field interpretations of the features in the Douglas Reservoir area were available for consideration by the CEUS SSC TI Team during their evaluation, but were not included in the calculation of Mmax for PEZ (i.e., they were given zero weight). The 10 percent weight also reflects considerable uncertainty in the relative and numerical ages of terraces containing these features.

To put this 10 percent value in perspective, it is useful to consider the CEUS SSC treatment of suspected paleoseismic features in southeastern Arkansas, northeastern Louisiana, and western Mississippi (collectively known as the ALM features), identified by Cox and other researchers (see Reference 2.5.2-1 for references). According to Cox and others, these features consist of: (1) roughly circular sandy deposits in aerial photographs along river valleys, which were interpreted as seismically induced sand blows; (2) trenched sandy deposits at seven locations, within which multiple sand-venting episodes can be identified and correlated between trench sites based on stratigraphic relationships and dating; and (3) evidence of Quaternary fault rupture in the Saline River area. The CEUS SSC study assigned a 20 percent weight to the ALM features in the calculation of Mmax for the ECC-GC source zone (which contains the ALM features). In the CRN SSHAC Level 2 deliberations, the paleoseismic evidence for the ALM features was deemed significantly stronger than the evidence for the Hatcher et al. (Reference 2.5.2-88) interpretation of the Douglas Reservoir evidence.

~~This~~ The sensitivity calculation ~~results in~~ shows no change in the Mmax distributions of MESEW, NMESE-N, and STUDY_R, and a very minor change in PEZ-N and PEZ-W. For PEZ-N, one magnitude in the distribution changes from **M** 7.4 to **M** 7.5. For PEZ-W, two magnitudes increase by 0.1; **M** 6.4 to **M** 6.5 and **M** 7.4 to **M** 7.5. These changes are largely an artifact of the discretization into 0.1 magnitude units. More importantly, the changes seen in the continuous distributions (i.e., shifts of approximately 0.02 magnitude units or less) are very small and much smaller than the standard deviations of these Mmax distributions. Therefore, ~~one can conclude~~ the TI Team concluded that the introduction of the two **M** 6.5 or greater paleoearthquakes proposed by Hatcher et al. (Reference 2.5.2-88) and Warrell (Reference 2.5.2-89) has a negligible effect on the Mmax distributions of these affected seismic sources.

The second sensitivity study was performed to evaluate whether the existing CEUS SSC 2012 model produces earthquakes in the ETSZ of sufficient size and frequency to explain the interpretations of paleoearthquakes from Hatcher et al. (Reference 2.5.2-88). This sensitivity study utilized the original Mmax distributions and rates from CEUS SSC 2012 and does not reflect the corrections made to Mmax distributions (Section 6.1 of Reference 2.5.2-1). As described above, ~~however,~~ the CEUS SSC 2012 model does not explicitly define a separate seismic source for the ETSZ. For the purpose of this hazard sensitivity study, the boundary of

the ETSZ as defined by the USGS NSHMP (Reference 2.5.2-10) was adopted (see Figure 2.5.2-26). Except for inputs developed by the CEUS SSC project, the choice of the ETSZ geometry defined by the USGS NSHMP is the only new input parameter required for this sensitivity analysis.

Magnitude frequency distributions were calculated for those portions (cell centers) of CEUS SSC 2012 sources (PEZ-N, PEZ-W, MESE-W, NMESE-N, and Study_R) that lie within the boundary of the NSHMP depiction of the ETSZ (Figure 2.5.2-26). Magnitude frequency distribution calculations used CEUS SSC 2012 annual seismicity rates, b-values, and extracted parameters of rate per cell area, cell-area, and values for each source. The final weighted magnitude frequency distribution was developed by applying CEUS SSC 2012 global logic tree weights to the calculated magnitude frequency distributions from each source. Using the final weighted magnitude frequency distribution, the approximate return periods for earthquake magnitudes ranging from **M** 6 to 7.5 are as follows:

- **M** 6.0 ~2,800 years
- **M** 6.5 ~13,000 years
- **M** 7.0 ~88,000 years
- **M** 7.5 ~850,000 years

These results indicate that the CEUS SSC 2012 model ~~appears to generate~~ generates moderate- to large-magnitude events (**M** > 6.5) with sufficient frequency in the ETSZ area to explain the Hatcher et al. (Reference 2.5.2-88) interpretation of field observations that implies the occurrence of two events of approximately **M** 6.5 or larger in the past 73 to 112 thousand years. Without any modification, the CEUS SSC 2012 model generates about seven **M** 6.5 events and one **M** 7.0 event in the ETSZ region every 100,000 years.

In summary, Mmax distributions for eight seismotectonic zones were corrected from the published values in Reference 2.5.2-1. The original CEUS SSC Mmax distributions and corrected Mmax distributions are shown in Table 2.5.2-15. The Mmax distribution for the ECC-AM was revised slightly to account for the occurrence of the 2011 **M** 5.8 Mineral, Virginia, earthquake (Table 2.5.2-14). These corrected and revised Mmax distributions were used in the CRN Site PSHA (Subsection 2.5.2.4). No other modifications were made to Mmax distributions.

Both of these sensitivity analyses, including the development of inputs, calculation procedures, and conclusions, were performed and documented as part of the SSHAC Level 2 study summarized in Subsection 2.5.2.2.5 and were subjected to SSHAC Level 2 peer review.

ENCLOSURE 2

SUPPLEMENTAL INFORMATION RELATED TO SSAR SUBSECTION 2.5.3 AND REVISED SSAR FIGURES OF THE EARLY SITE PERMIT APPLICATION FOR CLINCH RIVER NUCLEAR SITE

By letter dated May 12, 2016 (Reference 1), Tennessee Valley Authority (TVA) submitted an application for an early site permit for the Clinch River Nuclear (CRN) Site in Oak Ridge, TN. Subsequent to the submittal of the application, and consistent with interactions with NRC staff, TVA identified certain aspects of the application that it intends to supplement. By letter dated October 21, 2016 (Reference 2), TVA submitted supplemental information related to Geologic Characterization Information, Surface Deformation, and Stability of Subsurface Materials and Foundation in support of Early Site Permit Application (ESPA) for the CRN Site.

This enclosure provides additional supplemental information related Site Safety Analysis Report (SSAR) Subsection 2.5.3 and revised SSAR Figures of the ESPA provided in Reference 1 to support the NRC staff's review. This enclosure also includes proposed changes to the affected Site Safety Analysis Report (SSAR) Figures. These changes will be incorporated into a future revision of the ESPA.

The following Supplemental Items are provided:

1. SSAR Figures 2.5.2-56 and 2.5.4-26

   SSAR Figures 2.5.2-56 and 2.5.4-26, "Shear Modulus Reduction and Damping Curves for Firm Rock," have been corrected to reflect consistency with values in the text.

   Copies of the corrected Figures 2.5.2-56 and 2.5.4-26 are included in this enclosure.

2. SSAR Figure 2.5.1-30

   The cross section in Figure 2.5.1-30 is revised to include the Chestnut Ridge fault as well as the Shear Fracture Zone.

   A copy of the revised Figure 2.5.1-30 is included in this enclosure.

3. SSAR Figure 2.5.1-34 and Figure 2.5.1-35

   Figures 2.5.1-34 and 2.5.1-35 have been revised as discussed and copies provided in the response to Supplemental Information A, Enclosure 1 of Reference 2.

4. SSAR Figure 2.5.1-63, (Sheet 1 of 2)

   SSAR Figures 2.5.1-35, "Site Area Geologic Cross Section A-A'," and 2.5.1-63, "(Sheet 1 of 2), Geologic Cross-Section A-A' Ground Surface to Basement," have been revised to include the latest geological interpretation of the Chestnut Ridge Fault (see response to Supplemental Information A, Enclosure 2, for a full description of this process).

A copy of the revised Figure 2.5.1-35 was included in the Supplemental Information A response in Enclosure 1 of Reference 2. A copy of the revised Figure 2.5.1-63, (Sheet 1 of 2), is included in this enclosure.

5. SSAR Figure 2.5.1-62 and 2.5.1-63, (Sheet 2 of 2)

   SSAR Figures 2.5.1-62, "Map Showing the Location of Geologic Cross-Section A-A' to Basement, and 2.5.1-63, "(Sheet 2 of 2), Geologic Cross-Section A-A' Ground Surface to Basement," have been revised to:

   - correct the color coordination between the figures;
   - correct the inadvertent reversal of section labels A(NW) and A'(SE) between the figures;
   - correct the lower dimension of excerpted section B (A"-A') to match the outline shown on the larger profile (-4,000' vs. -7,000'); and,
   - provide larger and higher quality resolution figures.

   A copy of the revised Figures 2.5.1-62 and 2.5.1-63 are included in this enclosure.

   In addition to the revision to Figure 2.5.1-63, revisions to SSAR Subsection 2.5.1.1.3.1, "Valley Ridge Province," are being made. These revisions are included in this enclosure.

6. SSAR Figure 2.5.3-3, Sheet 2 of 2

   A new topographic profile, Profile B-B', will be added to better address the relationship of Quaternary terrace surfaces and the Copper Creek fault. The location of Profile B-B' is shown on new Figure 2.5.3-6, which was created for and included in the response to Supplemental Information A, Enclosure 1 of Reference 2.

   Profile B-B' will replace the previous profile presented on Figure 2.5.3-3, (Sheet 2 of 2) and a copy is included in this enclosure.

7. SSAR Figure 2.5.3-4

   SSAR Figure 2.5.3-4 has been modified to correct the indicated locations of the White Oak Mountain fault, Chestnut Ridge fault, and three intersections of the Copper Creek fault, and to add the locations of unnamed faults. Additionally, SSAR Figure 2.5.1-26, Sheet 5, "Quaternary Terrace Projections to the Clinch River for Creation of Longitudinal Profile" and Sheet 6, "Quaternary Terrace Projections to the Clinch River for Creation of Longitudinal Profile," were created to illustrate how Quaternary terraces were projected to create the longitudinal profile shown in SSAR Figure 2.5.3-4. SSAR Figures 2.5.3-2, Sheets 1 through 4, were provided in response to Supplemental Information A, Enclosure 1 of Reference 2 and have been updated to indicate a total of 6 Sheets due to the addition of Sheets 5 and 6.) Copies of these figures are included in this enclosure.

   The Clinch River baseline longitudinal profile was developed to represent the slope of the Clinch River riverbed, prior to the construction of the Watts Bar Dam. Historic United States Geological Society (USGS) topographic data, collected prior to the impoundment of Watts Bar Dam, was used to create the baseline longitudinal profile. This historic topographic data showed only a few contours crossing the approximately 15-mile length of the Clinch River; no obvious breaks-in-slope or knickpoints were noted. To honor the original data, the

baseline longitudinal profile was drawn as a smooth line connecting the limited topographic data now concealed by the Watts Bar reservoir.

The longitudinal profiles are the product of a simple linear regression model of terrace locations and elevation data within each relative age category. Providing the linear regression lines for each relative age category permits quantification and comparison of each longitudinal profile line with the slope of the modern Clinch River. The regression lines for Qht1, Qht2, Qht3, and Qpt1 closely match the baseline slope angle, determined for the modern Clinch River of y= -2 (10-4)x. The regression line for Qpt2 shows a flatter slope of y= -7 (10-5)x. The regression lines for Qpt3, Qpt4, and Qpt6 show a slightly steeper slope y= -3 (10-4)x. Qpt5 shows a near parallel slope angle to the Clinch River baseline that is based on limited pre-reservoir topographic data.

There are several factors that may explain the differences between regression lines and the Clinch River baseline. New panels were added as SSAR Figure 2.5.1-26 Sheets 5 and 6 to show how each terrace was projected to fit the 2D longitudinal profile. The distance a terrace is projected can introduce variability in the slope of the regression line due to location accuracy along the profile. Variations in slope because of location accuracy along profiles are more likely for the older terraces such as Qpt2, Qpt4, Qpt5, and Qpt6 that show more scatter within each dataset; however, there is also scatter in Qht3. These older terraces are located further away, both in horizontal distance and elevation, from the modern Clinch River and these greater projection distances may affect the slope of the regression lines due to projection inaccuracies.

Qpt2 produces a flatter linear regression line that is a function of the amount of scatter in the dataset, which in turn is a function of the size of the dataset and the projection variability that affects all older Quaternary terraces. The flatter slope of the single regression line for Qpt2 does not constitute evidence for tectonic deformation. Progressively tilting, warping, or sharply displaced longitudinal profiles would suggest tectonic deformation. It is permissible within the data evaluated in Figure 2.5.3-4 that no tectonic deformation associated with these northeast trending faults has occurred within the site area.

8. TVA has mapped the acceptance criteria in Revision 5 of NUREG-0800, “Standard Review Plan for the Review of Safety Analysis Reports for Nuclear Power Plants: LWR Edition,” Section 2.5.3, against locations of the pertinent information in the ESPA SSAR Subsection 2.5.3 provided in Reference 1. Table E2 provides an index of the SSAR subsection locations where each SRP 2.5.3 acceptance criterion is discussed.

Table E2
Index of Standard Review Plan 2.5.3 Acceptance Criteria Discussions Within Site Safety Analysis Report

SRP 2.5.3 Acceptance Criteria (NUREG-0800, Revision 5)	Location of Acceptance Criteria (CRN ESPA Reference)
1. Geologic, Seismic, and Geophysical Investigations.	
• Quaternary tectonics	2.5.1.2.2, Local Geologic History 2.5.1.2.4, Local Structural Geology 2.5.1.2.6.7, Residual Stresses in Bedrock 2.5.1.1.4.3.1, Current Stress Regime in the Eastern United States
• structural geology	2.5.1.2.4, Local Structural Geology
• stratigraphy	2.5.1.2.3, Local Stratigraphy and Lithology
• geochronologic methods used for age dating	2.5.1.1.1.3.2, Karst in the Interior Low Plateaus Province—Concerning dating of Green River Relics 2.5.1.1.2, Regional Geologic History and Tectonic Evolution 2.5.2.2.5.1, Geologic Investigations of the Eastern Tennessee Seismic Zone
• paleoseismology	2.5.1.1.4.3.2, Distribution of Seismicity in the ETSZ 2.5.2.2.5.1, Geologic Investigations of the ETSZ 2.5.3.1.2, Regional and Local Geologic Studies 2.5.3.6, Characterization of Capable Tectonic Sources 2.5.3.1.2,Regional and Local Geologic Studies (3rd paragraph discusses recent paleoseismic studies) New Subsection 2.5.3.2.6, Proposed Quaternary Deformation Features Along Douglas Reservoir, TN, added in response to Supplemental Information C, Enclosure 1 of Reference 2
• geologic history of the site vicinity, site area, and site location	2.5.1.1, Regional Geology 2.5.1.2, Local Geology (Subsection 2.5.1.2.2 specifically relates local stratigraphy to regional tectonic and eustatic events.

SRP 2.5.3 Acceptance Criteria (NUREG-0800, Revision 5)	Location of Acceptance Criteria (CRN ESPA Reference)
• site vicinity, site area, and site location-specific geologic maps and cross-sections constructed at scales adequate to clearly illustrate surficial and bedrock geology, structural geology, topography, and relationship of power plant foundations and site boundaries to these features	Figure 2.5.1-19, Site Region Geologic Map Figure 2.5.1-27, Simplified Site Vicinity Geologic Map Figure 2.5.1-34, Site Area Geologic Map Figure 2.5.1-35, Site Area Cross-Section Figure 2.5.1-37, Site Location Geologic Map Figure 2.5.1-29, Site Location Geologic Map Showing Borings Figure 2.5.1-30, Geologic Cross-Section K–K′ of the Clinch River Nuclear Site (revised in response to Supplemental Item 2 of Enclosure 2 of this letter) Figure 2.5.1-63, Geologic Cross-Section A-A' Ground Surface to Basement (revised in response to Supplemental Information A, Enclosure 1 of this letter) Plates for Site Vicinity and Site Area Geology provided in Part 8
2. Geologic Evidence for Surface Deformation.	
• Surface and subsurface information for the site vicinity, area, and location to confirm and characterize presence or absence of surface deformation from faulting	2.5.3.2, Geological Evidence, or Absence of Evidence, for Surface Deformation
• growth faulting	2.5.1.1.4.1.2, Cumberland Plateau 2.5.3.7, Designation of Zones of Quaternary Deformation in the Site Region

SRP 2.5.3 Acceptance Criteria (NUREG-0800, Revision 5)	Location of Acceptance Criteria (CRN ESPA Reference)
• subsidence or collapse related to dissolution of limestone, salt or gypsum deposits, or salt diapirism	<u>Subsidence</u> 2.5.1.1.1.3, Regional Karst Processes and Occurrence 2.5.1.2.5, Local Geologic Hazards 2.5.1.2.5.1.3, Potential Karst Hazards at the CRN Site 2.5.1.2.5.2, Other Geologic Hazards 2.5.1.2.6.5, Karst Features 2.5.3.4.3, Karst Collapse 2.5.3.8.2.1, Karst-Related Deformation <u>Dissolution (in addition to the above sections)</u> 2.5.1.2.5.1.1, Karst in the Site Vicinity Area 2.5.1.2.5.1.2, Karst Processes and Features at the Clinch River Nuclear Site 2.5.1.1.1.1.2, Interior Plateaus Physiographic Province 2.5.1.1.1.1.3, Appalachian Plateau Physiographic Province 2.5.1.1.5.1, Karst Hazard 2.5.1.2.5.3, Evaluation of Local Geologic Hazards 2.5.1.2.6.3, Fracture Zones 2.5.3.2.3, Karst 2.5.3.8.2.1, Karst Related Deformation 2.5.4.1.3.3, Weathered and Fracture Zones
• Paleoliquefaction	New Subsection 2.5.3.2.6, Proposed Quaternary Deformation Features Along Douglas Reservoir, TN, added in response to Supplemental Information C, Enclosure 1 of Reference 2
• Blind faults	2.5.1.2.4.1.2,Macroscopic Structures within the Site Area (5-mi Radius) 2.5.3.2.1, Geologic Evidence, or Absence of Evidence, for Surface Deformation - Bedrock Faults
3. Timing of Deformation	

SRP 2.5.3 Acceptance Criteria (NUREG-0800, Revision 5)	Location of Acceptance Criteria (CRN ESPA Reference)
• recognized surface deformation features (e.g., tectonic faults and non-tectonic features including growth faults) and features associated with a blind fault, are investigated in sufficient detail to constrain the age of the most recent surface deformation event	2.5.3.4, Ages of Most Recent Deformation
4. Correlation of Earthquakes with Tectonic Features	
• evaluates all reported historical earthquakes within the site vicinity with respect to accuracy of hypocenter location and source of origin, and with respect to correlation to tectonic features.	2.5.3.3, Correlation of Earthquakes with Tectonic Features
5. Relationship of Geologic Features in the Site Vicinity to Regional Geologic Features	
• evaluates the relationships between faults or other deformation features in the site vicinity and the regional framework	2.5.3.5, Relationship of Tectonic Structures in the Site Area to Regional Tectonic Structures Note: All of the faults within the site vicinity are in the same "family" as those within the site area.
6. Potential for Surface Deformation at the Site	
• provide sufficient geological, seismological, and geophysical information to clearly establish whether there is a potential for future surface deformation at the site	2.5.3.8, Potential for Tectonic or Non-Tectonic Deformation at the Site
• If the potential for future surface deformation exists at the site, the application must provide information that demonstrates the potential effects of surface deformation are within the design basis of the proposed facility	2.5.3.8 states, "The potential for tectonic surface deformation at the CRN Site is negligible based on evidence presented." 2.5.3.8.2 - Potential for Non-Tectonic Deformation -states, The potential for non-techonic surface deformation as a result of karst features represents the most significant geologic hazard to the CRN Site." 2.5.1.2.5.1.3, Potential Karst Hazard at the CRN Site 2.5.1.2.6.5, Karst Features 2.5.1.2.6.10, Unforeseen Geologic Conditions

References:

1. Letter from TVA to NRC, CNL-16-081, "Application for Early Site Permit for Clinch River Nuclear Site," dated May 12, 2016

2. Letter from TVA to NRC, CNL-16-162, “Submittal of Supplemental Information Related to Geologic Characterization Information, Surface Deformation, and Stability of Subsurface Materials and Foundation in Support of Early Site Permit Application for Clinch River Nuclear Site,” dated October 21, 2016

From Supplemental Item 5 of this Enclosure:

SSAR Subsection 2.5.1.1.3.1, the first paragraph on page 2.5.1-13 of the ESPA is revised as indicated below: (Note - deletions are shown as "~~strike-through~~" text and additions are shown as "underlined" text.)

2.5.1.1.3.1 Valley and Ridge Province

The CRN Site is located within the southwestern portion of the Valley and Ridge province. In the site vicinity, this province is underlain predominantly by lower to middle Paleozoic sedimentary rocks (Figures 2.5.1-27 and 2.5.1-14). The Paleozoic section consists of four major subdivisions: a basal, mainly clastic transgressive unit; a thick, extensive Cambrian to Ordovician carbonate shelf sequence; a thin, laterally variable shelf sequence of Ordovician to Lower Mississippian carbonate rocks and thin clastic units; and a Middle Mississippian to Pennsylvanian synorogenic clastic wedge. This sedimentary rock sequence was deposited on what has been interpreted as Grenvillian continental crust. ~~In support of the site response analysis described in Subsection 2.5.2.5, the stratigraphic units above the basement and below the Chickamauga Group are discussed in detail in this section. The location of a geologic cross-section showing stratigraphy, structure, and shear wave velocities from the basement to the ground surface is shown on a geologic map, Figure 2.5.1-62. A geologic cross-section drawn perpendicular to the strike direction is shown on Figure 2.5.1-63, Sheet 1 of 2. Figure 2.5.1-35 is an older, alternate interpretation of deep geologic structure and is drawn northwest of Figure 2.5.1-63 to illustrate the geometry of the Chestnut Ridge fault (Subsection 2.5.1.2.4.2.4). The stratigraphic unit symbols on the geologic map and cross-section are summarized on the cross-section explanation (Figure 2.5.1-63, Sheet 2 of 2) and are described in more detail in the following text. Chickamauga Group stratigraphy and the underlying upper Knox Group are described in greater detail in Subsection 2.5.1.2.3 (Local Stratigraphy and Lithology) since this information is derived from site-specific borings and site mapping.~~ The Grenville Province basement is ~~comprised~~ composed primarily of gneisses, granites, amphibolites, and other igneous and metamorphic rocks ranging in age from more than 2 Ga to approximately 980 Ma (Figure 2.5.1-2) based on province-wide geochronology studies (Reference 2.5.1-99). Although they have been deformed by Paleozoic orogenies, the rocks of the Blue Ridge province (Subsection 2.5.1.1.3.5) are Mesoproterozoic inliers interpreted as reworked amphibolite- to granulite –facies metamorphic rocks representative primarily of the Grenville orogeny and the crystalline basement beneath the CRN Site (Reference 2.5.1-99). Figure 2.5.1-35 presents a geologic cross section through the CRN Site area to illustrate the relationship between Paleozoic stratigraphy, northwest-directed Alleghanian thrust faults, and underlying Grenville basement rocks. An alternative interpretation that demonstrates the relationship between stratigraphy, structure, and shear wave velocities from the basement to the ground surface is also provided to support the discussion of site response (see Figures 2.5.1-62 and 2.5.1-63). ~~In support of the site response analysis described in Subsection 2.5.2.5, the stratigraphic units above the basement and below the Chickamauga Group are discussed in detail in this section.~~ Additionally, the lithologic descriptions of the stratigraphic units above the basement and below the Chickamauga Group, detailed in this section, support the site response analysis described in Subsection 2.5.2.5.

The fifth paragraph on page 2.5.1-17 is revised as indicated below:

The Chickamauga Group consists mainly of limestone toward the northwest and becomes increasingly clastic to the southeast. Its total thickness is more than 600 m (1970 ft) (Reference 2.5.1-105). On geologic maps within the CRN site region, the Chickamauga Group is subdivided into several formations with characteristics and nomenclature that vary between thrust sheets (References 2.5.1-9, 2.5.1-106, 2.5.1-107, and 2.5.1-108). Subdivisions of the Chickamauga Group in the CRN site vicinity are described below from oldest to youngest. The stratigraphy of the Chickamauga Group and the underlying upper Knox Group, derived from site-specific borings and mapping, are described in greater detail in Subsection 2.5.1.2.3

As a result of the changes described previously, the following existing figures are revised:

Figure 2.5.1-26.	(Sheet 1 of 6), Quaternary Terrace Map Adjacent to the Clinch River Arm of the Watts Bar Reservoir Within the Clinch River Nuclear Site Area, Location A
Figure 2.5.1-26.	(Sheet 2 of 6), Quaternary Terrace Map Adjacent to the Clinch River Arm of the Watts Bar Reservoir Within the Clinch River Nuclear Site Area, Location B
Figure 2.5.1-26.	(Sheet 3 of 6), Quaternary Terrace Map Adjacent to the Clinch River Arm of the Watts Bar Reservoir Within the Clinch River Nuclear Site Area, Location C
Figure 2.5.1-26.	(Sheet 4 of 6), Quaternary Terrace Map Adjacent to the Clinch River Arm of the Watts Bar Reservoir Within the Clinch River Nuclear Site Area, Location D
Figure 2.5.1-26.	(Sheet 5 of 6), Quaternary Terrace Projections to the Clinch River for creation of Longitudinal Profile
Figure 2.5.1-26.	(Sheet 6 of 6), Quaternary Terrace Projections to the Clinch River for creation of Longitudinal Profile
Figure 2.5.1-30.	Geologic Cross-Section K-K’ of the Clinch River Nuclear Site
Figure 2.5.1-62.	Map Showing the Location of Geologic Cross-Section A-A' to Basement
Figure 2.5.1-63.	(Sheet 1 of 2), Geologic Cross-Section A-A' Ground Surface to Basemen
Figure 2.5.1-63.	(Sheet 2 of 2), Geologic Cross-Section A-A' Ground Surface to Basement
Figure 2.5.2-56.	Shear Modulus Reduction and Damping Curves for Firm Rock
Figure 2.5.3-3.	(Sheet 1 of 2), Geologic Map and Topographic Profile B-B' of Quaternary Fluvial Terraces and Northeastern Projection of Copper Creek Fault
Figure 2.5.3-3.	(Sheet 2 of 2), Figure 2.5.3-3. (Sheet 2 of 2), Geologic Map and Topographic Profile B-B' of Quaternary Fluvial Terraces and Northeastern Projection of Copper Creek Fault
Figure 2.5.3-4	Longitudinal Profiles of Quaternary Terraces Along the Clinch River
Figure 2.5.4-26.	Shear Modulus Reduction and Damping Curves for Firm Rock

Copies of the new figures are provided on the following pages.

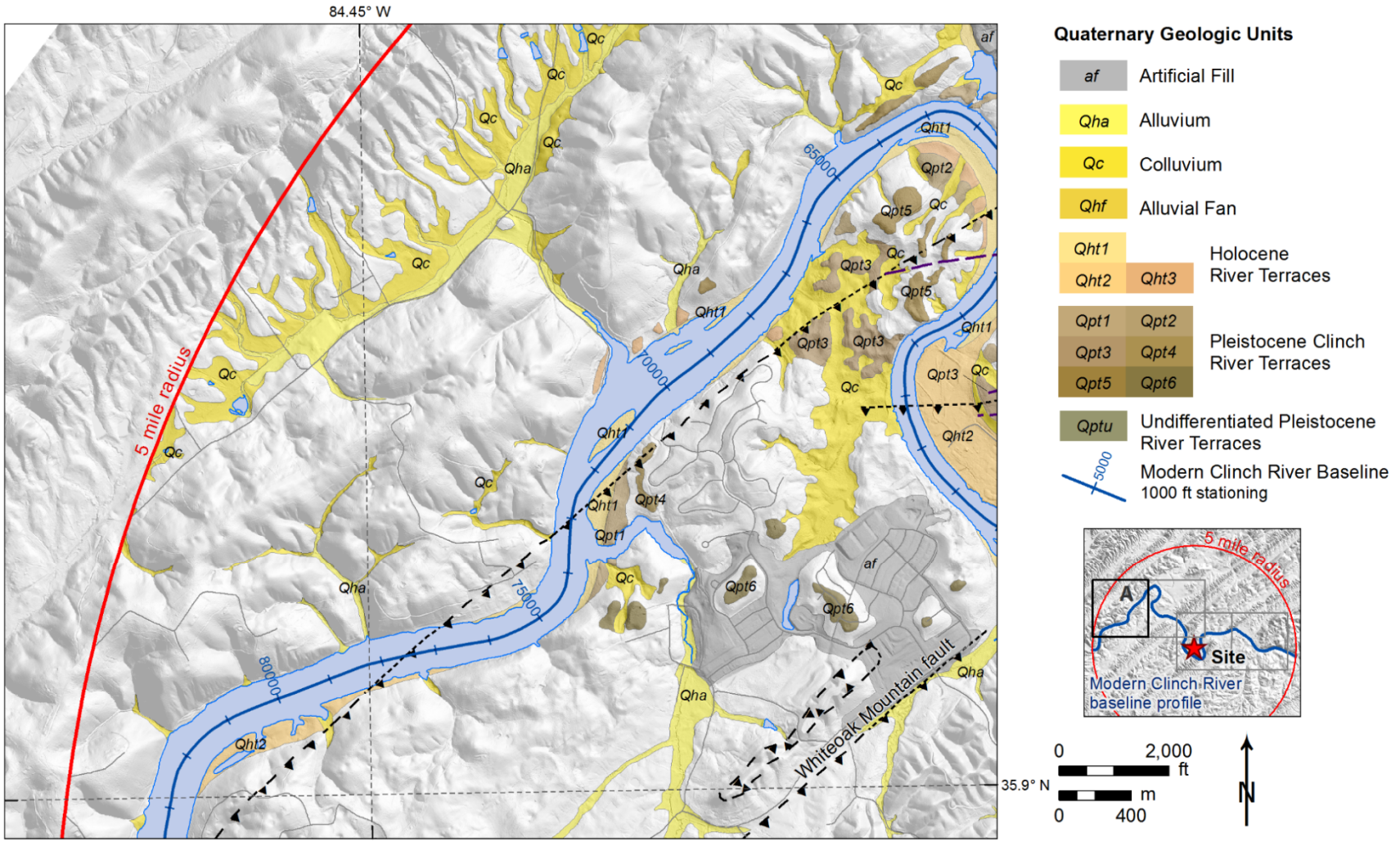

Figure 2.5.1-26. (Sheet 1 of 6), Quaternary Terrace Map Adjacent to the Clinch River Arm of the Watts Bar Reservoir Within the Clinch River Nuclear Site Area, Location A

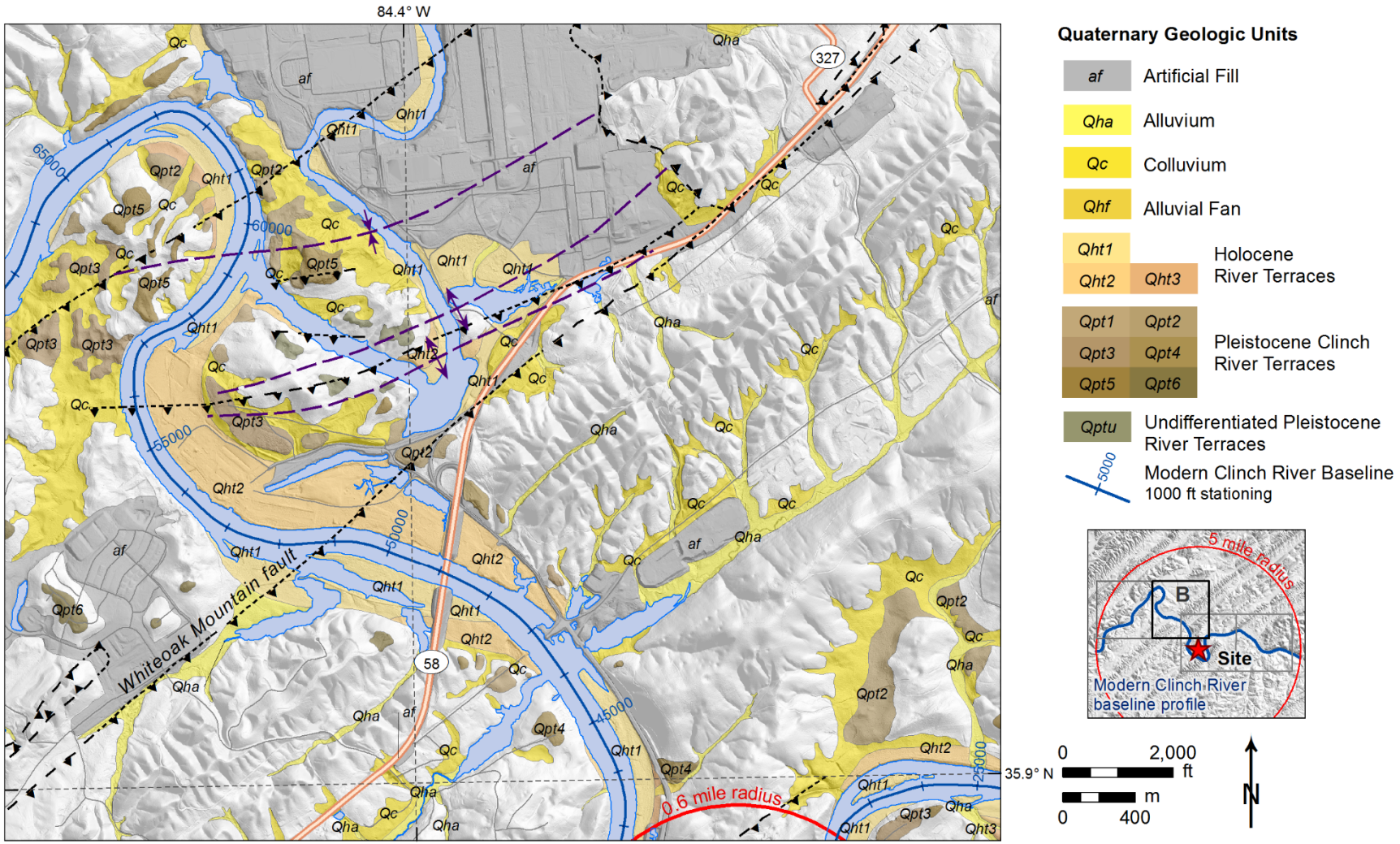

Figure 2.5.1-26. (Sheet 2 of 6), Quaternary Terrace Map Adjacent to the Clinch River Arm of the Watts Bar Reservoir Within the Clinch River Nuclear Site Area, Location B

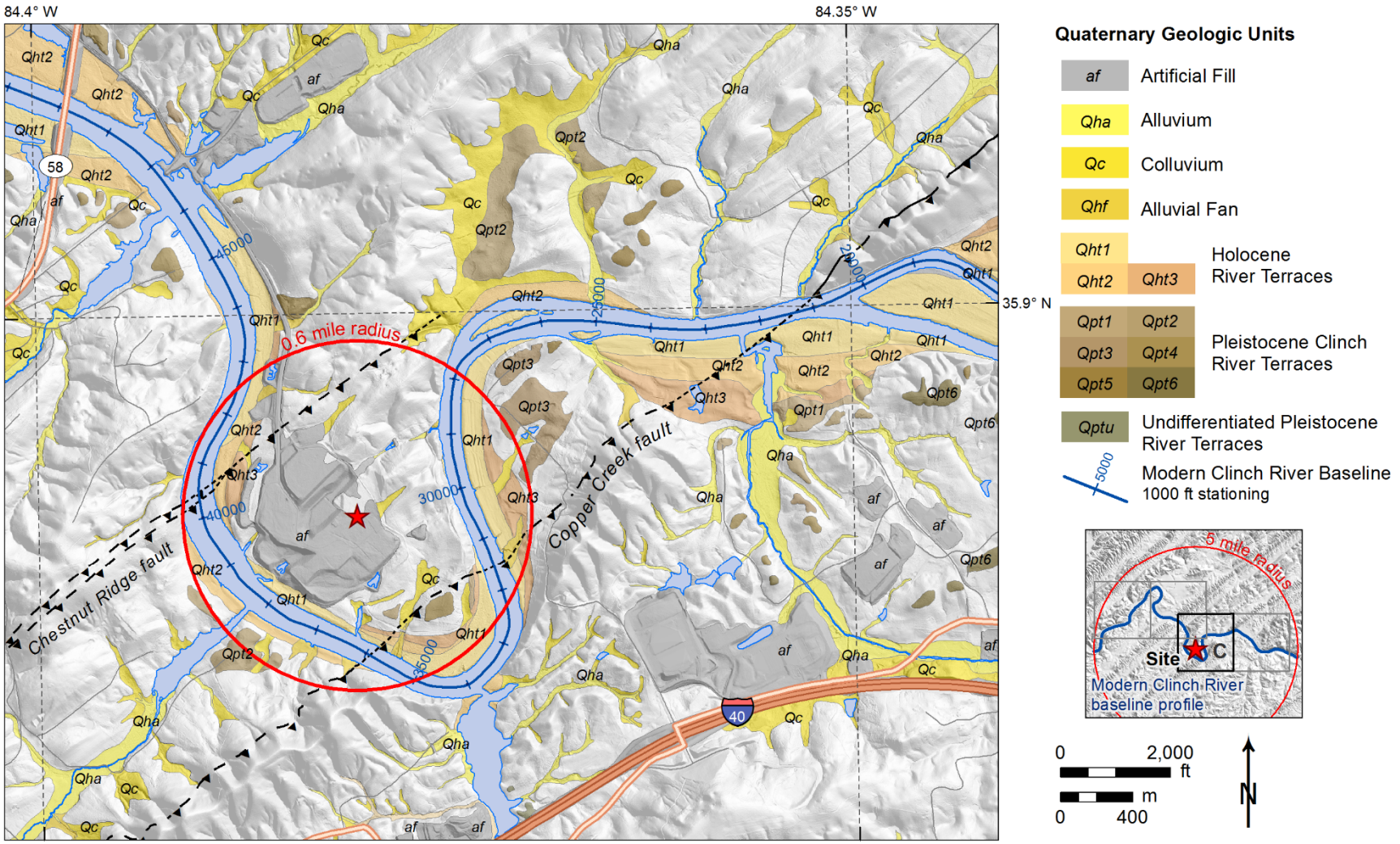

Figure 2.5.1-26. (Sheet 3 of 6), Quaternary Terrace Map Adjacent to the Clinch River Arm of the Watts Bar Reservoir Within the Clinch River Nuclear Site Area, Location C

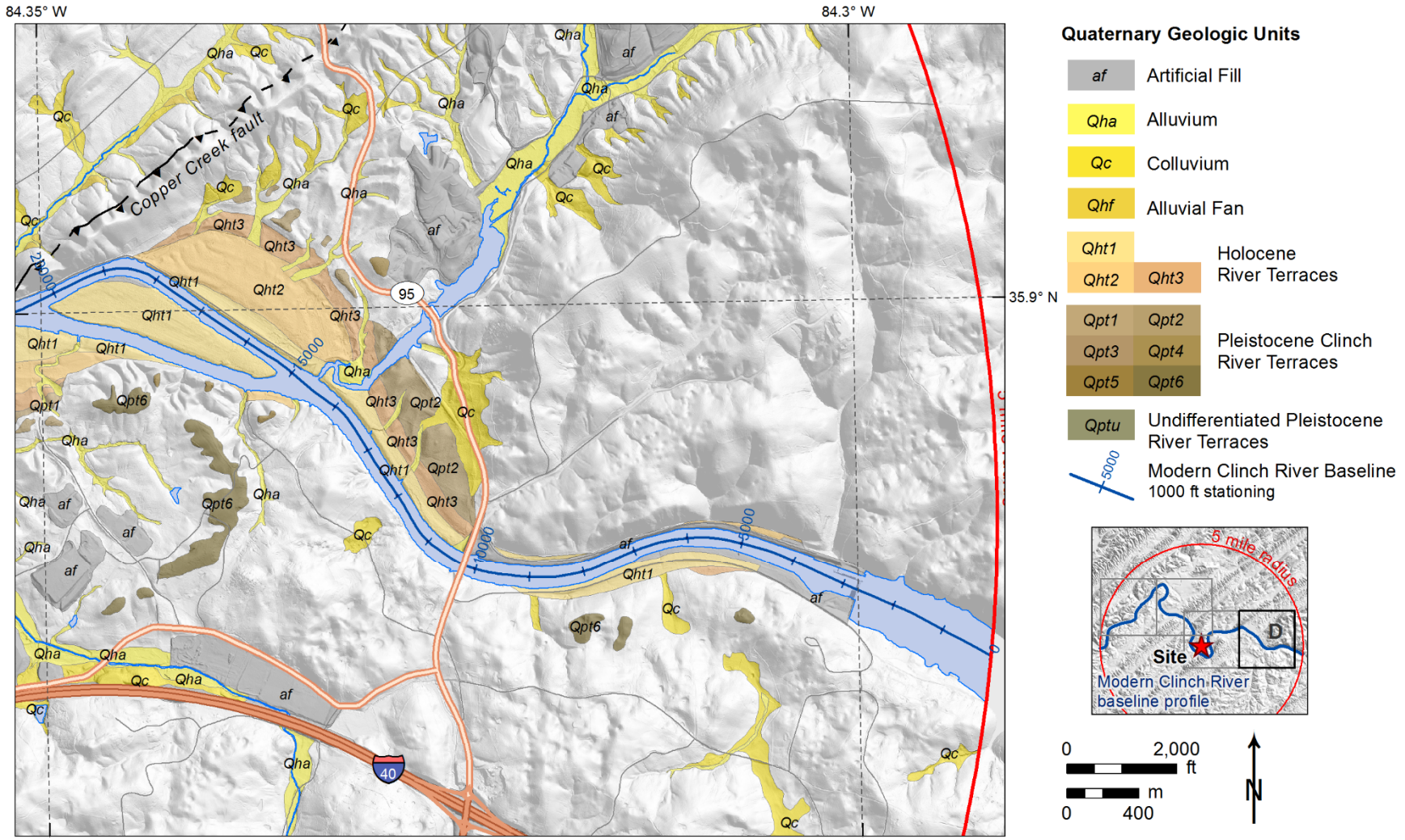

Figure 2.5.1-26. (Sheet 4 of 6), Quaternary Terrace Map Adjacent to the Clinch River Arm of the Watts Bar Reservoir Within the Clinch River Nuclear Site Area, Location D

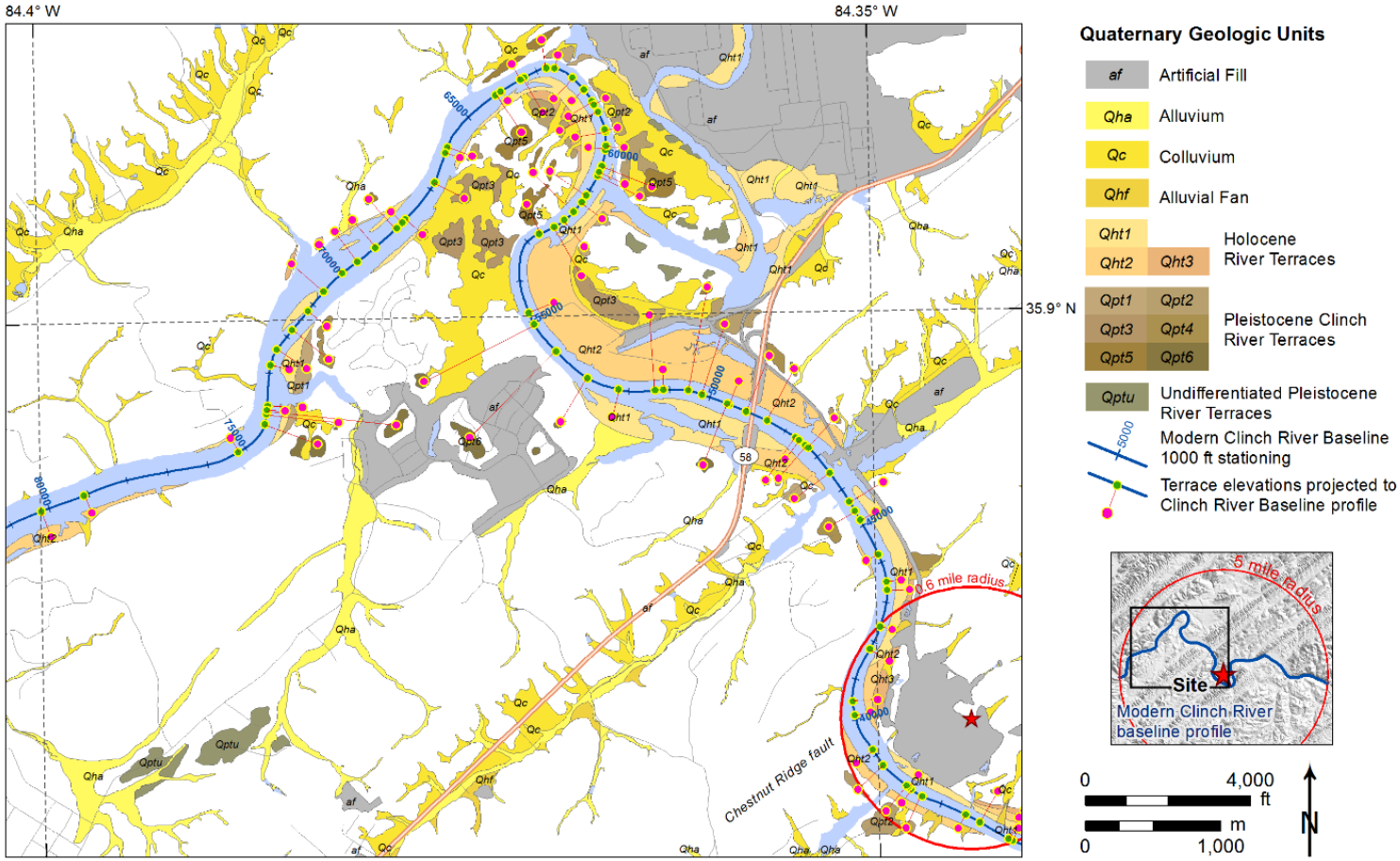

Notes:
See Figure 2.5.3-4 for Longitudinal Profiles of Quaternary Terraces along the Clinch River.
Quaternary mapping by Lettis Consultants International, Inc.

Figure 2.5.1-26. (Sheet 5 of 6), Quaternary Terrace Projections to the Clinch River for creation of Longitudinal Profile

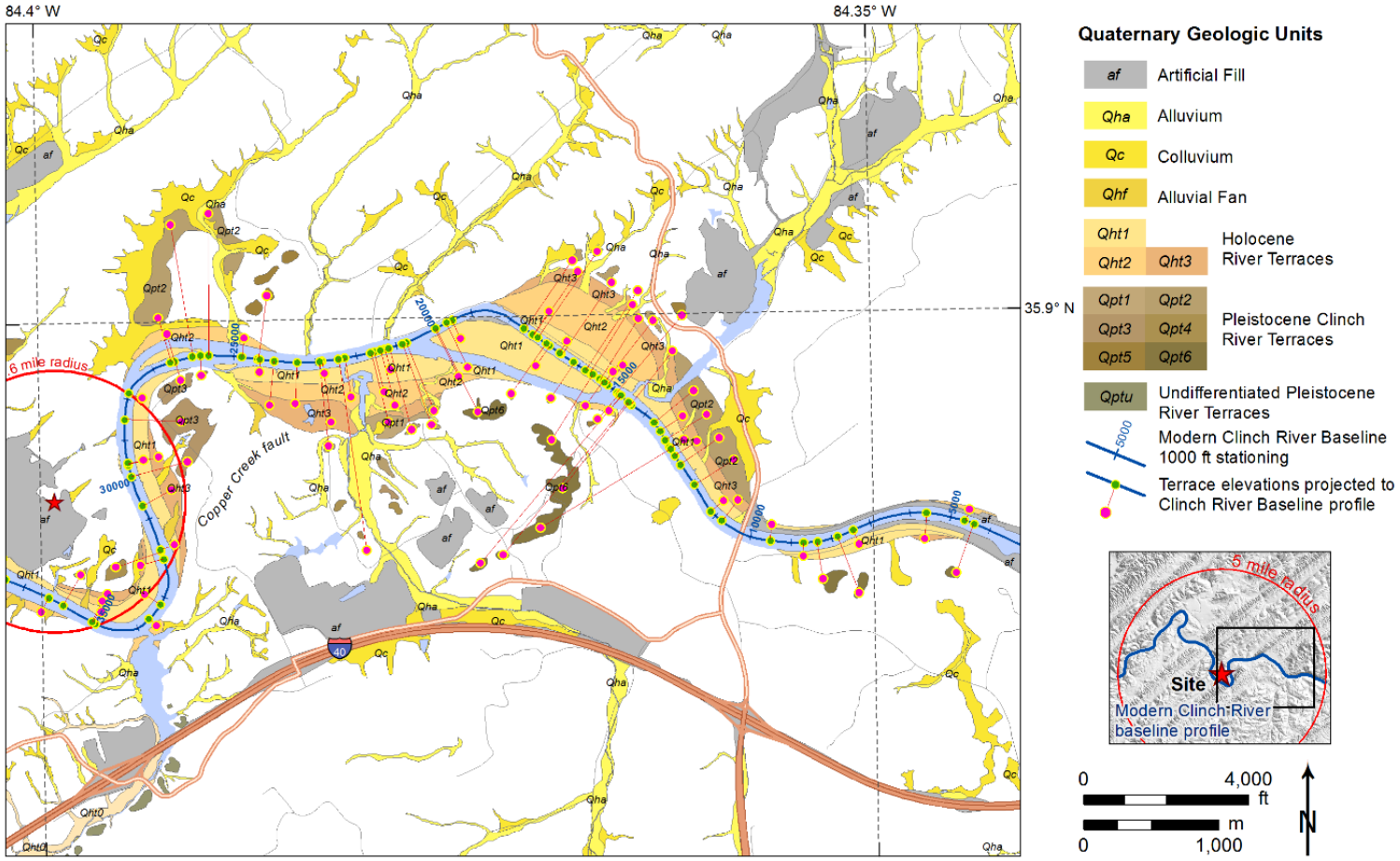

Notes:
See Figure 2.5.3-4 for Longitudinal Profiles of Quaternary Terraces along the Clinch River.
Quaternary mapping by Lettis Consultants International, Inc.

Figure 2.5.1-26. (Sheet 6 of 6), Quaternary Terrace Projections to the Clinch River for creation of Longitudinal Profile

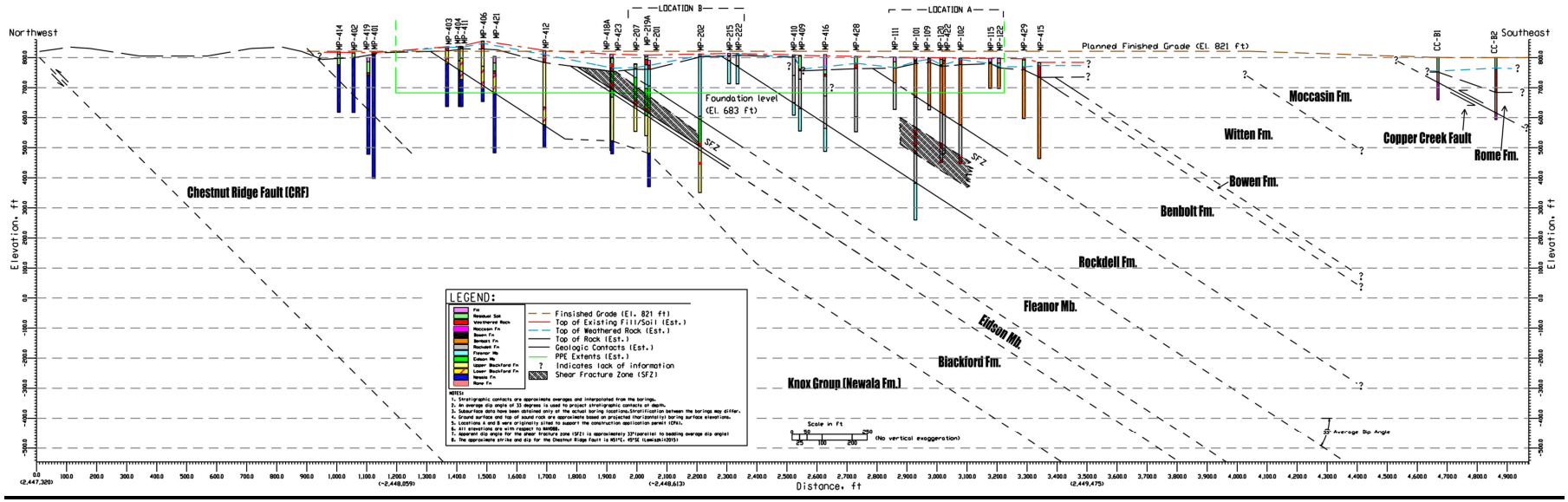

Figure 2.5.1-30. Geologic Cross-Section K–K′ of the Clinch River Nuclear Site

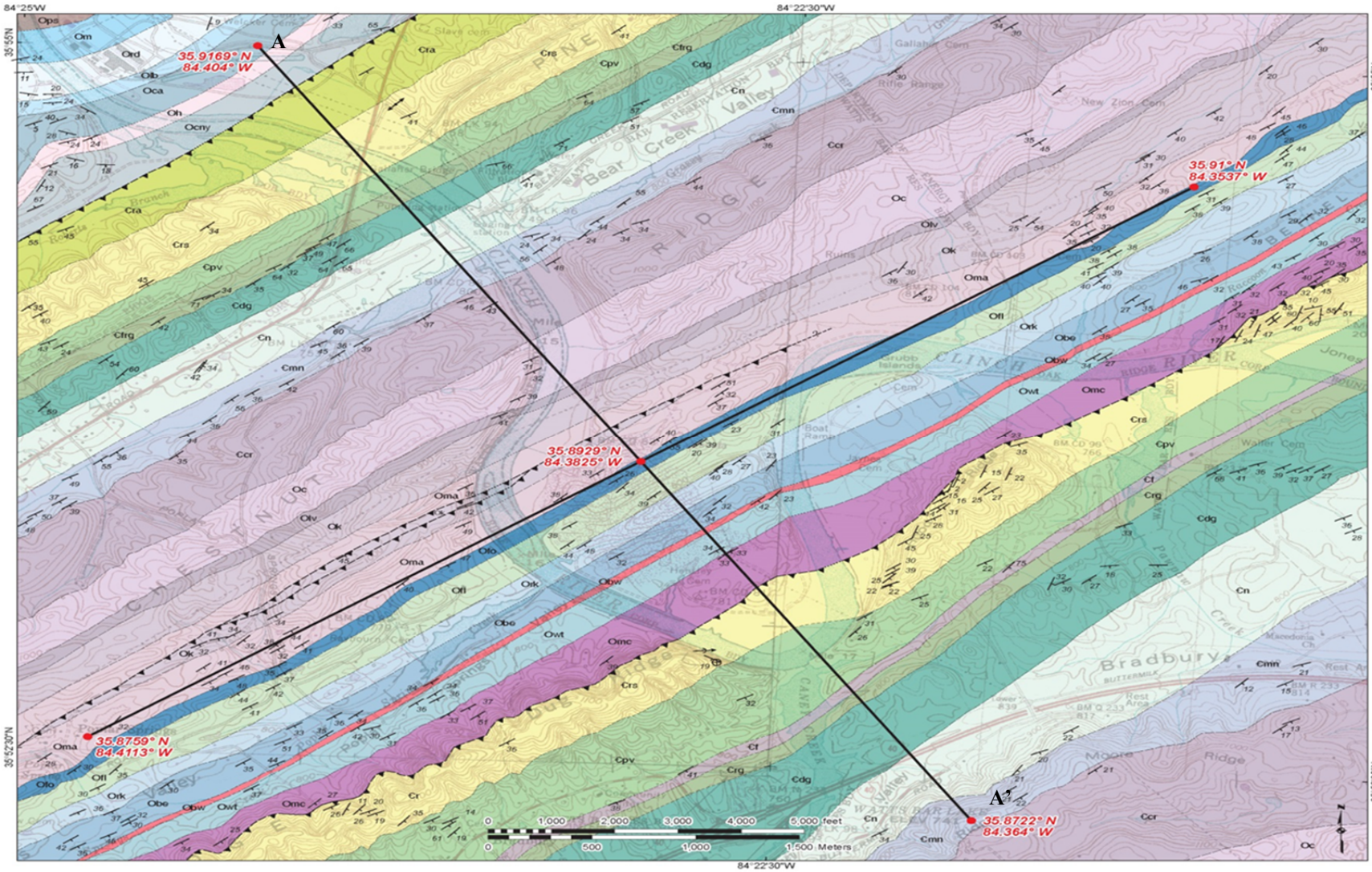

Note: Source: Reference 2.5.1-273.

Figure 2.5.1-62. Map Showing the Location of Geologic Cross-Section A-A' to Basement

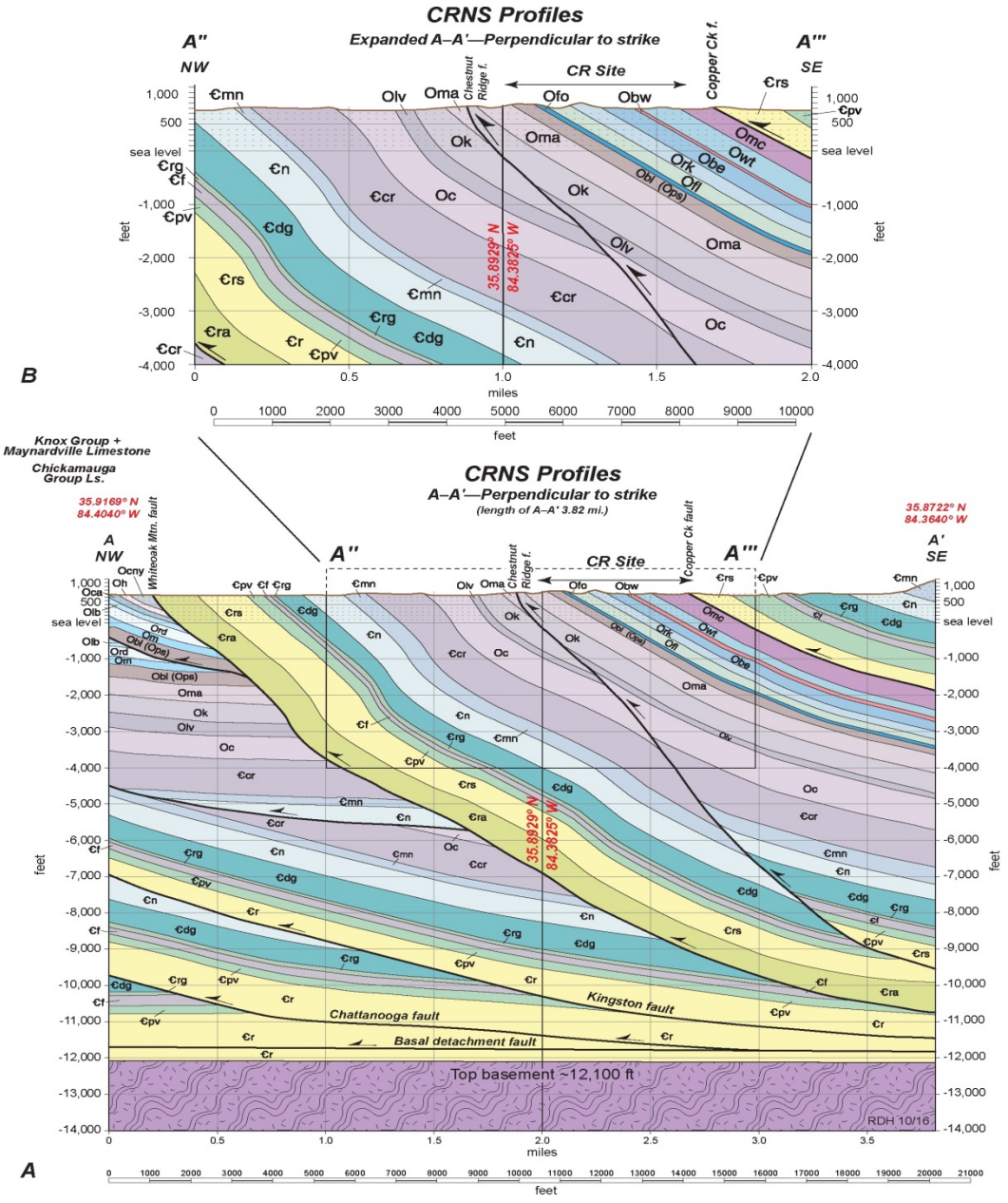

Figure 2. A. Across-strike geologic cross section A-A' with an expanded section, the location of which is indicated in the rectangle in the right center of the diagram. B. Upper part of Figure 2A with additional expansion indicated by the rectangle in the lower diagram. Location of section line is indicated in Figure 1.

Figure 2.5.1-63. (Sheet 1 of 2) Geologic Cross-Section A-A' Ground Surface to Basement

Note:
A. Across-strike geologic cross-section A-A' with an expanded section, the location of which is indicated in the rectangle in the center of the diagram.
B. Upper part of Figure A with additional detail. Location of section line is indicated in the geologic map on Figure 2.5.1-62.

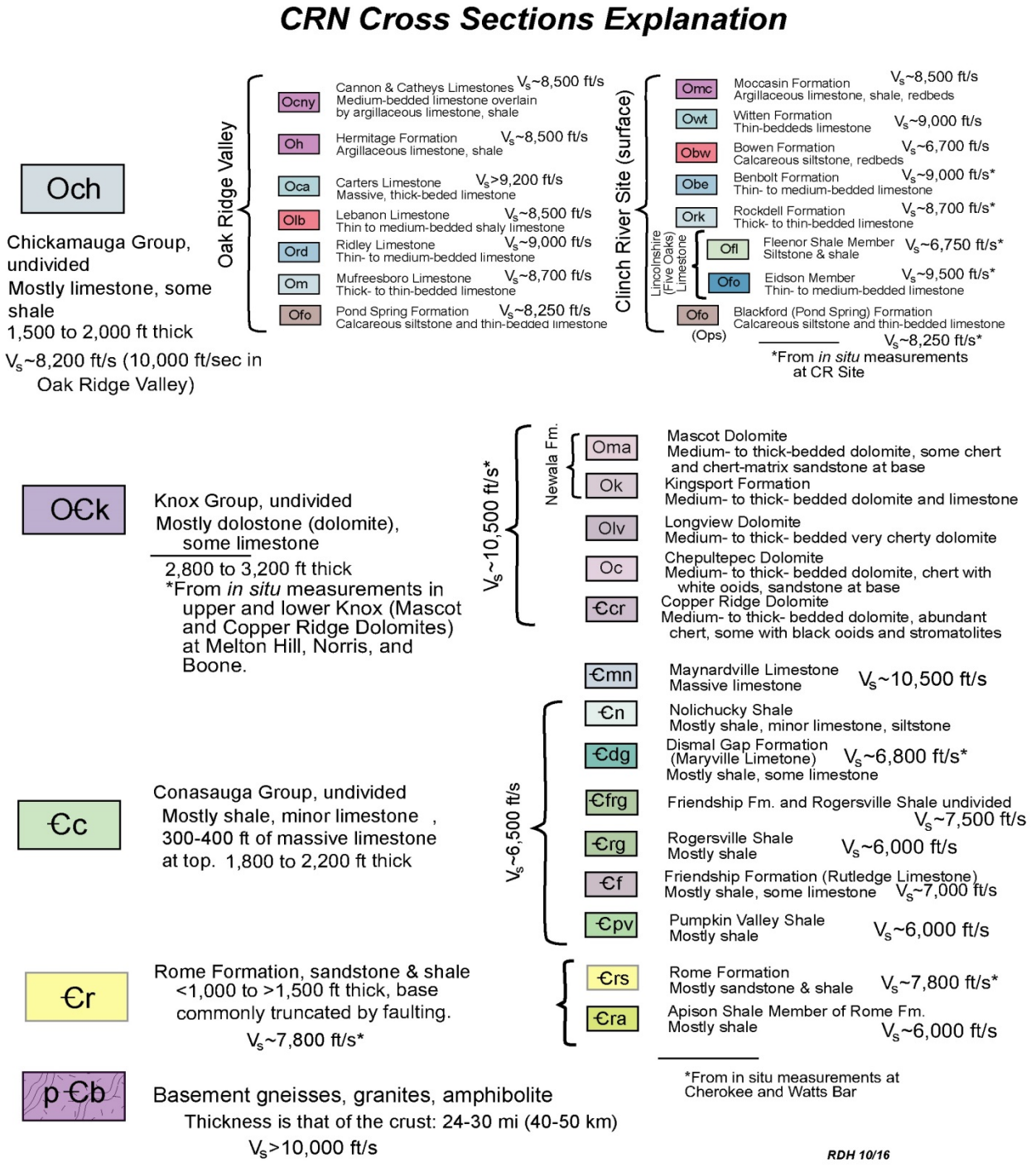

Figure 4. Explanation of symbols used to identify the different geologic units in Figures 2 and 3. Vs estimates are indicated, with asterisks showing the locations where the estimates are based on in situ borehole suspension-log measurements at different TVA sites.

Figure 2.5.1-63. (Sheet 2 of 2) Geologic Cross-Section A-A' Ground Surface to Basement

Note: Explanation of symbols used to identify the different geologic units in Figures 2.5.1-62 and 2.5.1-63

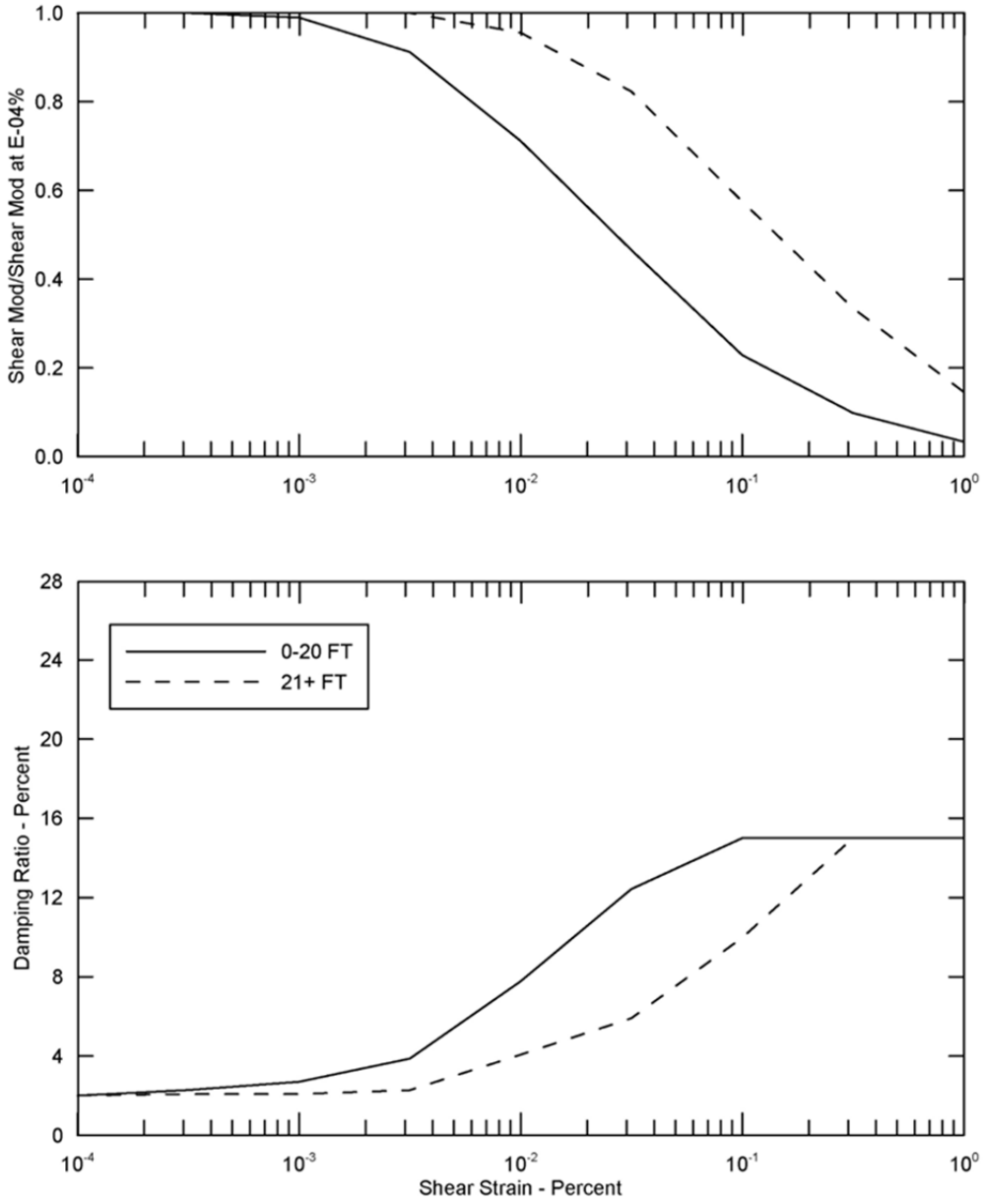

Figure 2.5.2-56. Shear Modulus Reduction and Damping Curves for Firm Rock

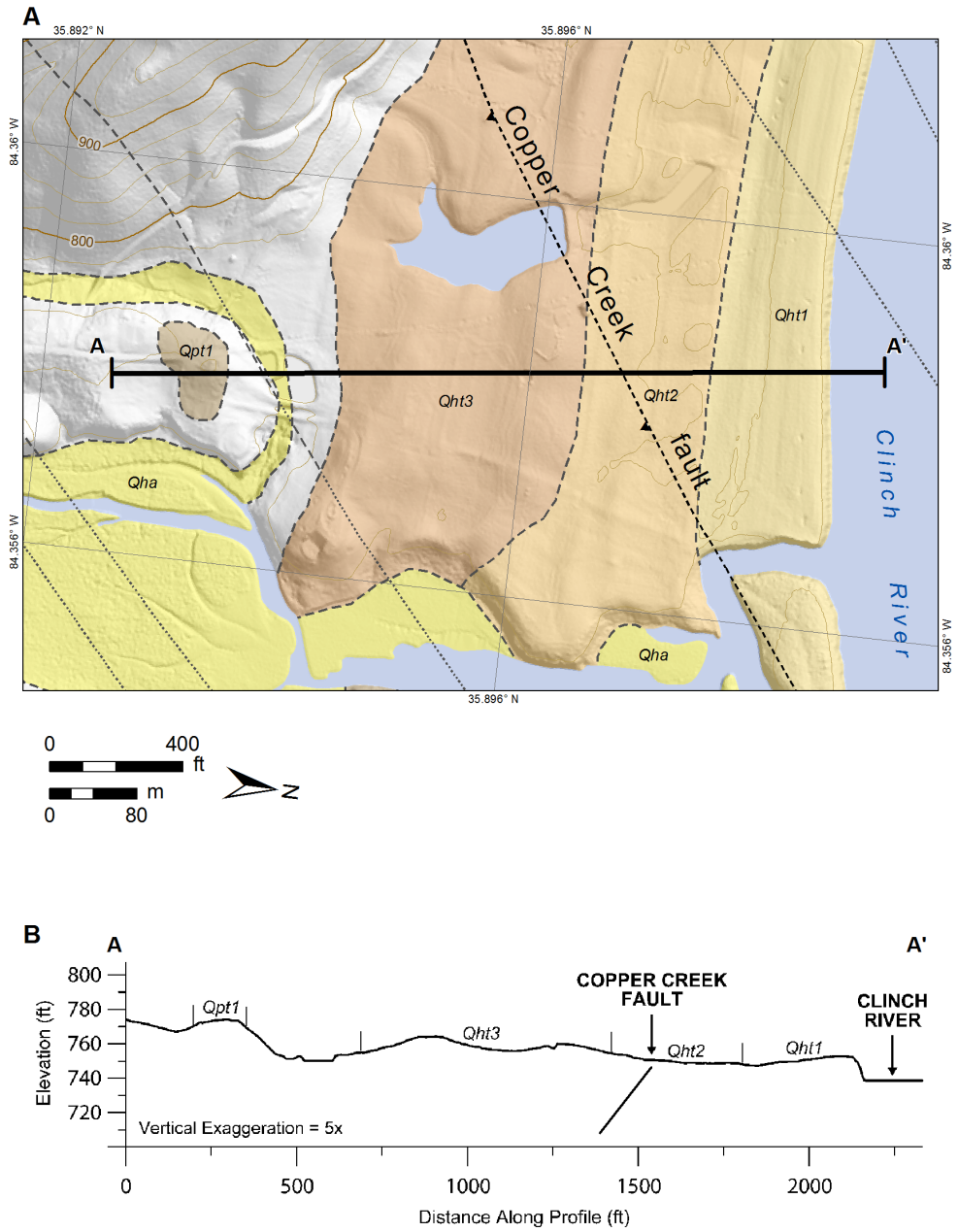

Note:
A.= Map of Clinch River terraces that overlie the Copper Creek fault
B = Topographic profile across terraces and Copper Creek fault
Location of Profile B-B' is shown on Figure 2.5.3-6
Location of Chestnut Ridge fault from Lemiszki (Reference 2.5.3-56)

Figure 2.5.3-3. (Sheet 1 of 2), Geologic Map and Topographic Profile B-B' of Quaternary Fluvial Terraces and Northeastern Projection of Copper Creek Fault

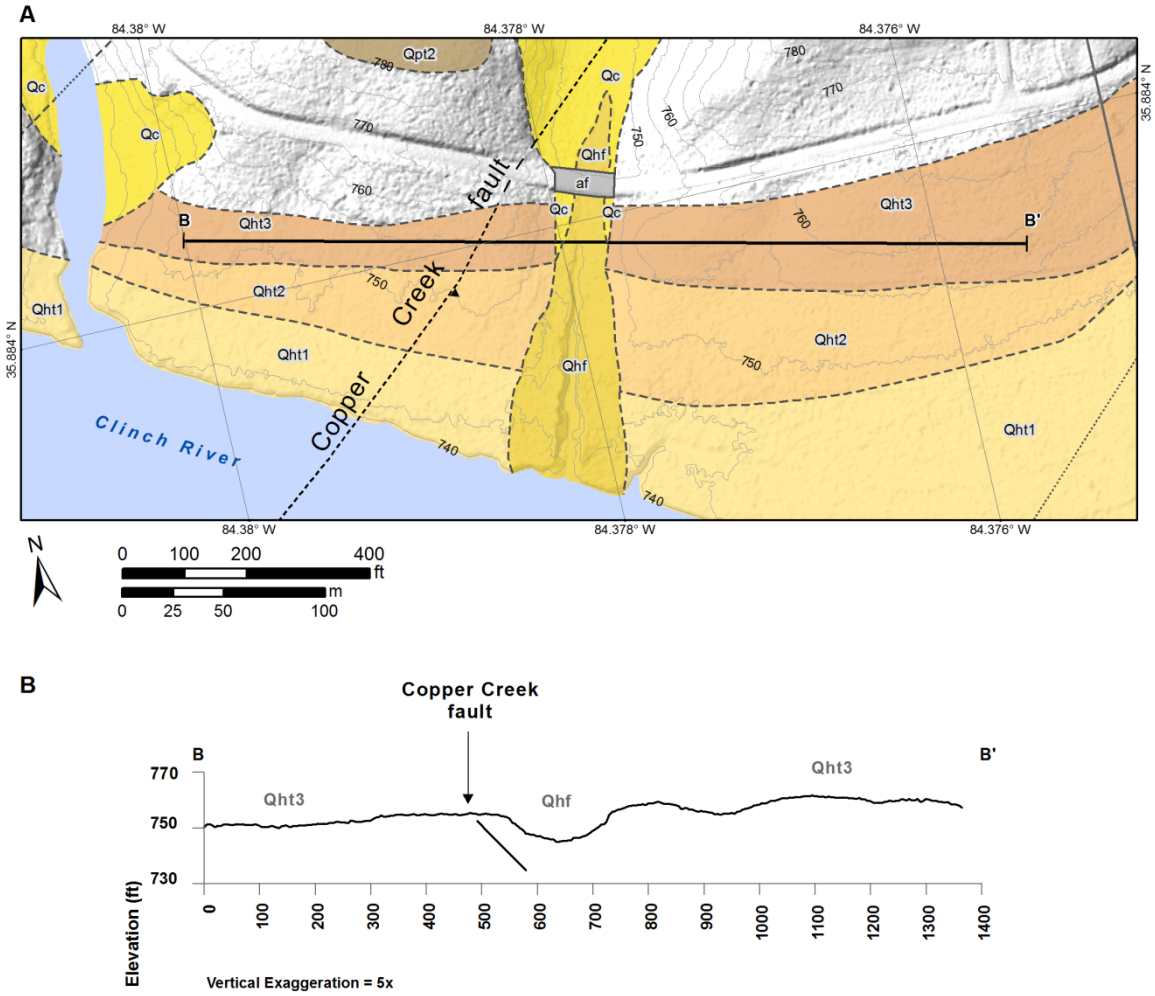

Note:
A.= Map of Clinch River terraces that overlie the Copper Creek fault
B = Topographic profile across terraces and Copper Creek fault
Location of Profile B-B' is shown on Figure 2.5.3-6
Location of Chestnut Ridge fault from Lemiszki (Reference 2.5.3-56)

Figure 2.5.3-3. (Sheet 2 of 2), Geologic Map and Topographic Profile B-B' of Quaternary Fluvial Terraces and Northeastern Projection of Copper Creek Fault

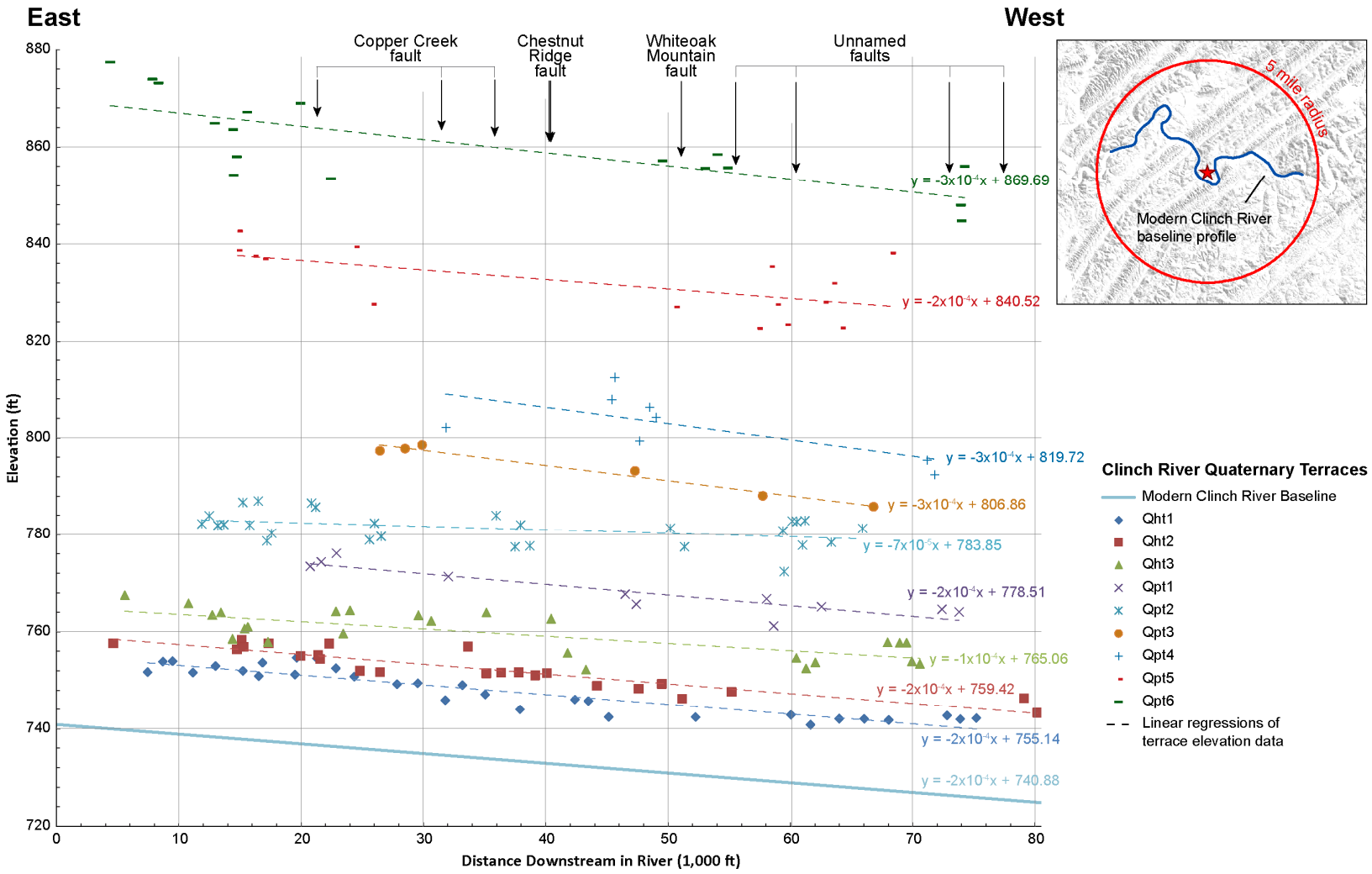

Notes:
See Figure 2.5.3-2A-D for Quaternary Terrace maps along the Clinch River.

Figure 2.5.3-4. Longitudinal Profiles of Quaternary Terraces Along the Clinch River

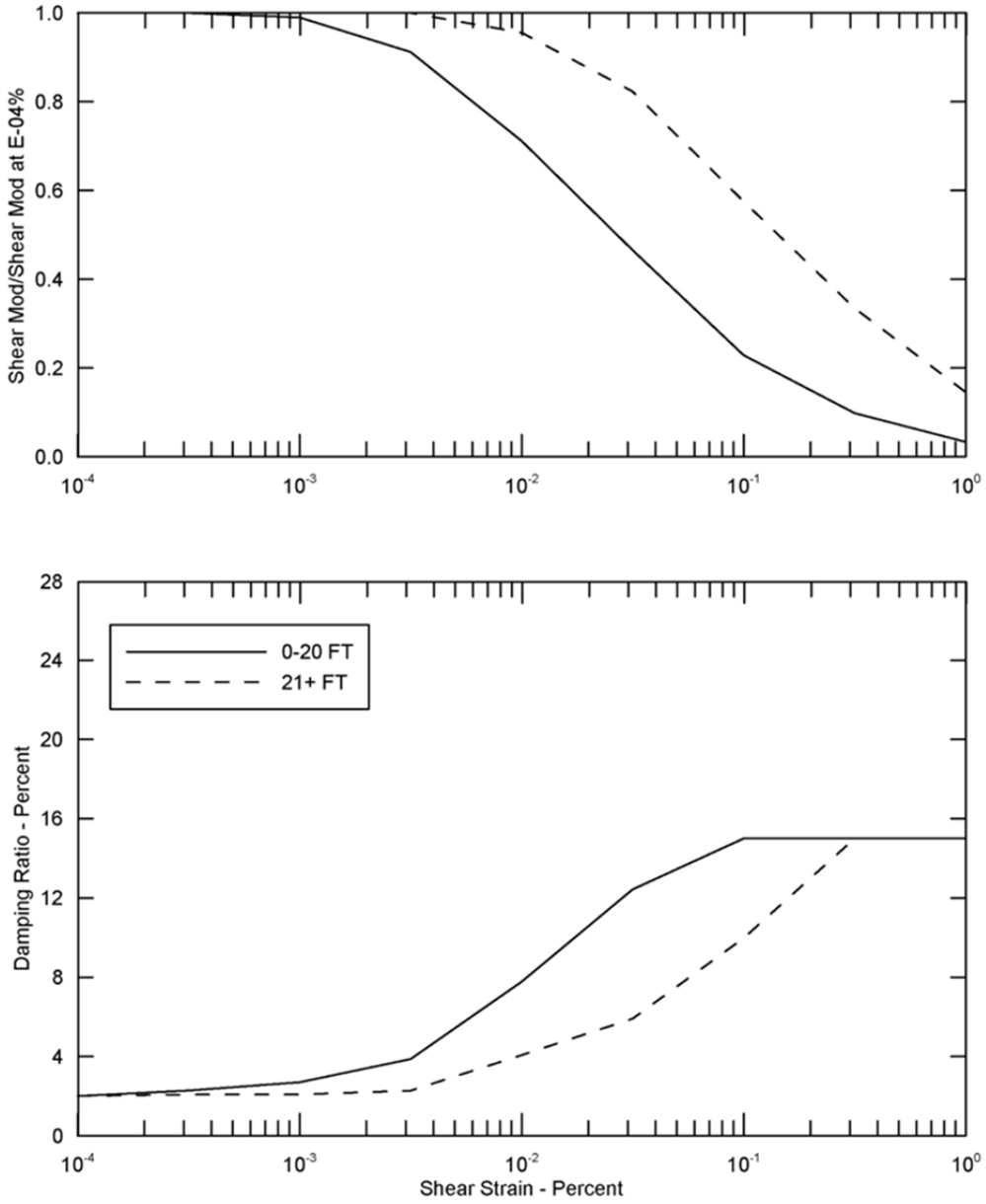

Figure 2.5.4-26. Shear Modulus Reduction and Damping Curves for Firm Rock